

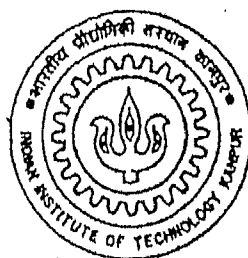
Liquid phase assisted sintering of alumina and silicon carbide based ceramics

*A thesis submitted in
Partial Fulfillment of the Requirements
for the Degree of*

MASTER OF TECHNOLOGY

by

Koushik Biswas



to the

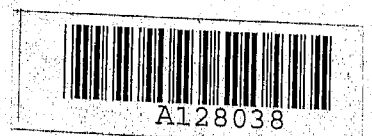
Department of Materials and Metallurgical Engineering
Indian Institute of Technology, Kanpur
India

May, 1999

25 MAY 1999 / MME
CENTRAL LIBRARY
I. I. T., KANPUR

Acc. No. A 128038

711
mme h 900/
B5482



Dedicated to my parents

Acknowledgements

The present work was accomplished in the period from June'96 to March'99 in Indian Institute of Technology, Kanpur, India and in the Pulvermetallurgisches Laboratorium of Max-Planck-Institut für Metallforschung, Stuttgart, Germany.

On successful completion of this project, I would like to thank all the personnel for their valuable contributions.

I am indebted to my thesis supervisors Prof. Dr. G. S. Upadhyaya (Indian Institute of Technology Kanpur, India), Prof. Dr. F. Aldinger (Max-Planck-Institute für Metallforschung, Stuttgart, Germany) and Dr. G. Rixecker (Max-Planck-Institute für Metallforschung, Stuttgart, Germany) for the guidance and support provided to me towards the consummation of this work.

I acknowledge the help extended to me by all colleagues, laboratory assistants and staffs in various stages of my work.

I express my sincere gratitude to my parents and younger brother for providing a constant source of motivation to me.

Koushik Biswas

Contents

Dedication	iii
Acknowledgements	iv
Contents	v
List of publications	xi
Abstract	xiii

Part I

Sintered alumina slurry coated with tungsten alloys

Certificate	xvii
List of Figures	xix
List of Tables	xx
Nomenclature	xxi
1 Introduction	3

1.1	Sintering aspects in laminar composites	4
1.2	Sintering of alumina	6
1.2.1	Sintering phenomena	7
1.2.2	Role of additives on sintering of alumina	8
1.2.3	Liquid phase sintering of alumina	11
1.3	Sintering of tungsten	14
1.3.1	Activated sintering of tungsten	16
1.3.2	Liquid phase sintering of tungsten	18
1.4	Alumina-tungsten cosintering	20
1.5	Scope of the present investigation	21
2	Experimental procedure	25
2.1	Preparation of substrate	25
2.2	Preparation of W-Cu-Ag premix slurries and the composites	26
2.3	Sintered density and densification parameter	27
2.4	Transverse rupture strength(TRS) evaluation	27
2.5	Scanning Electron Microscopy studies	28
3	Results and discussion	31
3.1	Effect of flux content in alumina substrate	31
3.2	Effect of lubricant in W-10Cu premix overlay	31
3.3	Effect of overlay sintering temperature	34
3.4	Effect of sintering atmosphere	34

3.5	Effect of copper content in W-overlay	34
3.6	Effect of silver addition in tungsten-copper overlay	40
3.7	Effect of pretreated silver/copper powders in tungsten overlay	40
4	Conclusions and future scope of work	47
	References	51

Part II

Optimization of an additive system for the liquid phase sintering of silicon carbide ceramics

Certificate	iii
List of Figures	v
List of Tables	vii
Nomenclature	viii
1 Introduction	3
1.1 SiC Powder Production	4
1.2 Solid State Sintering of Silicon Carbide	5
1.2.1 Pressureless sintering	5
1.2.2 Hot pressing	9
1.3 Liquid Phase Sintering	10
1.3.1 Effect of oxide additives	11

1.3.2	Effect of nitrides and other additives	14
1.4	Microstructural Aspects	16
1.4.1	Effect of B, Al and C	16
1.4.2	Role of oxide additives	16
1.4.3	Effect of nitride and other additives	18
1.5	Mechanical Properties	19
1.5.1	Strength	19
1.5.2	Fracture toughness	20
1.5.3	Creep and high temperature strength	21
1.5.4	Fatigue resistance	22
1.6	Oxidation Resistance	22
2	Experimental Procedure	25
2.1	Preparation of LPS-SiC Ceramics	25
2.1.1	Raw materials and greenbody fabrication	25
2.1.2	Sintering and HIPing	26
2.1.3	Annealing treatment	28
2.2	Characterization of the Ceramics	29
2.2.1	Sinter density and mass loss	29
2.2.2	X-ray diffractometry	29
2.2.3	Metallography	30
2.2.4	Microstructural analysis	30

2.3	Mechanical properties evaluation	30
2.3.1	Room temperature fracture toughness	31
2.3.2	Bending strength	31
3	Results and Discussion	35
3.1	Characteristic properties	35
3.1.1	Sinter density and mass loss	35
3.1.2	X-ray diffractometry	37
3.2	Mechanical properties	41
3.2.1	Fracture toughness	41
3.2.2	Bending strength	51
4	Conclusions and future scope of work	59
	References	63

List of publications

Following papers have been published based on the work presented in this thesis.

1. "Co-sintering of tungsten alloy slurry coated alumina composites and their properties", K. Biswas and G. S. Upadhyaya, Materials and Design, Vol. 19, 1998, pp.231-240.
2. "Flüssigphasensintern von Siliziumcarbid : das Additivsystem AlN-Y₂O₃", G. Rixecker, I. Wiedmann, K. Biswas und F. Aldinger, in Werkstoffwoche'98 - Band VII, Wiley - VCH, Weinheim, 1999, pp.215-218 (in German).

Abstract

Part I : Sintered alumina slurry coated with tungsten alloys

Alumina-tungsten composite systems have been in the forefront of electronic packaging materials because of their enhanced performances. In the present investigation, densification of alumina substrate was done using CaO-SiO_2 additive system and found that prefired flux(CaSiO_3) addition enhances densification with its greater proportion. Alumina substrate strengthening was also improved by dosing so.

Adhesion aspects between substrates and tungsten overlays are investigated in the light of lubricant addition, metal binder content in tungsten layer, sintering temperature and atmosphere. It was found that good adhesion occur in case of 1% micronized wax as lubricant. Good bonded layered composites were produced with alumina substrate containing 6wt% CaSiO_3 and the overlay(W-10Cu) premix containing 1% wax. Lower metal binder (5wt% Cu) in tungsten overlay produced a delaminated composite reflecting poor adherence due to insufficient liquid phase. Whereas addition of 20% Cu binder also gave rise to delamination owing to the stress generated due to excessive shrinkage. Change in the overlay system from W-10Cu to W-10Ag also produced delaminated composite due to poor wetting behaviour by silver. Partial substitution of copper by silver also produced the same result. Addition of pretreated metal binder system also result in delamination due to excessive shrinkage although a better wetting characteristics were observed in this system due to presence of less oxygen in the metal binder system. Elevated temperature(1300°C) cosintering results in a good bonded composites as compared to low temperature sintering(1200°C) owing to insufficient densification and poor wetting in the overlay. Effect of sintering atmosphere was observed and found that strength increases in case of layered composite sintered in H_2 as compared to argon. The better sintering behaviour in H_2 attributed to the fact that hydrogen reduces the oxide impurities facilitating a better wetting behaviour which enhances the overlay/substrate bonding. The

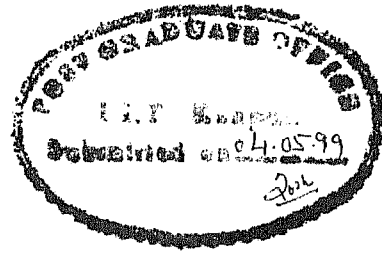
scanning electron microscope studies have been supplemented to correlate the structure properties behaviour.

Part II : Optimization of an additive system for the liquid phase sintering of silicon carbide ceramics

Silicon carbide has been recognized as an important structural ceramic, because of its unique combination of properties, such as excellent oxidation resistance, strength retention to high temperatures, high wear resistance, high thermal conductivity and good thermal-shock resistance. Several additive systems had been studied to obtain dense SiC ceramics. Using AlN-Y₂O₃ additive system, SiC ceramics sintered to the theoretical density were produced by pressureless sintering at 1950±30°C of β -SiC with α -SiC /coarse β -SiC seeds. Densification was observed for different additive compositions and it was found that a material with only 20mol% AlN in the additive system was hard to sinter. Hot isostatic pressing was also not fruitful to densify this material. For all the other systems annealing treatment was done at 1950°C for different times in order to obtain a platelet grain structure for better fracture toughness. The fastest transformation from β -to- α -SiC was observed in the materials with 60mol%AlN. This transformation was found to be important in respect of grain growth which in turn affects the fracture toughness. Mechanical properties like room temperature fracture toughness, bending strength and high temperature bending strength were measured. Fracture toughness of 6.5 MPa. \sqrt{m} was achieved in 4% α -SiC material after annealing for 32 hrs. The improved fracture toughness was attributed to crack bridging and crack deflection by the platelet grains. Room temperature bending strength of 635 MPa was attained in a material where α -SiC was substituted by coarse β -SiC. Bimodal microstructure was found to be the prerequisite for attaining such a high bending strength value. High temperature tests were done at 1000, 1200, 1400 and 1500°C and it was found that a material with 10vol% additive containing 60mol% AlN has an increased bending strength of 550 MPa at 1400°C. For other materials this phenomenon was observed at a 1200°C. This is explained in terms of oxidation of oxynitride phases close to the sample surface which induces a compressive stress due to the volume expansion associated with this transformation. SEM microstructural analysis and X-ray diffraction were performed in order to establish structure-properties relationship.

Part I

Sintered Alumina Slurry Coated with Tungsten Alloys



Certificate

It is certified that the work contained in the thesis entitled **Sintered alumina slurry coated with tungsten alloys** by **Koushik Biswas**, has been carried out under my supervision and it has not been submitted elsewhere for a degree.

A handwritten signature in black ink, appearing to read "G. S. Upadhyaya", with a long horizontal line extending to the right.

(Dr. G. S. Upadhyaya)
Department of Materials
Metallurgical Engineering
Indian Institute of Technology
Kanpur, India

List of Figures

1.1	Schematic illustration of the firing of thick film circuitry on the surface of a debased alumina substrate	5
1.2	Optimized $\text{CaO-Al}_2\text{O}_3\text{-SiO}_2$ phase diagram	12
3.1	SEM fractographs of different alumina substrates	33
3.2	SEM fractographs at interface region of layered composites sintered in H_2 .	36
3.3	Effect of temperature on contact angle of silver and copper melts over tungsten	38
3.4	SEM fractographs at interface region of layered composites sintered in Ar .	39
3.5	SEM micrographs at the surface of 1% waxed W-overlay with as received or pretreated binder	44

List of Tables

2.1	Characteristics of Al_2O_3 /metal powders	25
3.1	Effect of flux content on the properties of sintered alumina	32
3.2	Effect of substrate alumina composition and amount of lubricant in W-10Cu overlay on the sintered properties of layered composites	35
3.3	Effect of co-sintering temperature on the properties of layered Al_2O_3 /W-10Cu composites	37
3.4	Effect of sintering atmosphere on the properties of layered Al_2O_3 /W composites	37
3.5	Effect of copper content in tungsten on the properties of sintered Al_2O_3 /W layered composites	38
3.6	Effect of silver addition in tungsten-copper overlay on the properties of sintered Al_2O_3 /W layered composites	41
3.7	Effect of pretreated silver/copper powders on the properties of sintered Al_2O_3 /W layered composites	42

Nomenclature

a	...	Weight of the sintered compact in air	g
b	...	Weight of the xylene impregnated compact in air	g
c	...	Weight of the xylene impregnated compact in water	g
L	...	Length between two rolls	m
M	...	Width of the specimen	m
P	...	Fracture load	MN
T	...	Thickness of the specimen	m
ΔD	...	Densification parameter	

Chapter 1

Introduction

The need for advanced materials has been there since the early days of civilization. The demand for new and advanced materials has currently increased due to the rapid advancements in technology. Composite materials have been in the forefront of the drive for new materials having enhanced performances. Monolithic materials such as ceramics, metals and alloys have been incapable of meeting the property demands required by the modern materials. Ceramics generally have excellent strength, hardness, modulus and oxidation resistance, but are extremely brittle and have very poor toughness. On the other hand, metals and alloys normally have good ductility and toughness, but exhibit lower strength, hardness, modulus and oxidation resistance as compared to ceramics. Lamination of monolithic materials have led to effort in tailoring new material properties.

In the last two decades, most of the developments have been in the areas of particulate, whisker and continuous fiber architectures. Lesser attention has been devoted to laminated composites of metals and ceramics. Though laminated composites of metals and ceramics have great potential, practical problems associated with bulk processing have limited their widespread use. Several processing techniques such as physical and chemical vapour deposition and low pressure plasma deposition are presently being used to produce the laminated metal and/or ceramics[1]. Powder metallurgy techniques have the flexibility to economically produce bulk-laminated composite in a large scale and several P/M techniques have been used to form bulk-laminated composites[2]. Plain laminated composites consisting of alternating layers of two different materials could also have tremendous processing related problems such as stress at the interfaces produced due to dissimilarities cause delamination of materials. To overcome this, the concept of a new

composite architecture known as micro-infiltrated micro-laminated composite(MIMLC) was developed and several kinds of MIMLCs were fabricated[3, 4].

In the present era, most of the advancement occurs in the field of electronics and this gives rise to a widespread requirement for ceramic materials. One of the main uses includes insulating ceramic substrates to carry circuits and components and device packaging, which commonly involve different forms of alumina[5]. Alumina ceramics have much more structural flexibility and hermeticity than plastics, glass and other materials applicable to semiconductor device package. Ceramics are, therefore, frequently adopted for such packages when high quality and reliability are required. One of the most common ceramic-metal system is laminated alumina-tungsten system which finds its application in electronic packaging. In the present review the laminated composites of alumina-tungsten system have been emphasized.

1.1 Sintering aspects in laminar composites

Laminar composites essentially comprise of layered structure of two or more components. The compatibility of composite components is characterized by chemical and mechanical interactions between two or more material components within the composite. The creation and durability of compounds which was created as a result of reaction between several components[6] is connected with diffusive effects occurring under the increased temperatures. The kinetics of diffusion depends on the thermodynamic potential of forming the compounds of a given component. This thermodynamic potential depends on the conditions of specified composition of protective atmosphere which is used during sintering. The creation and durability of compounds formed in the intermediate layer is connected with diffusive effects occurring under high temperature. In addition, it was observed that a "saddle"(a spinel layer) occurs between the metallic layer and ceramics[6].

The bonding mechanism of metal to ceramic seal has been studied by several authors[7-13]. Pincus[7] reported the formation of interfacial spinel layer between alumina ceramic and Mo/Mn metallization. Cole and Hynes[8] observed the variation of seal strength as firing temperature and flux content changes. They concluded that presence of glassy phase is of prime importance and proper control of temperature and flux content give a maximum seal strength of metal-ceramic seal. The bonding mechanism is attributed to reduction of oxides present in the composite followed by metallurgical

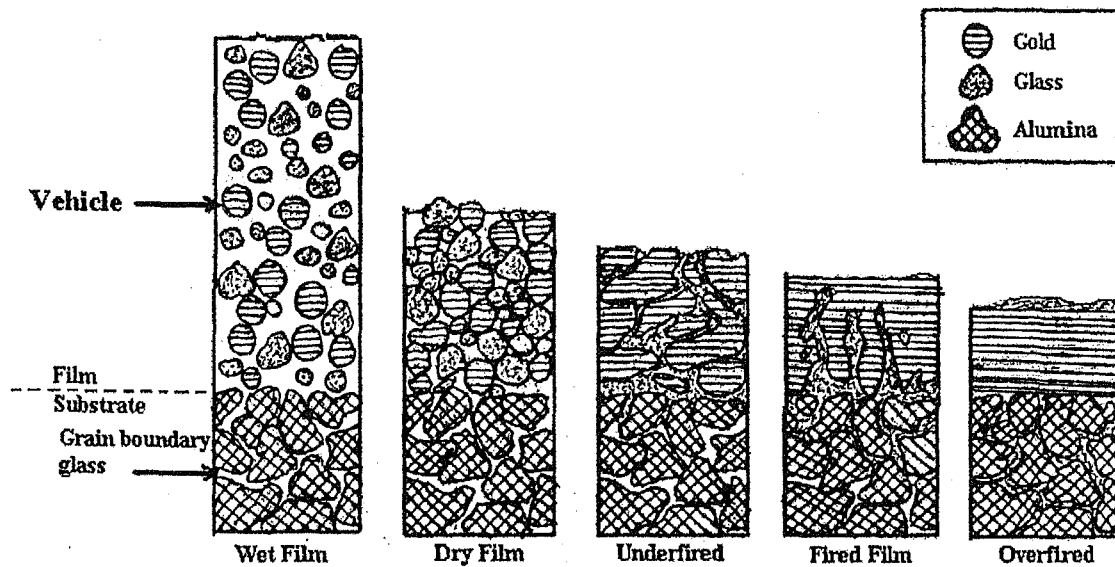


Figure 1.1: Schematic illustration of the firing of thick film circuitry on the surface of a debased(glass containing) alumina substrate. During firing the glass forms a mechanical interlock between the substrate and the metallic layer. If the system is overfired the glass is rejected entirely from the metal, resulting in a weak bond.

interaction. Pincus[7] suggested the formation of minor amount of oxide in molybdenum-ceramic system. The penetration of glassy phase into metallizing layer and simultaneous migration of different oxide phases in the ceramic layer gives rise to a higher metal to ceramic seal strength. Procedure such as thick-film circuitry[14] relies on the interactions during firing between the powder particles and pre-existing glass. Figure 1.1 shows a schematic of microstructural development in a thick film circuit. The thick film paste containing conductor metals painted on the desired region of the substrate. During firing, the metal particles fuse together to provide conduction path while glass particles fuse and begin to dissolve the more refractory glass in ceramic substrate and strong bond with graded properties are obtained. Floyed[11] studied the bonding mechanism, composition and crystal size of alumina-ceramic on Mo/Mn metallization and established the Metal-Alumina Reaction Theory and Glass Penetration Theory. Formation of reaction layer[10] is one of the possible mechanisms of forming bond between metal and ceramic. Denton and Rawson[12] investigated reactions at the interface between layers of Mo/Mn and Mo and Al_2O_3 ; reaction between MnO and Al_2O_3 ; MnO and SiO_2 ; MoO_3 and MgO; and MoO_3 and CaO were found to be most significant. Reed and Huggins[13] studied the ceramic-metal interfaces and observed MnO- Al_2O_3 reaction, migration of Mn and Ti oxides into ceramics and penetration of glassy phase into metallizing layer, diffusion of

glass/metal into the ceramic layer and penetration of brazing metal into the metallizing layer.

Several experiments were carried out to study the effect of various sintering parameters on the seal strength of ceramic-metallization layer. Arthur and fussel [15] studied the effect of time, temperature and sintering atmosphere in sintering of Mo-Mn metallization on alumina ceramics and concluded that these variables have appreciable effect on the strength of the bond. Wetting plays a very significant role in the bonding mechanism as well as in effective sintering. Williams and Nielsen[16] in their study on wetting of refractory metals by fused brazing materials pointed out that Ni directly wets Mo and W. However it poorly wets alumina. Hence other alloying elements(Ti, Co, Al, Mo) were added in order to lower the melting point of Ni and improve wetting[17, 18]. Best wetting is obtained when the liquid melts react with the ceramic[19].

On the basis of above discussion, it can be summarized that in order to obtain good adherence between metal to ceramic layer, appropriate flux should be incorporated which intensifies the sintering process by solution and recrystallization of ceramic phase. To obtain good adherence and low temperature sintering reactive additives in the metallizing layer have to be added.

1.2 Sintering of alumina

In most cases alumina is associated with other oxides such as Fe_2O_3 , TiO_2 , SiO_2 and Cr_2O_3 . Alumina is chemically inert and stable to its melting point of 2050°C . Commercial grade Al_2O_3 powder, assaying 99.8% or more Al_2O_3 is formed using various methods of molding and firing in an oxidizing atmosphere, upto $1920\text{-}1925^\circ\text{C}$ [20]. The body of sintered alumina is very strong, impervious to gases and liquids. The specific gravity of well sintered pure alumina is 3.90-3.92 and 3.86-3.88 depending on the sizes of crystallites. The actual density is essentially the theoretical value for corundum, usually a little below because of presence of some residual porosity.

Sintered alumina, fired at some lower temperature such as at $1760\text{-}1780^\circ\text{C}$ has a lesser specific gravity(3.78). The volume fraction of pores was estimated to be 4.5%[21].

The strength properties, in general, not only depend on their chemical nature but also influenced by several factors like grain size of the oxide ceramic body, strain energy

associated with the particles. control of particle size is very important since sintering rate is roughly proportional to the inverse of the particle size. Coble[22] showed the effect of particle size on the sintering of Al_2O_3 . He concluded that large particles even for 100 hrs sintering at 1600°C do not produce extensive sintering and as the particle size is decreased, the rate of sintering is raised. Kingery and Berg[23] observed that little sintering occurs at temperature near the melting point, i.e., approximately at 2020°C , for spherical particles of Al_2O_3 having $50\text{-}150\mu\text{m}$ size. But sintering rate increases as strain energy is introduced in the same particle when compacted at 280MPa .

The other variable that is subject to control is the diffusion coefficient, which can be affected by composition, temperature and heating rate. Addition of impurities and increase of temperature increases the volume diffusion. But at high sintering temperature, secondary grain growth can occur and due to this the pores are isolated from grain boundary. A rapid heating schedule may produce densification with a smaller concomitant grain size. Surface diffusion, which predominates at low temperature can cause grain coarsening, whereas fast heating increases the vacancy diffusivity and densification at a faster rate than diffusion causing grain coarsening. Fast firing with a minimum isothermal hold at the maximum temperature should be beneficial.

In order to control sintering process effectively, it is essential to maintain close control of initial particle size and sintering temperature. Dependence of sintering atmosphere on the sinterability of alumina was stated by Jones[24] who confirmed that sintering in dry hydrogen was faster than in other atmospheres such as helium, air or in vacuum. The reason for this was thought to be the creation of lattice defects formed due to the reduction of Al_2O_3 in hydrogen atmosphere. It had been supported by Bettinelli *et al.*[25]. But in the recent study, they reported that addition of silica based fluxes to Al_2O_3 produces a less densified body.

1.2.1 Sintering phenomena

In the light of above discussion one can see that the basic phenomena during sintering are (i) shrinkage, (ii) grain growth and (iii) pore growth. The driving force for the solid phase sintering is lowering of free energy of surfaces, grain boundaries, etc. To modify the rate of the three phenomena, one should select the experimental and compositional parameters depending on the mechanism.

Shrinkage

During sintering the predominant diffusion path could be the volume diffusion[26]. Reynen [27] and Readey[28] confirm this on the basis of their studies on the influence of non stoichiometry on sintering. An additional mechanism is grain boundary sliding which also leads to shrinkage. Grain boundary sliding is hampered with increase in grain size[29] which in turn stops shrinkage. It can also take place by grain boundary diffusion.

Grain growth

Large grains($>0.5\mu\text{m}$) can cause discontinuous grain growth[30]. Grain growth also depends on the volume diffusion. The characteristics of the above mentioned mechanisms are: relatively higher final porosity(5-10%), larger pores present at the intersections of grain boundaries and grains without presence of pores[30].

Pore growth

If the pores can follow the moving grain boundary they are in a favourable position to disappear(shrinkage) but they are also swept together by which the number of pores decreases and the pore size increases. As the number of vacancies emitted by a pore is independent of pore size, pore coalescence leads to a decreased sintering rate.

In nut shell, there is a competition between grain growth and diffusion process in the final stage of solid stage sintering and hence ultra-pure undoped ceramics can not be taken to 100% theoretical density by solid state sintering methods without additives.

1.2.2 Role of additives on sintering of alumina

The sintering of pure alumina is improved by addition of additives in amount of few percent. The sintering of pure alumina is enhanced by adding ~ 0.1 mol% of MgO, where dense translucent body can be obtained. Peelen[31] gave an excellent review of this problem in his doctorate thesis. The role of MgO was brought to be that of a second phase effect by which discontinuous grain growth was prevented. Johnson and Coble[32] developed theories for MgO additions to Al_2O_3 and these are the following types (1) solute

segregation to grain boundaries, preventing discontinuous grain growth by a solute drag mechanism (impurity segregation theory); (2) second phase pinning of grain boundaries preventing discontinuous grain growth (second phase pinning theory) and (3) enhancement of the sintering rate relative to grain growth rate, though the change in the defect structure introduced by the aliovalent (the element which changes its valency) solute (solid solution theory). Heuer[33] suggested that MgO permits sintering of Al_2O_3 to full density by enhancing surface diffusivities and thus increases pore mobility during the final stage of sintering and permitting an increase in grain size but not exaggerated growth. Bennison and Harmer[34] demonstrated that the MgO suppresses grain boundary migration rate by a factor of 50 times. Rodel and Glaeser[35, 36] further showed that the effect of MgO is dependent on the crystallography of individual grains. The effect of MgO doping in model experiments was to suppress the migration of the $\{11\bar{2}0\}$ planes. Rossi and Burke[37] studied the effect of additives on the microstructure of sintered alumina. They got almost pore free structure (99.9% theoretical density) in case of $\text{Al}_2\text{O}_3 + 0.25\% \text{MgO}$ sintered at 1900°C for 3 hrs. They studied alumina specimen doped with CaO, SrO, BaO, Y_2O_3 , ZrO_2 , etc., and yielded a similar microstructure obtained with the addition of 0.3wt% Y_2O_3 sintered at 1900°C . Microstructures differed somewhat in grain size and ultimate density but were very similar in general appearance. Smothers and Reynolds[38] studied the sintering and grain growth of Al_2O_3 as a function of the type of impurity (oxide) added. In their extensive review they pointed out that the addition of TiO_2 to Al_2O_3 creates larger internal voids in the Al_2O_3 crystals during firing. Vacuum of 0.05mm Hg at 1900°C was insufficient to reduce the inclusions in the alumina. The addition of small amounts of barium, strontium, zinc, calcium, cadmium, tantalum or thorium oxide to alumina to reduce these or voids in the Al_2O_3 crystals. Monazite sand is also mentioned as an additive to reduce these voids. Addition of certain amount of magnesia to alumina makes the recrystallization of Al_2O_3 more reliable. Addition of CaO (as tricalcium penta-aluminate), TiO_2 and SiO_2 cause the alumina to recrystallize at temperature below 1650°C . A study of sintering of Al_2O_3 includes the addition of Cu_2O , B_2O_3 , Fe_2O_3 , FeCl_3 , Mn_2O_3 , TiO_2 , ilmenite and magnesium titanates. The greatest increase in the sintering of Al_2O_3 at lower temperature is obtained by the addition of 2% to 5% TiO_2 . Addition of CoO and MgO to alumina gives a product having high strength and high density whereas addition of V_2O_3 to Al_2O_3 produces a stabilized heat exchange pebble. ZrO_2 , V_2O_3 , MoO_3 , H_3PO_4 and mullite addition reduce or stabilize the grain growth of Al_2O_3 (recrystallization). Metal fluorides, such as MgF_2 , also produces the same effect. Recently the effect of MoO_3 , ZrO_2 , MgO and V_2O_5 additives on the reduction of Al_2O_3 grain growth was published. Cahoon

and Christensen[39] in their work explained the result of addition of single additives. They found the addition of upto 5% cobalt oxide is to slightly decrease the sintering temperature of alumina. Further additions were deleterious to sintering. Small addition of 0.03% CoO reduces the grain size and equiaxed grains were produced. Addition of less than 2% Cr_2O_3 very little influences the sintering rate. Greater amount is deleterious. Larger grain growth occurs when it is added upto 1%. Above 2% grain growth is inhibited. Sintering of alumina was substantially enhanced by addition of iron oxide in an amounts of 1% and more. This is contrary to the findings of Smothers and Reynolds[38], where dense bodies were obtained at a firing temperature of 1700°C . Above 1% addition, crystal habit of grains changes to an equiaxed structure and the grains become smaller. It helps to eliminate small voids from the grain boundaries. Addition of manganese oxide also gives the similar effect. It exhibits the greatest effect in accelerating both sintering and growth rate of larger grains. Optimum densification is obtained by addition of 0.7% or more manganese oxide after sintering at 1600°C . Addition of copper oxide promotes sintering and grain growth when added upto 1.2%. More than 3% strongly inhibits the growth of larger grains. Additions of titania upto about 5% aids sintering. It also eliminates the voids from the periphery of the grains. Dense body was formed at 1600°C with addition of 1% titania. Silica has a deleterious effect on the sintering of alumina as it decreases the strength of the sintered body. Addition of 0.1% strongly inhibits the growth of large grains in alumina. Oxides of calcium, strontium and barium, when added increases the porosity. Addition of silica can control the deleterious effects of these oxides. Lithium, sodium and potassium also have same deleterious effect to the formation of good alumina bodies. Addition of phosphorus oxide to alumina also has adverse effects. It inhibits the growth of large grains at any sintering temperature. Popović, Gašić and Kinčević[40] studied the effect of MgO to $\gamma\text{-Al}_2\text{O}_3$. Addition of 1.5% increases the density and compressive strength of sintered body. $\gamma\text{-Al}_2\text{O}_3$ spinel formation attributes the strengthening and decrease the porosity. Reynen[41] found that the addition of TiO_2 , GeO_2 and SiO_2 decreases sintering rate of pure alumina. Both MgO and TiO_2 increase the sintering rate of pure alumina when added within solubility range. One is forced to accept that volume diffusion of aluminium ion is rate determining (in MgO containing samples with a vacancy mechanism and in TiO_2 containing sample with an interstitial mechanism) and that oxygen ions find an easier diffusion path along the grain boundaries. Addition of small amount (300 ppm) of MgO promotes grain growth and sintering, while larger amounts of MgO decreases grain growth and sintering rate. Along with the additions of additives, sintering atmosphere has also predominant effect to aid the sintering process. Gas trapped in close pores

will limit pore shrinkage unless the gas is soluble in the grain boundary and can diffuse from the pores. Al_2O_3 doped with MgO can be sintered to essentially zero porosity in H_2 and O_2 atmosphere, which are soluble, but not in air, which contains insoluble N_2 [42]. Heating in vacuum had no noticeable effect on sintering[38]. Chlorine atmosphere promotes the densification and its depends on the amount of chlorine present in the sintering atmosphere[38].

1.2.3 Liquid phase sintering of alumina

Pure alumina is denser, harder and stiffer and more refractory than most silicate ceramics so that increasing proportion of second phase in an alumina ceramic tends in general to decrease the density, Young's modulus, strength, hardness and refractoriness[43]. However, fabricating products with high alumina contents is expensive requiring pure starting materials and high firing temperature. Additions of CaO and SiO_2 are made to alumina for several reasons including: lowering the firing temperature, allowing cheaper, less pure starting materials to be used, improving rheology in shape forming and modifying the properties of the product[43].

A broad range of materials are commercially available with a concomitant broad range of properties. Most commercial alumina have additions of CaO and SiO_2 [44]. SiO_2 has low solubility in the alumina and segregates to grain boundaries forming a liquid phase at high temperature. Bettinelli *et al.*[25] show the effect of addition of SiO_2 and CaO to Al_2O_3 . The reaction of alumina with these oxides forms a eutectics whose melting point lies below 1400°C . Ternary diagram of Al_2O_3 -CaO- SiO_2 shows(*Figure 1.2*) the presence of eutectic point at 1392°C with CaO/ SiO_2 ratio of 1. The effect of MgO doping in liquid phase sintering is analogous to that observed for solid state sintering. The presence of MgO in liquid phase sintered alumina homogenizes the grain size distribution[44]. Platelike abnormal grains were observed in alumina doped with 0.25 mol% of $\text{Na}_2\text{O}+\text{SiO}_2$; $\text{CaO}+\text{SiO}_2$; $\text{SrO}+\text{SiO}_2$ and $\text{BaO}+\text{SiO}_2$. In case of $\text{MgO}+\text{SiO}_2$ the sintered compact exhibit equiaxed abnormal grains. Abnormal grains were also found in sintered Al_2O_3 compacts doped with $\text{MgO}+\text{CaO}+\text{SiO}_2$. They also observed the effect of CaO/ SiO_2 ratio on the sintered alumina and concluded that for the ratio of dopants $\text{CaO}/\text{SiO}_2 = 1$, the density of the plate like grains decreased as the doping amount increases(at sintering temperature of 1650°C for 2 hrs). Platelet grains increases in number as the result of this and microstructure contains only platelet grains when CaO/ SiO_2 dopant

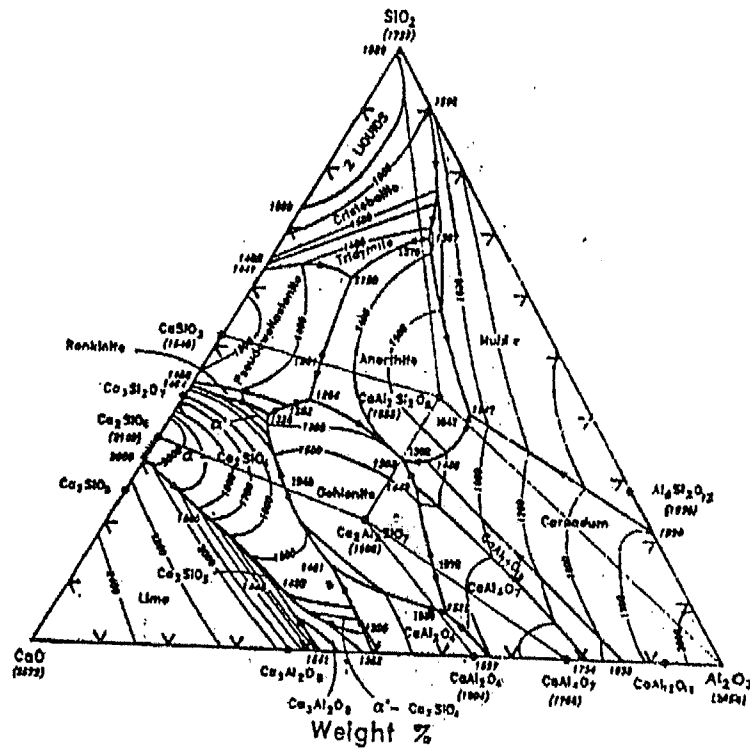


Figure 1.2: Optimized $\text{CaO-Al}_2\text{O}_3\text{-SiO}_2$ phase diagram calculated from the quasichemical model for the liquid with two ternary parameters.

added within the range of 3-10% in powder compact. Powell-Dogan and Heuer[45] have reported the characterization of the microstructure and micro chemistry of a number of commercial high alumina(96% Al_2O_3). They studied several samples all containing 2% to 3% SiO_2 with variable quantities of MgO , CaO and Na_2O . The dominant feature of the microstructure is the continuous glass phase containing the minor oxide constituents which allow densification at temperatures lower than that of the sintering temperature of pure alumina[46]. All the sintered materials contained large, randomly distributed spinel(MgAl_2O_4) grains. They also observed that the continuous glassy phase does not wet low angle grain boundaries which occurs in many high alumina ceramics[47, 48]. Among other intragranular and intergranular crystalline second phase, β -alumina is one which forms during sintering, nucleating within the glass pockets encapsulated within α -alumina by break way during grain growth and hence act as sintering aids. Other phases are calcium hexaluminate and small grains of spinel. Calcium hexaluminate helps to form intergrowth structure. Spinel is observed throughout the α -alumina matrix.

There are several grades of alumina ceramics. Very small amount of glassy phase is present with 99-99.7% alumina in alumina ceramics. As the glassy phase is less it

can be used in high temperature application. The coarse grained materials are preferred for electrical insulation. Alumina with 94.5-99% Al_2O_3 have significant amount of glassy phase. The grain boundary glassy phase is usually aluminosilicate containing additional oxides such as CaO , MgO . Microstructure of these alumina show a uniform distribution of alumina crystals separated by a glassy phase. High temperature sintering produces recrystallized alumina interconnected network. Although these alumina cannot be used in high temperature applications, it can be tailored for use in many electrical applications[44]. The presence of second phase depends on composition, firing temperature and cooling rate. Alumina with 80-94.5% Al_2O_3 are used as electrical insulators and they are fired generally at less than 1500°C .

Pejovnik *et al.*[49] studied the liquid phase sintering of alumina at different temperatures. From the shrinkage and porosity curve they suggested two sintering mechanisms, one below 1500°C and another above it. Microstructural analysis supported this fact. The Al_2O_3 sphere retain their shape upto 1400°C and disintegrate into individual grains above 1500°C . Two processes may control the observed changes (1) flow of glass into the contact area between particles and at higher temperatures into grain boundary or (2) sliding of particles or grains which are separated by glass layer. Main rate controlling process is *glass flow and penetration*.

It has been seen that multi phase ceramics should show poor sintering behaviour if grain boundary diffusion is the predominant mechanism while good sintering occurs if volume diffusion is the main transport mechanism[50]. Reynen and Firatli[50] studied this on the ternary system $\text{MgO-Al}_2\text{O}_3\text{-ZrO}_2$ and concluded that multiphase ceramics shows a good sintering behaviour because discontinuous grain growth is inhibited. Full density with small grains could not occur due to parasitic pore growth. Kiss *et al.*[51] investigated reaction sintering of $\text{Al}_2\text{O}_3\text{-MgO}$ mixture in $\text{MgO-Al}_2\text{O}_3\text{-SiO}_2$ system. They observed existence of non equilibrium phase at 1365°C along with other phases. Solid skeleton was formed which retarded the particle rearrangement in the presence of liquid phase.

In conclusion, it can be said that for effective densification to take place rapidly, it is essential to have (i) an appropriate amount of liquid phase in order to wet the ceramics completely (ii) an appreciable solubility of the solid in the liquid phase and (iii) complete wetting of the solid by liquid.

1.3 Sintering of tungsten

Solid state sintering of tungsten powder compacts is carried out at high temperature, generally at temperature in excess of 2600°C in order to increase the density of the compacted body to a minimum level of 85% of the theoretical density. In practice tungsten is generally sintered under a reducing gaseous atmosphere, such as hydrogen, because this will eliminate oxygen content of the powder to a large extent. Otherwise the oxide film coated at the surface of tungsten powder particles impedes the sintering and bonding processes and desired density of the product will never be achieved[52]. At elevated temperature, a green compact is basically an unstable material in which the large surface area provides a driving force for densification during sintering. At that temperature strongly bonded bridges and necks are established at powder particle contacts through diffusional process. The mechanisms of mass transport for the sintering of pure tungsten powder involve self diffusion at external surfaces, along the grain boundaries at the neck region and through the lattice from grain boundaries to neck[53, 54]. Other mechanisms have negligible effect on neck growth and shrinkage[54]. The sintering methods, according to the furnace construction, are classified into direct sintering and indirect sintering[52, 55].

Direct sintering

Small dimension objects(compacted) are generally sintered by this method. Prior to sintering, green body is presintered at $1000\text{-}1200^{\circ}\text{C}$ for 30 mins or so to obtain appreciable strength to withstand handling and clipping during sintering. During presintering, the oxide film surrounding the particles is reduced to metal and a better cohesive strength between particles results[52]. The final sintering is carried out in water cooled bell jars in hydrogen atmosphere at the temperatures of 3000°C or near to that. The current may be raised gradually so that gradual temperature rise is there, otherwise density of sintered product decreases[56]. The duration at the maximum temperature ranges from 30 to 60 mins. Density after final sintering reaches $17.6\text{-}18.2\text{ g/cm}^3$.

Indirect sintering

This process is viable for large objects sintering. For this purpose, an indirect resistance and induction furnace is used. In indirect resistance furnace, surface of the objects

densify more than interior when heated upto 800°C and hence permeability of surfaces goes down and thus preventing the escape of gases. So slow rate of heating is the prime requirement[52]. Control of temperature at higher temperature region is also important in order to avoid deleterious effect of thermal stresses. The final temperature for indirect sintering[1600-2200°C], depending on the particle size and compacting pressure, is generally lower than that of direct sintering. The sintered density obtained is minimum of 85% of theoretical density. Depending on the sintering temperature the grain size changes[52].

The main difference between induction furnace sintering and indirect resistance furnace sintering is that the former uses a helium gas atmosphere and maintains a positive pressure gradient whereas latter process uses a hydrogen atmosphere having a lesser pressure than atmospheric. In induction furnace process, the final sintering temperature ranges from 2100°C to 2700°C depending upon the particle size and pressure used for compacting. Gradual heating rate is maintained and holding time is within the range of 6 to 10 hrs[52].

Assessing the overall discussion, it can be said that the quality of sintered products depends upon the properties of raw material(tungsten powder). Characterization of a powder includes purity, particle size, shape, porosity, microstructure, lattice defects, specific surface, particle size distribution, apparent density of bulk powder, tap density, flowability and compressibility. Irregular and finer particles produce less dense green compacts. Apparent density increases proportionally with particle size and finer powder produces larger grains[56].

To promote and assist the sintering process, two techniques have been developed which involve the use of metallic sintering additives. These are known as liquid phase sintering and activated sintering. In liquid phase sintering the refractory metal powders are sintered in presence of one or more metals – such as copper or iron – at temperature above the melting point of the additive, so that sintering occurs in a molten binder phase which may be present in substantial amount, for example upto 40% by weight or so. In contrast to liquid phase sintering, activated sintering is performed in the presence of small amount of metal additives, again often transition metals, but in the solid state at temperature below the melting point of the additive.

1.3.1 Activated sintering of tungsten

Since Vacek[57] reported the enhancement of sintering by additions of small quantities of transition metals to tungsten in 1959, making it possible to lower the sintering temperature substantially, a great deal of work has been carried out in the activated sintering of tungsten particularly with additives of Group VIII transition metals[57-65]. Much work has involved the use of platinum group metals which has been reported to be very effective as sintering activator[66]. Brophy and coworkers[58, 62] found that of the added elements explored to date, palladium appears to have the greatest effect. The effectiveness of the activators in promoting enhanced sinter of tungsten were found to be in the order:

$$\text{Pd} > \text{Ni} > \text{Rh} > \text{Pt} > \text{Ru}$$

They also found that with 0.25 w/o palladium densities of 93.5% and 99.5% of theoretical density were obtained after sintering of 30 mins and 16 hrs respectively at 1100°C in hydrogen atmosphere. In comparison, nickel activated sintered bodies have densities of 92% and 98% of theoretical density under the same sintering conditions. Toth and Lockington[60] in their review noted that presence of powdered nickel(0.5 to 2%) decreases the sintering temperature of tungsten from about 3000°C to 800°C or so. They also studied the rate of sintering of tungsten and tungsten with 2% thoria compacts with Pd and Ni activators in the sintering temperature range of 850°C to 1100°C and found the optimum amounts to be 0.317wt% Pd and 0.13wt% Ni for W-powder of 3.3μm average particle size. Kaysser *et al.*[67] also observed the influence of Ni-dopant on sintering of W during different stages of sintering and concluded that addition of transition metals of group VIII to refractory metals increases grain boundary self diffusion of the refractory metal by several orders of magnitude and thus leading to "activated sintering". The addition of small quantities of 0.25 wt% Ni to W enhances the surface diffusion. The presence of Ni at W grain boundaries increases the grain boundary mobility considerably. The typical values obtained was $2.4 \times 10^{-15} \text{ m}^4/\text{Js}$ for tungsten and $1 \times 10^{-3} \text{ m}^4/\text{Js}$ for nickel doped tungsten. Although transition elements increase the sintering kinetics of tungsten an opposite effect was observed when iridium was added to tungsten[68]. The probable reason for it is that iridium decelerates the interfacial diffusion of W-atoms and slower densification occurs as volume self diffusion of W possibly predominates. Addition of copper to W for enhanced sintering was observed by several authors[69, 70, 73, 74]. From

the view point of electronic properties, role of this element is very significant. Bregel *et al.*[69] reported that tungsten and copper are mutually insoluble in solid state. Powder metallurgy can produce complete range of composition but still some amount of porosity remain when W-Cu mixture is sintered below the melting point of Cu[70]. German and Munir[59] also observed that the addition of copper to the tungsten had no appreciable effect on the sintering kinetics. They also reported that the basic mechanism of densification is grain boundary diffusion process and postulated that sintering enhancement by the transition metals follows sintering models based on the electron concentration approach to the diffusion process. Apart from enhancement of sintering kinetics, variation of electrical resistivity of tungsten compacts with respect to compaction and sintering time had been reported by Moon *et al.*[71]. They found that addition of 0.2 wt% Ni increases the electrical conductivity of presintered W by several factors and is strongly depended on sintering parameters. They also observed that although Ni addition enhances the electrical conductivity of presintered W compacts, this alloying process in W-Ni system increases the electrical resistance during sintering. Moon[72] reported that shrinkage and density of compacts is larger when sintered in an atmosphere of H_2 + moisture due to chemical activation and there is a decrease in electrical resistivity of the specimen.

It is known that trace elements of group VIII especially Ni, can significantly accelerate the sintering of tungsten. At the same time Ni-addition appears to produce better wetting of W by Cu[70]. Haufe *et al.*[73] investigated the sintering kinetics and reported that 0.1 to 0.5 wt% Ni addition should be used as a sintering aid however the electrical conductivity of the composite decreases at the upper limit of Ni concentration. Decrease of electrical conductivity occurs after certain critical concentration of Ni. They also studied the effect of particle size of tungsten on thermal conductivity and found that large W particles cause poorer thermal conductivity. Moon and Lee[74] studied the beneficial effect of Cobalt as an activating agent. This is due to the fact that Co reacts with W forms W_6Co_7 phase at W-Cu interface. German and Rabin[75] reported on 98wt% W alloy containing various mixtures of iron, cobalt and nickel and found a direct relation between second phase melting temperature and densification. Densification and shrinkage improved in the order iron – cobalt – nickel at sintering temperature of 1200°C.

Sinterability of doped tungsten powder was studied by several authors[71,76-78]. It was observed that as presintering increases, sinterability decreases. Shrinkage, observed during the initial stage of sintering, was found to be inversely proportional to the particle size. Kims and Moon[78] discussed the sinterability of Ni doped W-compact and found

that sinterability increases as the particle size reduces as diffusion of Ni increases. The fine nickel powder at sintering temperature(1100-1400°C) might be in liquid phase below the melting point of nickel. This was also observed by Moon and Kim[77]. Mechanism for increased densification rate proposed by Hyden and Brophy[58] who suggested that activating elements on tungsten particle surface forms a "carrier phase" layer and mass transport occurs through this layer. In this process solid state sintering mechanism is selectively accelerated.

1.3.2 Liquid phase sintering of tungsten

Liquid phase sintering is an important technology for the production of contact materials, heavy alloys and several other alloys for different applications. For production of tailor-made alloys of W for electronic industries, it is the prime root among other processes. Liquid phase sintering of pure tungsten required very high temperature(melting point $\sim 3410^\circ\text{C}$). So to enhance the sintering kinetics and also to lower the liquidus temperature, some additive elements were added to the tungsten. This additive phase forms a binder phase which is an alloy of additive phase and base metal. Ekbohm and Eliasson[79] studied the liquid phase sintering of several alloying elements + W and found that W-Ni(9vol%) had the higher particle growth rate. Cobalt along with it gives a much higher particle growth rate in all microgravity experiments. Huppmann *et al.*[80] studied the liquid phase sintering of W-Ni system. They found the probable mechanism of liquid phase sintering of W-Ni system at the sintering temperature of 1500°C . Basic mechanisms observed during the liquid phase sintering are particle disintegration, coalescence of particles and solution reprecipitation process. Kwon and Yoon[81] found that the liquid phase sintering of W-Ni can be divided into three stages: agglomeration of liquid phase and high density region formation, outward liquid flow and expansion of this dense region and filling of isolated pores by liquid. They varied the nickel content within 2 to 8wt% at liquid phase sintering temperature of 1550°C and found that mass transport through liquid phase is important in liquid phase sintering. Reigger *et al.*[82] also observed the densification and grain growth behaviour of 8wt% Ni added to W at 1550°C . The sintering behaviour of tungsten copper is reported by Hens *et al.*[83]. They observed that initial size and powder preparation technique effect the final properties of sintered W-Cu. At the sintering temperature of 1250°C , they obtained 99% of theoretical density with 15wt% Cu addition. Improved sinterability was reported by Moon and Lee[84]. Huppmann and Reiger[85] studied the processes of rearrangement in tungsten-copper system at the sin-

tering temperature of 1100°C. Johnson and German[86] in their study on W-Cu system discussed the effect of various elements such as Pd, Ni, Fe, Co, etc. on their sintering properties. Nickel is commonly added to increase sintering behaviour however it decreases the electrical conductivity of the system[87, 88]. They also studied the effect of transition elements such as Co, Ni, Fe, Pd on the activated liquid phase sintering of tungsten copper. Nickel enhances the solution reprecipitation process. Nickel however degrades the electrical and thermal properties. So Fe and Co were added and it was found that sintering behaviour was greatly enhanced by addition of these elements. Co addition gave the highest densification among all other elements. This was also observed by Moon and Lee[84]. The amount of additives added were in the range of 0.35 to 0.5% and sintering temperature was varied between 1250-1400°C. The probable mechanism is that Co and Fe forms intermetallics and segregate to W grain boundaries and provide a high diffusivity solid phase. This is not observed in the case of Ni and Pd and so they are much less effective as activators[86, 89]. Lavrinenko and Naidich[90] studied several systems, like W-Cu, W-Ag in which solubility of components is absent and observed the influence of wettability of W by Cu or Ag on the growth rate and shrinkage. They observed that shrinkage sharply increases with the rise in temperature. Prill and coworkers[91] studied the system of 99%W and 1%Cu-Ni(by weight) and reported the shrinkage mechanisms, one solution controlled and other diffusion controlled. Bettinelli *et al.*[25] after their extensive study found that addition of Ti, Co, Al reduced the melting point of nickel. For thicker metallization layer they performed the tests with the addition of Cu-Cr and Cr-Ti alloys, both of which improved tungsten densification.

Other properties of tungsten metallization are also effected by additions of alloying elements and this was observed by several authors[83, 92]. Hens *et al.*[83] studied W-Cu system and showed that coefficient of thermal expansion varies linearly at low copper content (~3wt%) and attain coefficient of thermal expansion of Al₂O₃ ceramics at 10wt% copper. Silver addition improved the thermal and electrical characteristics but a high coefficient of expansion is obtained and hence the Ag content is usually limited to 15wt%[92]. The use of copper in place of silver results in slightly lower coefficient of thermal expansion and lower electrical conductivity and it is more prone to corrosion than silver additive[92].

1.4 Alumina-tungsten cosintering

Traditional ceramic packages were usually made by cofired multilayer ceramic techniques[93]. In this technology, green sheets of ceramic hold together by a organic binder are metallised with refractory metals by sreen printing method. These metallized sheets are then stacked laminated and cofired resulting a tough, hermetic, monolithic ceramic structure with burred conductors and vias(a metallic path has been provided for interconnection of two metallized layers deposited on the two sides of the ceramic layer)[93, 94]. The cofired approach had its own advantages and disadvantages. One advantage to the overall process is that the adhesion of the cofired metal to the ceramic is very good[93].

In microelectronic applications new materials with unique combinations of mechanical, thermal and electrical properties has been developed. An ideal ceramic packaging material is an inexpensive, low dielectric constant, low dielectric loss, high thermal conductivity ceramic that has a thermal expansion match to the semiconductor chip and could be cofired with high electrical conductivity metallization[95].

The use of alumina as a multilayer ceramic substrate is not an old one[96]. As already described, pure alumina has a high melting point so, cofired substrates or packages incorporate a glass phase to promote sintering of alumina. The other reason of addition of glassy phase to alumina is to achieve thermal expansion matching between the internal metal and the ceramic[97]. This matching is very important so that the packaging substrate and metallized layer "fuse" together at the same temperature(cofired) to form the desired multilayer construction[98].

Al_2O_3 and the metallized layer are fired or sintered at high temperature. In high temperature systems, the metallization is by a refractory metal or combination of refractory metals which was usually tungsten[98]. Tungsten was used because metals other than those which are refractory would either melt or/and oxidize so completely that they would not retain the desired shape and dimensions[98]. The metallization over the alumina surface provides a hermetic seal.

Several authors[25,97,99-101] studied various aspects of alumina-tungsten system. Foster *et al.*[97] compared the 99.6% Al_2O_3 cofired system with 90-94% Al_2O_3 (conventional high temperature cofired system) system. They found that 99.6% Al_2O_3 -W system would be better in respect of thermal, electrical and mechanical properties. Chance[100] studied

the metallization of green alumina and concluded that pure tungsten adhere strongly to pure fine grained alumina. Metal particle diameter is the main controlling factors in cosintered metal/ceramic system as it controls the shrinkage, residual stress which ultimately contributes to high adhesion. The author selected sintering temperature in the range 1550-1600°C and found that excessive reorientation and grain growth of the tungsten layer causes loss of mechanical bonds. Use of low temperature sintering is thus beneficial. Bettinelli *et al.*[25] studied alumina ceramics metallized and cofired with tungsten system at significantly lower cofiring temperature(1400°C). They used CaO-SiO₂ prefired flux and additives to alumina to obtain higher sintering density, enhance sintering kinetics and grain growth. Enhancement of tungsten sintering kinetics at that temperature was obtained by addition of Ni-based additives. The results obtained is dense ceramic(95% of theoretical density) having good adhesion to metal and ceramic substrate and increased metal conductivity due to better densification.

Tummala[99] studied the basic phenomena of sintering of ceramic-metal system. He reported that sintering of the substrate stage begins with the densification of glass which leads to glass alumina reactions causing crystallization. The crystals however melts at ~1450°C resulting in a fluid glass, the viscosity of which keeps on dropping until the maximum temperature is reached. The screening paste is tailor made for various use and consists of refractory metal powder(generally W or Mo) which is uniformly dispersed in a resin and solvent mixture. This metal paste, during sintering goes through organic removal by volatilization of organic materials at high temperature and densification progresses. The glass phase enters into porous W or Mo metal vias thus providing the mechanical anchoring in addition to chemical reaction. The bonding depends on the oxygen partial pressure of the furnace atmosphere.

1.5 Scope of the present investigation

Tungsten layered alumina composites have been in the forefront of electronic packaging materials because of their enhanced performances. Alumina ceramic substrate were extensively used to carry circuits and components and device packaging because of structural flexibility and hermeticity than plastics, glass and other materials applicable to semiconductor device package[5]. Addition of CaO and SiO₂ are made to alumina for lowering of firing temperature, allowing cheaper, less pure starting materials to be used, improving rheology in shape forming and modifying the properties of product[43]. The other reason

of addition of glassy phase to alumina is to achieve thermal expansion matching with the metal[97]. The importance of this matching between packaging substrate and metallized layer lies in the fact that these two layers 'fuse' together to form the desired multilayer construction[98].

In general, the metallizing layer is found to be of a refractory metal or combination of refractory metals which is usually tungsten[98]. Extensive studies have been carried out on the alumina-tungsten system by several authors[25,97-101]. Foster *et al.*[97] reported conventional high temperature($\sim 1600^{\circ}\text{C}$) cofired Al_2O_3 -W system would be the better in respect of thermal, electrical and mechanical properties. But Chance[100] observed excessive reorientation and grain growth of the tungsten layer at high temperature($\sim 1600^{\circ}\text{C}$) causing loss of mechanical bonds. Use of low temperature sintering is thus beneficial. Enhancement of tungsten sintering at low temperature was obtained by addition of Ni-based additives and other additives[25].

In the present investigation, CaO and SiO_2 is taken to densify alumina substrate at comparatively lower temperature(1400°C). Tungsten metallization along with Cu/Ag binder is selected in order to investigate the bonding mechanism. The selection of Cu/Ag metal binder to tungsten is to obtain an improved conductive overlay and better bonding with alumina substrate. A newly developed slurry coating technique is being investigated in this work with varying sintering atmosphere and temperature for sintering of tungsten metallization layer over sintered alumina substrate.

Chapter 2

Chapter 2

Experimental procedure

2.1 Preparation of substrate

Before assessing the optimization of preparation method and end properties of the composites, it was necessary to study the densification of alumina with fluxes like CaO and SiO₂. The characteristics of alumina powder is given in *Table 2.1*.

Table 2.1: Characteristics of Al₂O₃/metal powders

Charac- teristics	Al ₂ O ₃	W	Cu	Ag
Source	Indal, Calcutta (India)	Wolfram Bergbau and Huttengesell- schaft, Austria	Amrut Industrial product, Mumbai (India)	Bonds, New Delhi (India)
Average par- ticle size(μm)	4.05	3.05	31	27.5
Apparent density(g/cm ³)	0.75	4.53	1.41	0.88
Flow rate	Non-free flowing	Non-free flowing	Non-free flowing	Non-free flowing

Al_2O_3 was densified by following two routes. In one case, 1, 2 and 3 wt% of CaO and SiO_2 were added and premixes were prepared by conventional ball milling. Wet milling of the powders in acetone was performed for 15 minutes in a Fritsch 'Pulverisette-5' centrifugal type ball mill using 1.8×10^{-2} m diameter WC balls. The ratio of feed to ball by mass was kept at 1:6. In the latter case, CaO and SiO_2 mixture in equal mol% was first prefired at 1200°C for 4 hrs to form Wollastonite (CaSiO_3) and then milled with alumina. One or two drops of 0.5 mass% PVA solution was added to the green substrate to facilitate handling. In both cases the sintering was carried out at 1400°C for 1hr after green compaction of premixes at 400 MPa. Sintering was done in a molybdenum resistance heated muffle furnace with a heating rate of $9^\circ\text{C}/\text{min}$ and then furnace cooled.

2.2 Preparation of W-Cu-Ag premix slurries and the composites

The characteristics of tungsten, copper and silver powders are given in *Table 1*. Tungsten powder was initially mixed with 10 wt% copper powder. Different premix slurries were obtained by wet milling of W-Cu in acetone medium with 0, 1 and 4 wt% lubricant (micronized wax). In second stage of experiment, keeping 1 wt% lubricant constant, various amounts of copper binder (5, 10 and 20 wt%) were added to tungsten. In addition, compositional variation of premix slurries was done by diluting the copper by silver in W-10Cu premix. In a separate set of experiments, pretreated silver (heated at 300°C for 1/2 hr in air) and copper (reduced at 600°C for 1/2 hr in hydrogen) powders were added in tungsten powder in order to observe the effect of pretreated binders on tungsten slurries.

The overlay slurries thus prepared, were manually spread over the already sintered alumina pellets (average thickness 2 mm) and dried in air to evaporate acetone. The average thickness of the coated slurry was 0.4 mm.

Dewaxing of the layered composites was carried out in a silicon carbide resistance heated tubular furnace at 450°C for 45 mins under dry hydrogen (dew point -35°C) and argon atmospheres respectively. The hydrogen used as atmosphere was dried and cleaned by passing through a purification train before introducing it into the furnace. The hydrogen purification train consisted of a hydrogen purifier, DEOXO, model 0.15/3.5 of Engelhard Industries, Gloucestershire (U. K.) and tubes containing calcium chloride for drying and

glass wool/cotton for removing any suspended particles. The dewaxed composites were sintered in the same tubular furnace by varying the temperature to 1200°C and 1300°C with heating rate of 9°C/min and then furnace cooled. The sintering period in all cases was kept constant as 15 mins.

2.3 Sintered density and densification parameter

The sintered densities of substrate and overlay were measured according to the following formula as suggested by Arthur[102] by using displacement method:

$$\text{SinteredDensity}(g/cm^3) = \frac{a}{b - c} \quad (2.1)$$

where, a = weight of the sintered compact in air(g)

b = weight of the xylene impregnated compact in air(g)

c = weight of the xylene impregnated compact in water(g)

The densification parameter(ΔD) was, also, calculated from the formula:

$$\Delta D = \frac{\text{sintered density} - \text{green density}}{\text{theoretical density} - \text{green density}} \quad (2.2)$$

The theoretical densities of the alloys were calculated from the rule of mixture. The densities of alumina, tungsten, copper and silver powders were taken as 3.96, 19.3, 8.96 and 10.49 g/cm³ respectively.

2.4 Transverse rupture strength(TRS) evaluation

TRS of as sintered specimens was determined under three point loading as per ASTM specifications(B406-76). The specimens were placed in a fixture having two WC rolls

of 3mm diameter and 15mm length which were kept 14.9mm apart. The testing was performed in an Instron 1195 machine with a cross head speed of 0.1mm/min. The maximum rupture load at the failure point of the test piece was used for calculating the TRS according to formula:

$$TRS(MN/m^2) = \frac{3 P L}{2 W T^2} \quad (2.3)$$

where, P = fracture load(MN)

L = length between the two rolls(m)

W = width of the specimen(m)

T = thickness of the specimen(m)

The average value after three testings was reported in each case.

2.5 Scanning Electron Microscopy studies

The fractured samples from TRS test were mounted and observed under scanning electron microscope of model JSM 840A. For alumina pellets, fractographs were taken arbitrarily from different places at 5000 magnification. For layered composites, photomicrographs were taken at interface region at 350 magnification. SEM microstructures of W-overlays were taken at 3500 magnification.

Chapter 3

Chapter 3

Results and discussion

3.1 Effect of flux content in alumina substrate

The results(*Table 3.1*) show that in case of premix flux addition, there is no regular pattern for either densification of alumina or TRS variation with increase in the amount of flux. However in case of prefired flux, both densification and TRS values increase uniformly with increase in the amount of flux.

The SEM fractographs of sintered pellets corresponding to substrates containing different amounts of CaSiO_3 flux are given in *Figure 3.1*. These show more linkages with the grains with increase in the flux content, which contribute in overall strengthening. The reason for this is that at presently selected sintering temperature, viz. 1400°C , formation of liquid phase occurs in Al_2O_3 – CaSiO_3 system(eutectic point 1392°C) which promotes densification. Increase in flux content increases the amount of liquid phase; hence more particle rearrangement and solution reprecipitation occurs resulting higher densification.

3.2 Effect of lubricant in W–10Cu premix overlay

Variation in the amount of micronized wax addition in W-10Cu premix shows that 1% lubricant is the optimum amount from the point of view of adhesion between the overlay and the substrate(*Table 3.2*). With no wax in the overlay, delamination occurs, whereas in case of 4% wax, the overlay cracks. Good bonded layered composites are produced when

Table 3.1: Effect of flux content on the properties of sintered alumina.

Composition (wt%)	Avg.G.D. (g/cm ³)	Green porosity (%)	Avg.S.D. (g/cm ³)	%Th.D.	ΔD	Avg.TRS (MN/m ²)
Al ₂ O ₃	2.26	43	2.46	62	.12	44
98 Al ₂ O ₃ - 1 CaO- 1 SiO ₂	2.14	46	2.56	65	.23	91
96 Al ₂ O ₃ - 2 CaO- 2 SiO ₂	2.12	46	2.67	68	.30	51
94 Al ₂ O ₃ - 3 CaO- 3 SiO ₂	2.04	48	2.50	64	.25	45
98 Al ₂ O ₃ - 2 CaSiO ₃	2.26	43	2.72	69	.30	84
97.75 Al ₂ O ₃ - 2.25 CaSiO ₃	2.24	43	2.80	71	.33	89
96 Al ₂ O ₃ - 4 CaSiO ₃	2.24	43	2.86	73	.38	119
94 Al ₂ O ₃ - 6 CaSiO ₃	2.19	44	2.90	74	.40	135

Sintering parameters: temperature 1500°C(Al₂O₃) and 1400°C(Al₂O₃-Flux system), time 1hr, atmosphere Air

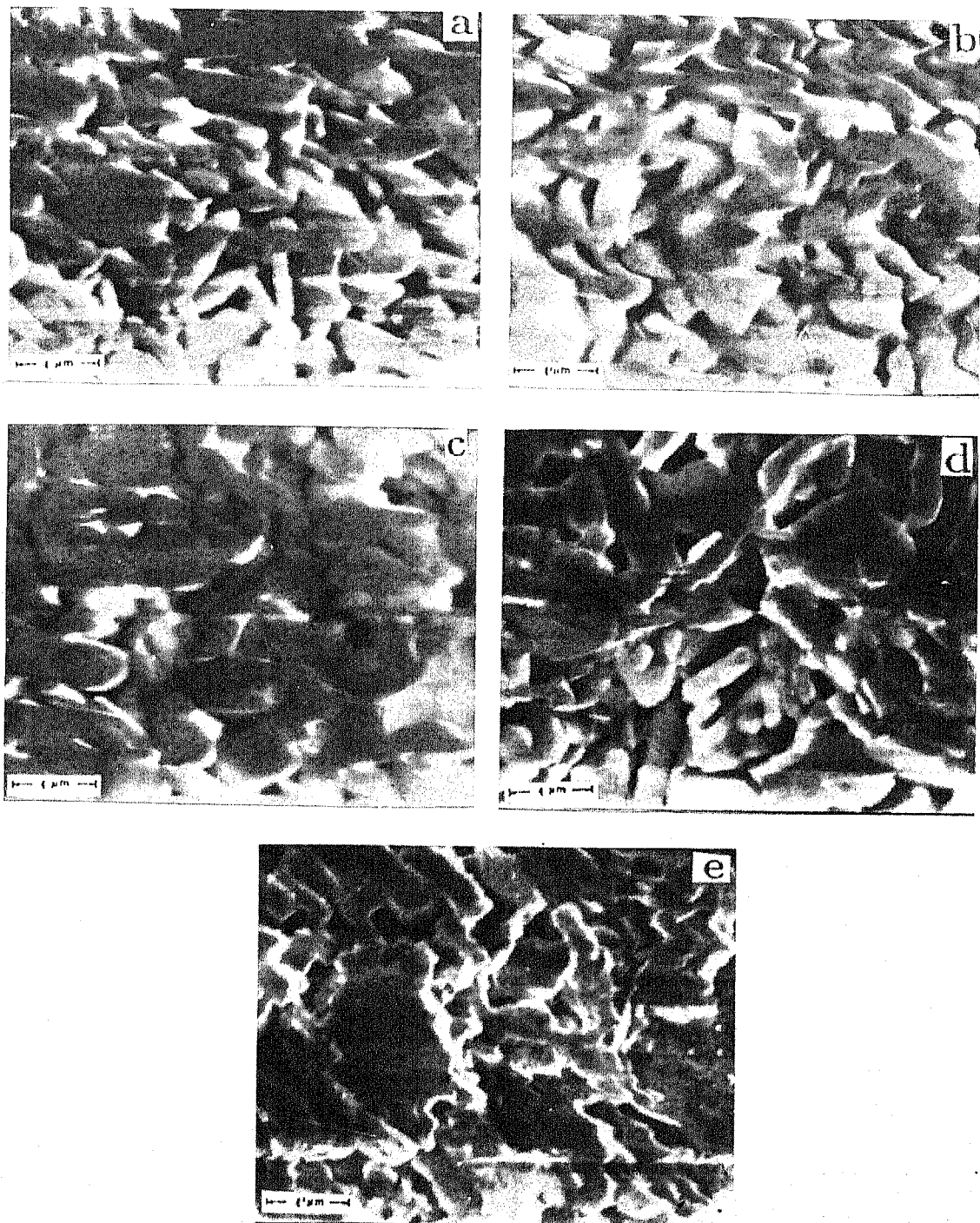


Figure 3.1: SEM fractographs of alumina substrates containing: (a) 0% CaSiO_3 ; (b) 2% CaSiO_3 ; (c) 2.25% CaSiO_3 ; (d) 4% CaSiO_3 and (e) 6% CaSiO_3 .

the substrate Al_2O_3 contains 6 wt% CaSiO_3 and the overlay(W-10Cu) premix contains 1% wax. This is confirmed from the SEM fractographs(*Figure 3.2*).

3.3 Effect of overlay sintering temperature

Elevated temperature sintering, viz. 1300°C gave rise to successful composites, whereas lower temperature sintering(1200°C) causes the overlay to delaminate(*Table 3.3*). The optimized amount of lubricant(1%) was used for all subsequent sinterings. Insufficient densification is noted in case of lower temperature sintered composites. It is evident from the *Figure 3.3* that increase in temperature from 1000°C to 1300°C decreases the contact angle for wetting[103], hence better densification is observed at higher temperature.

3.4 Effect of sintering atmosphere

Our results demonstrate that, among hydrogen and argon, former gives rise to more sound layered composites. This is confirmed by TRS results(*Table 3.4*), which showed the values in case of hydrogen sintering is greater than that in argon. However, the SEM fractographs(*Figure 3.4*) are not revealing this subtle difference. The main reason behind the better role of hydrogen sintering is the fact that hydrogen reduces the oxide impurities present in the overlay. This facilitates better wetting by the melt, which enhances the overlay/substrate bonding.

3.5 Effect of copper content in W-overlay

Table 3.5 shows that system having 5 wt% copper does not sinter too well. Here the amount of liquid phase appears to be insufficient to promote the adherence of the overlay over the substrate. On the other hand, addition of 20 wt% copper gives rise to excessive amount of liquid phase. This gives rise to high %shrinkage which causes a stress along the interface. At the same time the incomplete reduction of oxide may prevent adequate bonding between the layer. Upadhyaya and German[104], while studying dilatometric plots of W-Cu premix and comilled powders, observed more swelling during heating the former, which was interpreted by them due to more disturbance caused by reduction of

Table 3.2: Effect of substrate alumina composition and amount of lubricant in W-10Cu overlay on the sintered properties of layered composites.

Substrate composition(wt%)	Wt% wax in overlay premix	Avg.TRS (MN/m ²)	%Th.D Substrate	%Th.D overlay	Remarks
Al ₂ O ₃	0	—	62	—	delaminated, poor sintering
	1	73	62	51	—
	4	—	62	36	overlay cracked
Al ₂ O ₃ - 2 CaSiO ₃	0	—	69	—	delaminated, poor sintering
	1	236	69	50	—
	4	—	69	36	overlay cracked
Al ₂ O ₃ - 2.25 CaSiO ₃	0	—	71	—	delaminated, poor sintering
	1	214	71	50	—
	4	—	71	35	overlay cracked
Al ₂ O ₃ - 4 CaSiO ₃	0	—	73	—	delaminated, poor sintering
	1	235	73	52	—
	4	—	73	36	overlay cracked
Al ₂ O ₃ - 6 CaSiO ₃	0	—	74	—	delaminated, poor sintering
	1	327	74	52	—
	4	—	74	35	overlay cracked

Sintering parameters: temperature 1300°C, time 15mins, atmosphere H₂

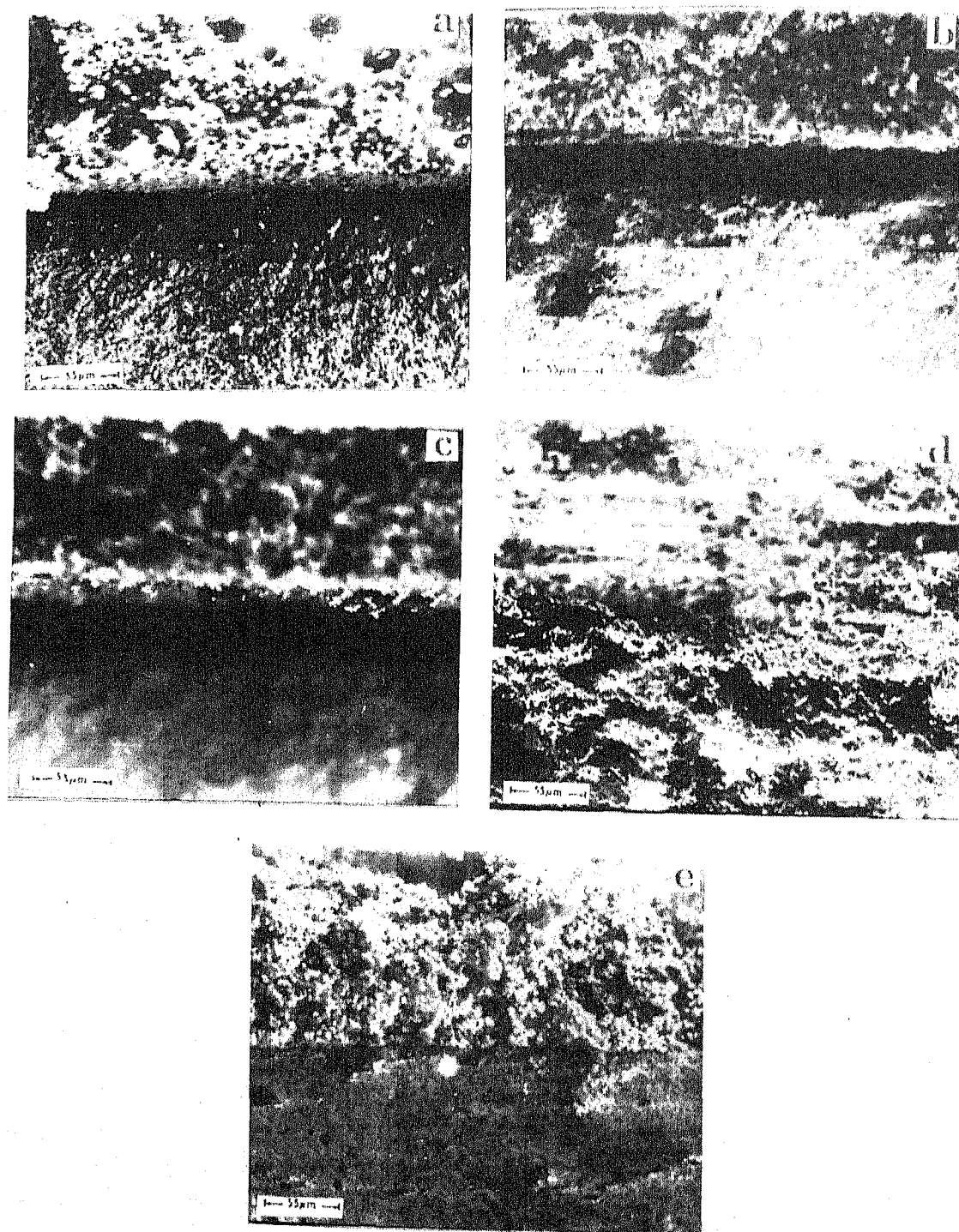


Figure 3.2: SEM fractographs at interface region of layered composites sintered in H_2 ($1300^\circ C$ for 15 min): (a) Al_2O_3 substrate; (b) Al_2O_3 -2% $CaSiO_3$ substrate; (c) Al_2O_3 -2.25% $CaSiO_3$ substrate; (d) Al_2O_3 -4% $CaSiO_3$ substrate and (e) Al_2O_3 -6% $CaSiO_3$ substrate.

Table 3.3: Effect of co-sintering temperature on the properties of layered Al_2O_3 /W-10Cu composites.

Substrate composition(wt%)	Sintering temperature($^{\circ}C$)	Avg. TRS (MN/m ²)	%Th.D		Remarks
			Substrate	overlay	
Al_2O_3	1200	–	62	–	delaminated, poor sintering
	1300	73	62	51	–
Al_2O_3 - 2 CaSiO ₃	1200	–	69	–	delaminated, poor sintering
	1300	236	69	50	–
Al_2O_3 - 2.25 CaSiO ₃	1200	–	71	–	delaminated, poor sintering
	1300	214	71	50	–

Overlay W-10Cu(1%wax), sintering period 15mins, atmosphere H₂

Table 3.4: Effect of sintering atmosphere on the properties of layered Al_2O_3 /W composites.

Substrate composition(wt%)	Sintering atmosphere	Avg. TRS (MN/m ²)	%Th.D		Remarks
			Substrate	overlay	
Al_2O_3 - 4 CaSiO ₃	Ar	213	73	49	good adhesion
	H ₂	235	73	52	better adhesion
Al_2O_3 - 6 CaSiO ₃	Ar	312	74	50	good adhesion
	H ₂	327	74	52	better adhesion

Overlay W-10Cu(1%wax), sintering temperature 1300 $^{\circ}C$, time 15mins

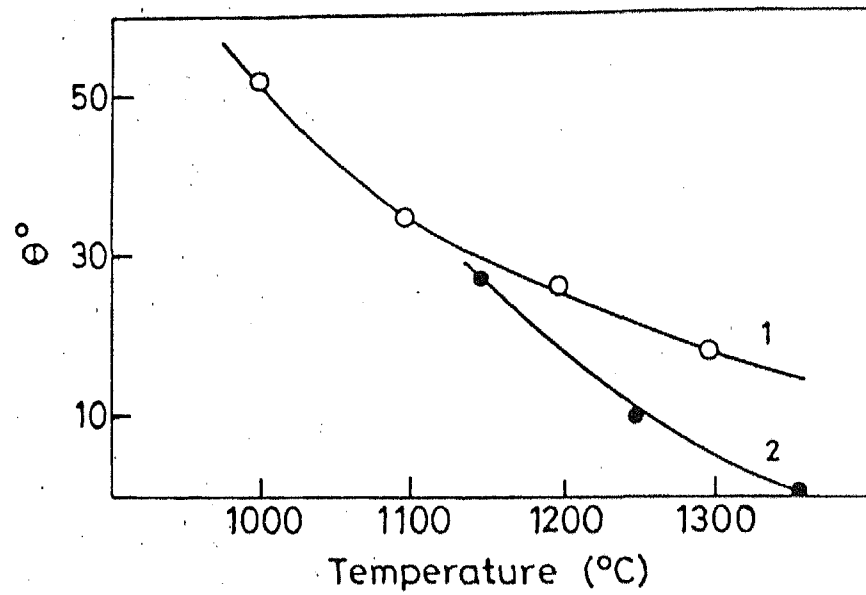


Figure 3.3: Effect of temperature on contact angle of silver(1) and copper(2) melts over tungsten(after Naidich[103]).

Table 3.5: Effect of copper content in tungsten on the properties of sintered Al_2O_3/W layered composites.

Substrate composition(wt%)	Wt% Cu content in W-1%wax	Avg.TRS (MN/m ²)	%Th.D Substrate	%Th.D overlay	Remarks
Al_2O_3	5	—	62	35	delaminated
	10	73	62	51	—
	20	—	62	44	delaminated
Al_2O_3 - 2 $CaSiO_3$	5	—	69	36	delaminated
	10	236	69	50	—
	20	—	69	44	delaminated

Sintering parameters: temperature 1300°C, time 15mins, atmosphere H_2

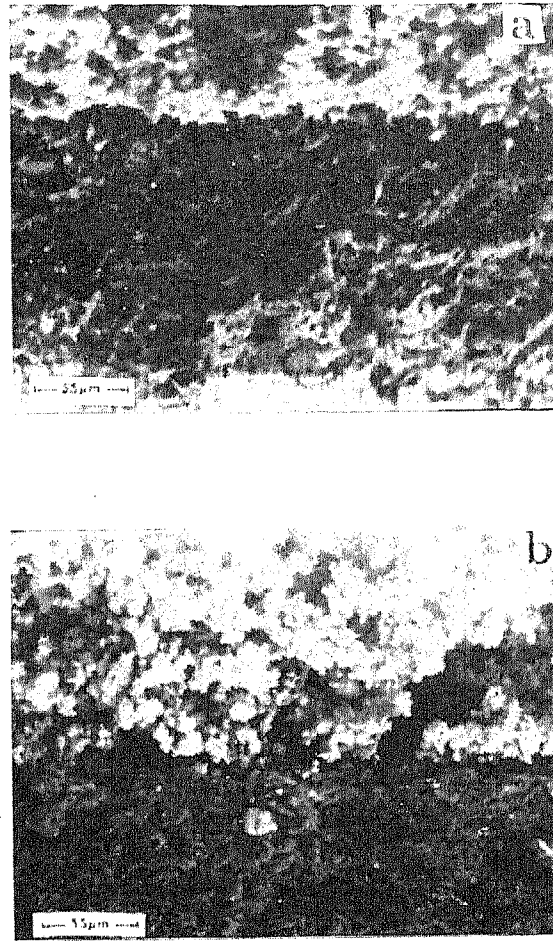


Figure 3.4: SEM fractographs at interface region of layered composites sintered in Ar (1300°C for 15 min): (a) Al_2O_3 -4% CaSiO_3 substrate and (b) Al_2O_3 -6% CaSiO_3 substrate.

copper oxide by hydrogen. In the present case, in case of 20 wt% copper in the overlay the enhanced amount of oxygen does a similar effect, causing relatively poor bonding. However, it is interesting to note that in the report of Upadhyaya and German[104], comilling was carried out for 24 hours, whereas in the present investigation it was only 15 mins. This more or less behaves similarly to their premix compacts. In case the comilling was continued for a much longer period, it is expected to have sound bonding in case of even W-20Cu overlay composition. Copper content of 10 wt% in tungsten is, therefore, the optimized amount irrespective of the composition of the substrate.

3.6 Effect of silver addition in tungsten-copper overlay

With change in the overlay system from W-10Cu to W-10Ag, all composites invariably got delaminated(*Table 3.6*). When copper binder was diluted by silver, the results are similar to those corresponding to pure silver binder. In case where copper binder was diluted by relatively larger proportion of silver(i.e. 80Cu-20Ag); the densification of the overlay is more or less similar to W-9Cu-1Ag composition(*Table 3.6*). Naidich[103] discussed the effect of silver or copper melts on the wettability of tungsten. It is evident from *Figure 3.3* that with increase in temperature from 1000°C to 1300°C the contact angle for wetting decreases, such that the decrease is more pronounced for copper melts as compared to silver. This finding directly correlates with our results as any overlay composition which contained silver got delaminated after sintering.

3.7 Effect of pretreated silver/copper powders in tungsten overlay

Table 3.7 shows that W-9Cu-1Ag(prefired Ag) premix overlay did not adhere to the substrate. In case of W-10Ag(prefired) the results were similar to that of W-9Cu-1Ag(prefired Ag) and significant shrinkage was observed. Similar trend was also observed when hydrogen prerduced copper powder was in the binder. In this case, also, excessive shrinkage was noticed. *Figure 3.5* shows scanning electron micrographs of as sintered surface of the W-overlay with as received and pretreated binders. From particle and porosity distribution, it is clear that in case of as received binders, infiltration action was very poor causing

Table 3.6: Effect of silver addition in tungsten-copper overlay on the properties of sintered Al_2O_3/W layered composites.

Substrate composition(wt%)	overlay(1% waxed) composition(wt%)	Avg.TRS (MN/m ²)	%Th.D Substrate	%Th.D overlay	Remarks
Al_2O_3	W-10Cu	73	62	51	–
	W-8Cu-2Ag	–	62	–	delaminated, poor sintering
Al_2O_3 - 2 $CaSiO_3$	W-10Cu	236	69	50	–
	W-8Cu-2Ag	–	69	–	delaminated, poor sintering
Al_2O_3 - 2.25 $CaSiO_3$	W-10Cu	214	71	50	–
	W-9Cu-1Ag	–	71	–	delaminated, poor sintering
	W-8Cu-2Ag	–	71	–	delaminated, poor sintering
	W-10Ag	–	71	49	delaminated
Al_2O_3 - 4 $CaSiO_3$	W-10Cu	235	73	52	–
	W-9Cu-1Ag	–	73	–	delaminated, poor sintering
	W-10Ag	–	73	50	delaminated
Al_2O_3 - 6 $CaSiO_3$	W-10Cu	327	74	52	–
	W-9Cu-1Ag	–	74	–	delaminated, poor sintering
	W-10Ag	–	74	49	delaminated

Sintering parameters: temperature 1300°C, time 15mins, atmosphere H_2

Table 3.7: Effect of pretreated silver/copper powders on the properties of sintered Al_2O_3/W layered composites.

Substrate composition(wt%)	overlay(1% waxed) composition(wt%)	Avg. TRS (MN/m ²)	%Th.D		Remarks
			Substrate	overlay	
Al_2O_3 - 2.25 CaSiO ₃	W-10Cu	214	71	50	—
	W-10Cu (prereduced)	—	71	54	delaminated, excessive shrinkage
	W-9Cu-1Ag	—	71	—	delaminated, poor sintering
	W-9Cu-1Ag (prefired)	—	71	49	delaminated, excessive shrinkage
	W-10Ag	—	71	49	delaminated
	W-10Ag (prefired)	—	71	50	delaminated, excessive shrinkage
	W-10Cu	327	74	52	—
	W-10Cu (prereduced)	—	74	55	delaminated, excessive shrinkage
Al_2O_3 - 6 CaSiO ₃	W-9Cu-1Ag	—	74	—	delaminated, poor sintering
	W-9Cu-1Ag (prefired)	—	74	50	delaminated, excessive shrinkage
	W-10Ag	—	74	49	delaminated
	W-10Ag (prefired)	—	74	51	delaminated, excessive shrinkage

Sintering parameters: temperature 1300°C, time 15mins, atmosphere H₂

a less porous surface. On the other hand in case of pretreated binders, more porous surface suggests that liquid melt, with less amount of oxygen in it was driven down the free surface by the capillary force. It can be therefore, concluded that wetting behaviour by melts of prefired silver or pretreated copper is better than those corresponding to as received silver or copper. Lesser amount of oxide impurities gives rise to better wetting characteristics and hence more shrinkage. The main cause of delamination is mismatch between the shrinkage rates of overlays and substrates.

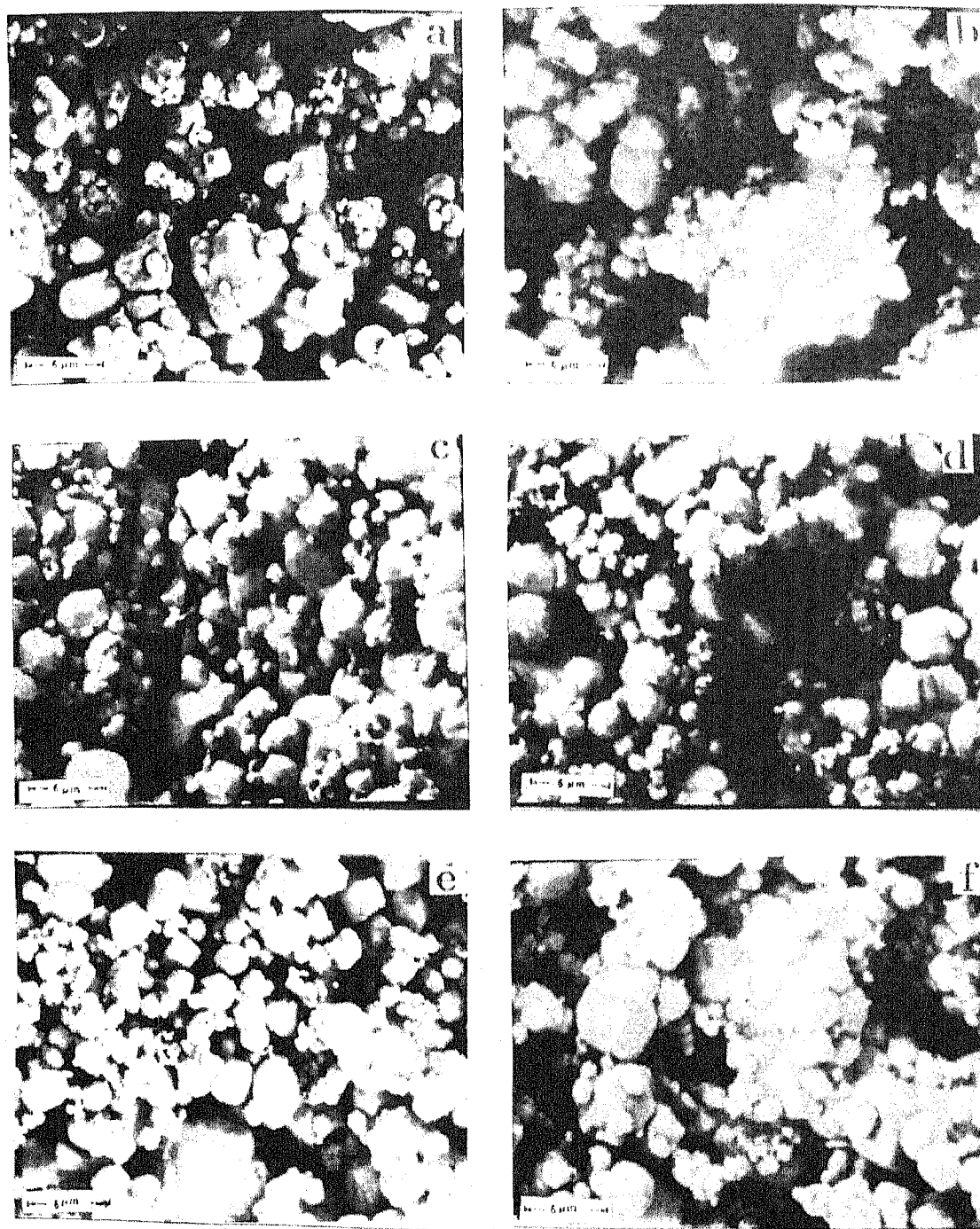


Figure 3.5: SEM micrographs at the surface of 1% waxed W-overlay with as received or pretreated binder: (a) 10% Cu(as received); (b) 10% Cu(prereduced); (c) 9% Cu-1% Ag(as received); (d) 9% Cu-1% Ag(prefired); (e) 10% Ag(as received) and (f) 10% Ag(prefired).

Chapter 4

Chapter 4

Conclusions and future scope of work

Prefired flux(CaSiO_3) addition to alumina enhances densification with concomitant strengthening with its greater proportion. Further addition of CaSiO_3 can improve the sintered density and can strengthen the alumina substrate to a greater extent.

Good bonded layered composites are produced with optimized W-10Cu premix overlay containing 1% wax. For higher wax contained overlay bonding with alumina was good but it results in cracked overlay. Delamination and poor sintering occur in case of overlay containing no wax. Delaminated overlay was also obtained with lower and higher copper content overlay.

Elevated temperature cosintering gives densified overlay due to good wetting behaviour. One can proceed to still higher temperature to observe these effect in more details. Sintering in hydrogen atmosphere as compared to argon gives better wetting by the melt and thus better strength effect. Partial or full substitution of copper binder by silver results in delaminated composite due to poor wettability of tungsten by silver. Pre-treated silver or copper powders cause excessive shrinkage in the overlay system resulting in delamination effect on the cosintered composites.

Bibliography

- [1] D. Tench and J. White, *Metall. Trans.*, **Vol. 15A**, 1984, p.2039.
- [2] P. Boch, T. Chartier and M. Huttepain, *J. Am. Ceram. Soc.*, **Vol. 69**, 1989, p.C-191.
- [3] A. Bose, *Adv. in P/M and Particulate Materials*, **Vol. 9**(compiled by J. M. Campus and R. M. German), Metal Powder Industries Federation, Princeton, N. J., 1992, p.57.
- [4] A. Bose, and J. Lankford, *Adv. in P/M and Particulate Materials*, **Vol. 5**(compiled by C. Lall and A. J. Neupaver), Metal Powder Industries Federation, Princeton, N. J., 1994, p.411.
- [5] K. B. Guy and D. M. Jacobson, *Designing Interfaces for Technological Applications: Ceramic-Ceramic, Ceramic-Metal Joining*, (Ed. S. D. Peteves), Elsevier, N. Y., 1989, p.33.
- [6] W. Wlosinski, *Sintering-Theory and Practice*, *Matl Sc. Monographs*, **Vol. 14**, (Eds. D. Kolar, S. Pejovnik and M. M. Ristic), Elsevier, Amsterdam, 1982, p.539.
- [7] A. G. Pincus, *J. Am. Ceram. Soc.*, **Vol. 36**, No.5, 1953, p.152.
- [8] S. S. Cole, Jr. and F. J. Hynes, Jr., *Am. Ceram. Soc. Bull.*, **Vol. 37**, No.3, 1958, p.135.
- [9] M. Hirota, *Trans. of the Japan Ins. of Metal*, **Vol. 16**, No.4, 1968, p.266.
- [10] S. Morozumi, M. Kikuchi and T. Nishino, *J. Matl. Sc.*, **Vol. 16**, 1981, p.2137.
- [11] J. R.Floyd, *Am. Ceram. Soc. Bull.*, **Vol. 42**, No.2, 1963, p.65.
- [12] E. P. Denton, and H. Rawson, *Trans. Br. Ceram. Soc.*, **Vol. 42**, No.2, 1963, p.65.
- [13] L. Reed and R. A. Huggins, *J. Am. Ceram. Soc.*, **Vol. 48**, No.8, 1965, p.421.

CENTRAL LIBRARY
I. I. T., KANPUR

No. A 128038

- [14] D. H. Harris and P. Lall, Handbook of Electronic Package Design, (Ed. M. Pecht), Marcel-Dekker, N. Y., 1991, p.101.
- [15] M. E. Arthur and L. E. Fussell, Am. Ceram. Soc. Bull., Vol. 50, No.12, 1971, p.982.
- [16] J. C. Williams and J. W. Nielsen, J. Am. Ceram. Soc., Vol. 42, No.5, 1959, p.229.
- [17] G. S. Upadhyaya, Materials Sc. Monographs, Vol. 25, (Ed. G. S. Upadhyaya), Elsevier, Amsterdam, 1984, p.46.
- [18] E. M. Uygur, Materials Sc. Monographs, Vol. 25, (Ed. G. S. Upadhyaya), Elsevier, Amsterdam, 1984, p.305.
- [19] R. M. German, Liquid Phase Sintering, Plenum Press, N. Y., 1985, p.45.
- [20] E. Ryshkewitch, Oxide Ceramics, Academic Press Inc., N. Y., 1960, p.205.
- [21] E. Ryshkewitch, Oxide Ceramics, Academic Press Inc., N. Y., 1960, p.136.
- [22] R. L. Coble, J. Am. Ceram. Soc., Vol. 41, 1958, p.51.
- [23] W. D. Kingery and M. Berg, J. Appl. Phys., Vol. 26, part.3, 1955, p.1205.
- [24] W. D. Jones, Fundamental Principle of Powder Metallurgy, Edward Arnold (Pub.) Ltd., 1960, p.422.
- [25] A. Bettinelli, J. Boissier, J. Guille, J. C. Bernier, High Tech Ceramics, Vol. 38b, (Ed. P. Vincenzini), Elsevier sc. Pub. B. V., Amsterdam, 1987, p.1567.
- [26] G. Kuczynski, Trans. AIME, Vol. 185, 1949, p.169.
- [27] P. Reynen, Problems of Nonstoichiometry, (Ed. A. Rabenau), North-Holland Publ. Co., Amsterdam, 1970, p.219.
- [28] D. W. Readey, J. Am. Ceram. Soc., Vol. 49, 1966, p.366.
- [29] T. Nishikawa et al., J. Ceram. Soc. Japan, Vol. 87, 1979, p.217.
- [30] P. Reynen, Sintering Process, Matl. Sc. Research, Vol. 13, (Ed. G. C. Kuczynski), Plenum Press, N. Y., 1979, p.362.
- [31] J. G. J. Peelen, PhD Thesis, Technical University Eindhoven, Netherlands, 1977.
- [32] W. C. Johnson and R. L. Coble, J. Am. Ceram. Soc., Vol. 61, No.3-4, 1978, p.110.

- [33] A. H. Heuer, J. Am. Ceram. Soc., Vol. 62, No.5-6, 1979, p.317.
- [34] S. J. Bennison and M. P. Harmer, J. Am. Ceram. Soc., Vol. 73, No.4, 1990, p.833.
- [35] J. Rödel and A. M. Glaeser, J. Am. Ceram. Soc., Vol. 73, No.11, 1990, p.3292.
- [36] J. Rödel and A. M. Glaeser, J. Am. Ceram. Soc., Vol. 73, No.11, 1990, p.3302.
- [37] G. Rossi and J. E. Brrke, J. Am. Ceram. Soc., Vol. 56, No.12, 1973, p.654.
- [38] W. J. Smothers and H. J. Reynolds, J. Am. Ceram. Soc., Vol. 37, No.12, 1954, p.588.
- [39] H. P. Cahoon and C. J. Christensen, J. Am. Ceram. Soc., Vol. 39, No.10, 1956, p.337.
- [40] J. Katanić-Popović, M. Gašić and D. Kinčević, Matl. Sc. Monographs 6, Vol. 14, (Eds. D. Kolar, S. Pejovnik and M. M. Ristić), 1982, p.153.
- [41] P. Reynen, Proc. of 6th Inter. Symp. on the Reactivity of Solids, Schenectady, 1968, Wiley Inter. Sc., 1969, p.99.
- [42] J. S. Reed, Introduction to the Principles of Ceramic Processing,, Wiley Inter. Sc. Publ., N. Y., 1988, p.459.
- [43] R. Morrell, Handbook of Properties of Technical and Engineering Ceramics, part 2, Data Reviews(HMSO Publication Centre, London), Sec. I, High-alumina ceramics, 1987, p.1.
- [44] J. D. Cawley and W. E. Lee, Material Sc. and Tech., Structure and Properties of Ceramics, Vol. 11(Vol. Ed. M. V. Swain), (Eds. R. W. Chan, P. Haasen, E. J. Kramer), VCH Publ. Inc., N. Y., Chapter 2, 1994, p.97.
- [45] C. A. Powell-Dogan and A. H. Heuer, J. Am. Ceram. Soc., Vol. 73, No.12, 1990, p.3670.
- [46] W. H. Gitzen, Am. Ceram. Soc., Columbus, OH., 1970, p.127.
- [47] S. Lartique and L. Priester, J. Phy., Vol. 46, C-4, 1985, p.101.
- [48] K. J. Morrissey and C. B. Carter, J. Am. Ceram. Soc., Vol. 67, 1984, p.292.

- [49] S. Pejovnik, D. Kolar, W. J. Huppmann and G. Petzow, *Sintering Sc. and Tech.*, (Ed. D. P. Uskoković), Printed in Yugoslavia, 1977, p.103.
- [50] P. Reynen and A. C. Firatli, *Sintering-Theory and Practice*, Matl. Sc. Monographs, Vol. 14, (Eds. D. Kolar, S. Pejovnik and M. M. Ristic), Elsevier, Amsterdam, 1982, p.209.
- [51] S. J. Kiss, D. Cerovic and E. Kostic, *Sintering-Theory and Practice*, Matl. Sc. Monographs, Vol. 14, (Eds. D. Kolar, S. Pejovnik and M. M. Ristic), Elsevier, Amsterdam, 1982, p.251.
- [52] S. W. H. Yih and C. T. Wang, *Tungsten: Sources, Metallurgy, Properties and Applications*, Plenum Press, N. Y., 1979, p.163.
- [53] N. C. Kothari, *J. Less-Common Metals*, Vol. 5, 1963, p.140.
- [54] S. Gowri and J. A. Lund, *Tungsten and Tungsten Alloys-1992*, (Eds. A. Bose, R. J. Dowding), Metal Powder Industries Federation, Princeton, N. J., 1992, p.183.
- [55] D. J. Jones, *J. Less-Common Metals*, Vol. 2, 1960, p.76.
- [56] H. Yamamoto, *The Metallurgy of Doped/Non-sag Tungsten*, (Eds. E. Pink, L. Bartha), Elsevier Appl. Sc., London and N. Y., 1989, p.31.
- [57] V. J. Vacek, *Planseeber: Pulvermetall.*, Vol. 7, 1959, p.6.
- [58] H. W. Hayden and J. H. Brophy, *J. Electrochem. Soc.*, Vol. 110, p.805.
- [59] R. M. German and Z. A. Munir, *Metall. Trans. A*, Vol. 7A, 1976, p.1873.
- [60] I. J. Toth and N. A. Lockington, *J. Less-Common Metals*, Vol. 12, 1967, p.353.
- [61] G. V. Samsonov and W. I. Jakowlew, *Z. Metallkunde*, Vol. 62, 1971, p.621.
- [62] J. H. Brophy, L. A. Shepard and J. Wulff, *Powder Metallurgy*, (Ed. W. Leszynski), AIME-Metal Powder Industries Federation, Inter Sc. Publ., N. Y., 1961, p.113.
- [63] R. M. German and Z. A. Munir, *J. Less-Common Metals*, Vol. 46, 1976, p.333.
- [64] J. H. Brophy, H. W. Hayden and J. Wulff, *Trans. Met. Soc. AIME*, Vol. 221, 1961, p.1225.

- [65] J. H. Brophy, H. W. Hayden and J. Wulff, *Trans. Met. Soc. AIME*, **Vol. 224**, 1962, p.797.
- [66] C. W. Corti, *Int. J. Refractory and Hard Metals*, **Vol. 6**, No.1, 1987, p.28.
- [67] W. A. Kaysser, M. Hofmann-Amtenbrik and G. Petzow, *Sintering '85*, (Eds G. C. Kuczynski, D. P. Uskokovic, H. Palmour and M. M. Ristic), Plenum Press, N. Y., 1987, p.121.
- [68] H. W. Hayden and J. H. Brophy, *J. Less-Common Metals*, **Vol. 6**, 1964, p.214.
- [69] T. Bregel, W. K. Vogt, R. Michal and K. E. Saeger, *IEEE Trans. on Compts. Hybrids and Manuf. Tech.*, **Vol. 14**, No.1, 1991, p.8.
- [70] G. H. Gessinger and K. N. Melton, *Powder Metall. Int.*, **Vol. 9**, No.2, 1977, p.67.
- [71] J. H. Moon, J. S. Lee and I. S. Ahn, *Sintering '85*, (Eds G. C. Kuczynski, D. P. Uskokovic, H. Palmour and M. M. Ristic), Plenum Press, N. Y., 1987, p.143.
- [72] I. H. Moon, *Int. J. Powder Met. and Powder Tech.*, **Vol. 11**, 1975, p.27.
- [73] W. Haufe, W. Reichel and H. Schriener, *Z. Metallkunde*, **Vol. 63**, 1972, p.651.
- [74] J. H. Moon and J. S. Lee, *Powder Met.*, **Vol. 22**, No.1, 1979, p.5.
- [75] R. M. German and B. H. Rabin, *Powder Met.*, **Vol. 28**, No.1, 1985, p.7.
- [76] I. H. Moon, J. S. Kim and Y. L. Kim, *J. Less-Common Metals*, **Vol. 102**, 1984, p.219.
- [77] I. H. Moon and J. S. Kim, *Sintered Metal Ceramic Composites*, *Materials Sc. Monographs*, **Vol. 25**, (Ed. G. S. Upadhyaya), Elsevier Sc. Publ. B. V., Amsterdam, 1984, p.269.
- [78] Y. L. Kim, J. S. Kim and I. H. Moon, *Modern Developments in Powder Metallurgy, Principles and Process*, **Vol. 15**, (Eds. E. N. Aqua and C. I. Whitman), Metal Powder Industries Federation, American Powder Met. Inst., Princeton, N. J., 1985, p.541.
- [79] L. B. Ekbom and A. Eliasson, *Tungsten & Tungsten Alloys – 1992*, (Eds. A. Bose and R. J. Dowding), Metal Powder Industries Federation, Princeton, N. J., 1993, p.97.

- [80] W. J. Huppmann, H. Reigger and G. Petzow, Sintering – New Developments, Material Sc. Monographs, Vol. 4, (Ed. M. M. Ristic), Elsevier Sc. Publ. Co., 1979, p.272.
- [81] O. J. Kwon and D. N. Yoon, Sintering Processes, Material Sc. Monographs, Vol. 13, (Ed. G. C. Kuczynski), Plenum Press, N. Y., 1980, p.203.
- [82] H. Reigger, J. A. Pask and H. E. Exner, Sintering Processes, Material Sc. Monographs, Vol. 13, (Ed. G. C. Kuczynski), Plenum Press, N. Y., 1980, p.219.
- [83] K. F. Hens, J. L. Johnson and R. M. German, Metal and Ceramic Injection Moulding, Adv. in P/M and Particulate Materials – 1994, Vol. 4(compiled by C. Lall and A. J. Neupaver), Metal Powder Industries Federation, Princeton, N. J., 1994, p.217.
- [84] I. H. Moon and J. S. Lee, Powder Met. Int., Vol. 9, 1977, p.23.
- [85] W. J. Huppmann and H. Reiger, Acta Metallurgica, Vol. 23, 1975, p.965.
- [86] R. L. Johnson and R. M. German, Sintering, Adv. in P/M and Particulate Materials – 1992, Vol. 3(compiled by J. M. Capus and R. M. German), Metal Powder Industries Federation – APMI, Princeton, N. J., 1992, p.35.
- [87] H. H. Hausner, Metals and Alloys, Vol. 18, 1943, p.437.
- [88] A. Lawley, Copper Based P/M, (Ed. P. W. Taubenblat), Metal Powder Industries Federation, Princeton, N. J., 1980, p.147.
- [89] J. L. Johnson and R. M. German, Metall. Trans., Vol. 24A, 1993, p.2369.
- [90] I. A. Lavrinenko and Y. V. Naidich, Powder Metallurgy World Congress, Vol. II, European Powder Metallurgy Association, 1994, p.1549.
- [91] A. L. Prill, H. W. Hayden and J. H. Brophy, Trans. Met. AIME, Vol. 230, 1964, p.769.
- [92] S. W. H. Yih and C. T. Wang, Chapter 5, Tungsten: Sources, Metallurgy, Properties and Applications, Plenum Press, N. Y., 1979, p.335.
- [93] F. A. Lindberd, IEEE Trans. on Compts. Hybrids and Manuf. Tech., Vol. 14, No.4, 1991, p.790.

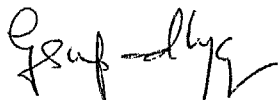
- [94] H. D. Kaiser, F. J. Pakulski and A. F. Schmeckenbecher, Solid State tech., **Vol. 15**, No.5, 1972, p.35.
- [95] K. G. Ewsuk and L. W. Harrison, Manufacture of Ceramic Components, Ceram. Trans., **Vol. 49**, (Eds. B. Hiremath, A. Bruce and A. Ghosh), Am. Ceram. Soc. Inc., OH., USA, 1995, p.197.
- [96] A. J. Blodgett and D. R. Bardour, IBM J. Res. Develop., **Vol. 26**, No.1, 1982, p.30.
- [97] B. C. Foster, F. J. Bachner, E. S. Tormey, M. A. Occhionero and P. A. White, IEEE Trans. on Compts. Hybrids and Manuf. Tech., **Vol. 14**, No.4, 1991, p.784.
- [98] S. G. Konsowski, Electronic Materials and Processes, Second Edition(Eds. C. A. Harper and R. N. Sampson), McGraw-Hill, Inc., 1994, p.11.1.
- [99] R. R. Tummala, Am. Cearm. Soc. Bull., **Vol. 67**, No.4, 1988, p.752.
- [100] D. A. Chance, Metall. Trans., **Vol. 1**, 1970, p.685.
- [101] K. Otsuka, T. Usami and M. Sekihata, Am. Cearm. Soc. Bull., **Vol. 60**, No.5, 1981, p.540.
- [102] G. Arthur, J. Inst. Met., **Vol. 84**, 1955, p.327.
- [103] Y. V. Naidich, Contact Phenomena in Metallic Melts, Naukova Dumka, Kiev, 1972, p.152.
- [104] A. Upadhyaya and R. M. German, IJPM, **Vol. 34**, 1998, p.43.

Part II

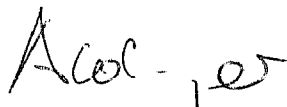
Optimization of an Additive System for the Liquid Phase Sintering of Silicon Carbide Ceramics

Certificate

It is certified that the work contained in the thesis entitled **Optimization of an additive system for the liquid phase sintering of silicon carbide ceramics** by **Koushik Biswas**, has been carried out under our supervision and it has not been submitted elsewhere for a degree.



(Dr. G. S. Upadhyaya)
Department of Materials and
Metallurgical Engineering
Indian Institute of Technology
Kanpur, India



(Dr F. Aldinger)
Max-Planck-Institut für Metallforschung
Institut für Nichtmetallische Anorganische
Materialien der Universität Stuttgart
Pulvermetallurgisches Laboratorium
Heisenbergstraße 5, Stuttgart, Germany

List of Figures

1.1	The Influence of boron compounds on the sintered density of silicon carbide	7
1.2	Effect of additives on grain growth and densification in sintering of SiC . .	7
1.3	Effect of temperature on sintered density for B-doped, Al-doped and B+Al-doped silicon carbide	8
1.4	Effect of Al ₂ O ₃ and carbon on sintered density of SiC	10
1.5	SiC-Al ₂ O ₃ stability diagram	12
1.6	Sintered density variation of SiC as a function of Al ₂ O ₃ additive and sintering time	13
1.7	Change of sintered density of SiC with Y ₂ O ₃ addition	13
1.8	Plot of density versus amount of sintering aids for SiC-AlN samples	15
1.9	Quasibinary phase diagram of AlN-Y ₂ O ₃	15
1.10	Schematic microstructure development of β -SiC during pressureless sintering	17
1.11	The variation of bend strength with temperature in hot pressed SiC	20
2.1	Schematic diagram of sample preparation method	27
2.2	Schematic diagram of sintering cycle	28
2.3	Percentage α -SiC obtained as a function of intensity ratio	30
2.4	Schematic drawing of 4-point bending strength specimen	32
3.1	SEM micrographs of HIPed material	36
3.2	X-ray diffraction pattern of hot isostatically pressed material	38
3.3	X-ray diffraction pattern of 90 β /10A/60AlN sample	39

3.4	X-ray diffraction pattern of 90 β /7A/60AlN sample	39
3.5	X-ray diffraction pattern of 90 β -10 β' /10A/60AlN sample	40
3.6	$\beta \rightarrow \alpha$ -SiC phase transformation as a function of annealing time	40
3.7	Fracture toughness variation as a function of AlN-content in the additive system	43
3.8	Scanning electron micrographs of as sintered specimens containing different mol% AlN in AlN + Y ₂ O ₃ additive system	44
3.9	Differences in crack propagation in the globular and platelet materials . . .	45
3.10	Scanning electron micrographs of as sintered specimens containing different vol% of additive	46
3.11	Scanning electron micrographs of as sintered specimens containing different amounts of α -SiC seeds	47
3.12	Fracture toughness variation as a function of annealing time and with different AlN-contents in the additive system	49
3.13	Effect of prolong annealing on grain size and aspect ratio	50
3.14	Fracture toughness variation with annealing time and additive content . . .	51
3.15	Fracture toughness variation as a function of annealing time and with different α -SiC content in additive system	52
3.16	SEM micrograph of 96 β /10A/60AlN after 32 hrs of annealing	52
3.17	Bending strength variation with AlN-content in additive system	53
3.18	High temperature bending strength variation with AlN-content in additive system	53
3.19	Bending strength variation with additive content	55
3.20	High temperature bending strength variation with additive content	55
3.21	Bending strength variation with initial α -SiC content	56
3.22	High temperature bending strength variation with initial α -SiC content . .	56

List of Tables

2.1	Characteristics of initial powders	25
2.2	Specifications of the starting powders	26
3.1	Sinter density and mass loss data	35
3.2	Phase analysis data as a function of annealing time	41
3.3	Fracture toughness and hardness variation data for the materials containing different mol% AlN in the additive system	42
3.4	Fracture toughness and hardness variation data for the materials containing different vol% of additive	48
3.5	Fracture toughness and hardness variation data for the materials containing different vol% of additive	48

Nomenclature

b	...	Breadth of the specimen	mm
d_H	...	Diagonal length of Vickers indentation	μm
E	...	Elastic modulus	GPa
F	...	Force	N
h	...	Height of the specimen	mm
H	...	Vickers hardness	GPa
K_{IC}	...	Fracture toughness	$\text{MPa}\cdot\sqrt{\text{m}}$
l_o	...	Length between two outer supports of 4-point bending strength fixture	mm
l_i	...	Length between two inner supports of 4-point bending strength fixture	mm
L	...	Crack length	μm
m_G	...	Mass of green body	g
m_s	...	Mass of sintered body	g
m_w	...	Mass of sintered body in water	g
Δm	...	Mass loss	%
ρ_{rel}	...	Relative density	%
ρ_s	...	Sinter density	g/cm^3
ρ_{th}	...	Theoretical density	g/cm^3
ρ_w	...	Density of water at room temperature	g/cm^3
σ_{4P}	...	4-point bending strength	MPa
γ_{GB}	...	Grain boundary energy	J/m^2
γ_{SV}	...	Surface energy	J/m^2

Chapter 1

Chapter 1

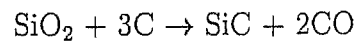
Introduction

Development of silicon carbide ceramics during the last 20 years has proceeded at a rapid pace. Their characteristics include high hardness, heat and corrosion resistance and high temperature strength. These properties make SiC the main material for structural components such as high temperature furnace components (heating elements, core tubes, refractory bricks, etc.)[1]. These applications, however, do not necessarily require high density sintered bodies. The development of SiC compacts as structural materials with high density was initially begun with the objective of application to gas turbine engines. Application of SiC compacts as structural materials can be broadly divided into two categories: (i) abrasion and corrosion resistant components and (ii) heat resistant components.

Silicon carbide occurs with many different crystal structure[1, 2]. This includes α -SiC, which is represented as a combination of zinc blende structure and the similar structure of wurtzite, and β -SiC, which has a zinc blende structure. α -SiC exhibits polytypism, i.e. the stacking sequence changes but the layer unit remains same. The relationship between Si-atoms and C-atoms in SiC is such that each Si atom is tetrahedrally bonded to four C-atoms and similarly four Si-atoms are tetrahedrally bonded to each C-atom. This type of structure leads to the strongly covalent character.

1.1 SiC Powder Production

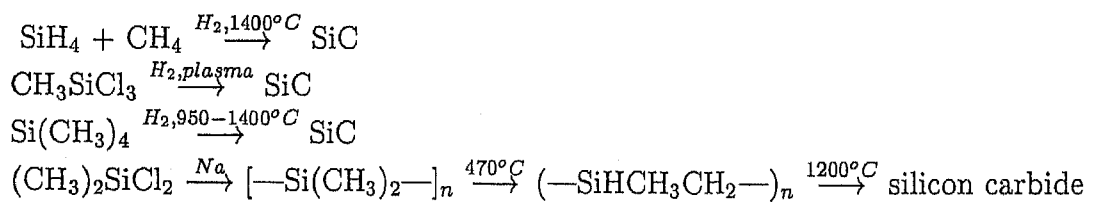
Silicon carbide is manufactured most frequently on an industrial scale using the **Acheson method**. In this technique, two solid electrodes are connected with graphite powder, a mixture of silica and coke is packed in the surrounding area, and the whole assembly is electrically heated to produce SiC chiefly by the reaction:



SiC crystal blocks from the reaction are then ground, refined and classified to produce SiC powders. The SiC grades thus prepared are characterized as α -SiC having a coarse grained structure with a mean particle size of $5\mu\text{m}$. This requires a further refining process to produce ultrafine-grain powders for sintering [3].

β -SiC powders are produced using solid phase and vapour-phase reactions. β -SiC is also produced by the Acheson method at low temperature (1500-1800°C) and hence it is possible to manufacture fine grained β -SiC powders.

Vapour-phase methods use the reaction of SiH_4 [4] or SiCl_4 with hydrocarbons such as CH_4 and C_3H_8 or the thermal decomposition of CH_3SiCl_3 , $(\text{CH}_3)_4\text{Si}$ [5], or polycarbosilane[6] to produce β -SiC. The steps leading to the production of SiC can be summarized as follows:



Particle size and chemical composition are controlled by varying reaction temperature, gas concentration and gas flow rate.

Other solid-phase methods include the direct reaction of silicon and carbon[7] and the gas evaporation method[8], in which the raw material surface is heated and melted using an arc discharge in a mixed gas (consisting of an inert gas and H_2 or N_2) to form

ultrafine SiC particles.

A new synthesis process has been developed[9, 10] to produce small, high purity non-agglomerated powders of SiC. In this process, the ceramic powder is synthesized by rapidly heating a reactant gas(silane(SiH_4) mixed with methane(CH_4) or ethylene(C_2H_4)). The characteristics of the powders are controlled by cell pressure, the reactants, their flow rates and flow ratios and temperature distribution within the reaction zone. Luce *et al.*[11] further studied on the same process and by varying the reaction conditions (laser power, flow rates and ratio of reacting gases) synthesized SiC ranging from amorphous to crystalline mixture.

1.2 Solid State Sintering of Silicon Carbide

Because silicon carbide has a high covalency, simple heating of powder compacts is insufficient to produce sintered bodies. As a result, a variety of SiC sintering methods have been developed, the three representative technologies being hot-pressing with a sintering aid, pressureless sintering with a sintering aid and reaction sintering.

1.2.1 Pressureless sintering

Pressureless sintering is considered the most important from an industrial standpoint because it allows the manufacture of large or complex-shaped pieces, it offers good mass producibility and low cost, and it can produce products with superior performance. Because of its strong covalency, however, SiC is difficult to sinter. The absence of densification during sintering of pure silicon carbide is the result of its high amount of energy required for the formation and migration of defects in the structure, which leads to lower self diffusion coefficient and hence sintering by volume and grain boundary diffusion would not occur[12]. However to obtain a high density in the sintered products, these mechanisms are necessary since surface diffusion does not lead to elimination of the pores. Prochazka[13] found the necessary conditions for good sinterability of silicon carbide powder. He mentioned that very fine particle size and additives promote the sinterability by enhancing volume diffusion and retarding surface diffusion. A similar behaviour was also observed by Hausner[14]. He observed the effect of boron and carbon addition on the sintering of β -SiC. In his review, he pointed out that high grain boundary to surface energy ratio

(γ_{GB}/γ_{SV}) hinders the densification process. He found that addition of boron decreases the grain boundary energy (γ_{GB}) and carbon increases the effective surface energy (γ_{SV}). The proposed mechanism was removal of surface oxide layer of silicon carbide by carbon and segregation of boron onto grain boundaries causes a reduction of grain boundary energy. Suzuki and Hase[15] studied the kinetics of densification in the initial stage of sintering of SiC by addition of boron and carbon. They proposed that materials transport along boundary phase was the rate controlling factor. Murata and Smoak[16] observed that solid solution between SiC and boron compounds (BN, BP and B₄C) occurred during densification and maximum density was obtained at the concentration of maximum solubility of additives(*Figure 1.1*). Addition of carbon also plays an important role in densification as well as in inhibition of grain growth of SiC-crystals.

Another proposed mechanism for the enhanced sintering effect of carbon and boron was that of grain growth inhibition[12]. Carbon and boron inhibit silicon carbide grain growth caused by surface diffusion during increasing temperature thereby maintaining the driving force of sintering upto higher temperature where volume diffusion induced densification becomes active. Addition of carbon or boron alone cannot be effective for such activated sintering mechanism(*Figure 1.2*). Stutz *et al.*[17] studied the effect of boron with carbon and aluminium with carbon in sintering of β -SiC and found that minimum B concentration of 0.3 wt% or above was required to promote densification. Carbon must be present to the tune of 2 wt%. But addition of only 1% Al with 1.5% C could not densify the cubic SiC powders to high density. The effectiveness of aluminium as a SiC sintering additive was discovered by Alliegro *et al.*[18] and he observed that aluminium was the most effective additive after boron. Bröcker *et al.*[19] first reported the pressureless sintering with addition of aluminium-carbon additives. The mechanism of densification was the same as with the B-C additive system. Al-C sintering additives act on the grain boundaries but the quantity of aluminium required was somewhat greater than that of B-C additive system because the solubility limit of aluminium in silicon carbide was larger as compared to boron and the Al₄SiC₄ and Al₄C₃ produced during sintering are easily volatilised. It was also found that less grain growth occurred with aluminium additive system than with B-additive system(*Figure 1.3*). A similar investigation was done by Shinozaki *et al.*[20] and they found that addition of Al, B and C to fine grained β -SiC enhanced the β to α transformation and subsequent growth of α -SiC platelets. The excess carbon present was reduced by Al, and Al₄C₃ was formed in C-rich regions which helps to reduce the formation of large graphite particles.

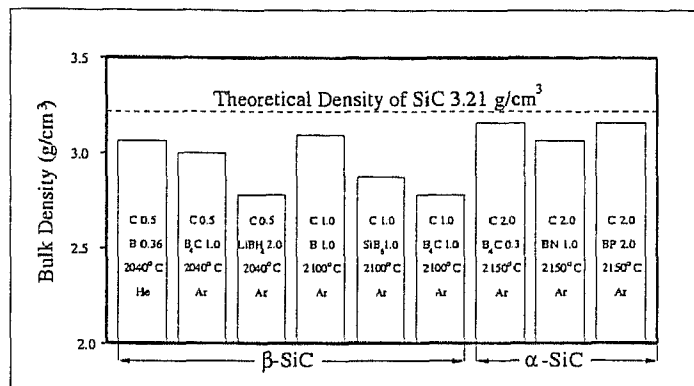


Figure 1.1: The Influence of boron compounds on the sintered density of silicon carbide (additives in wt%)[14].

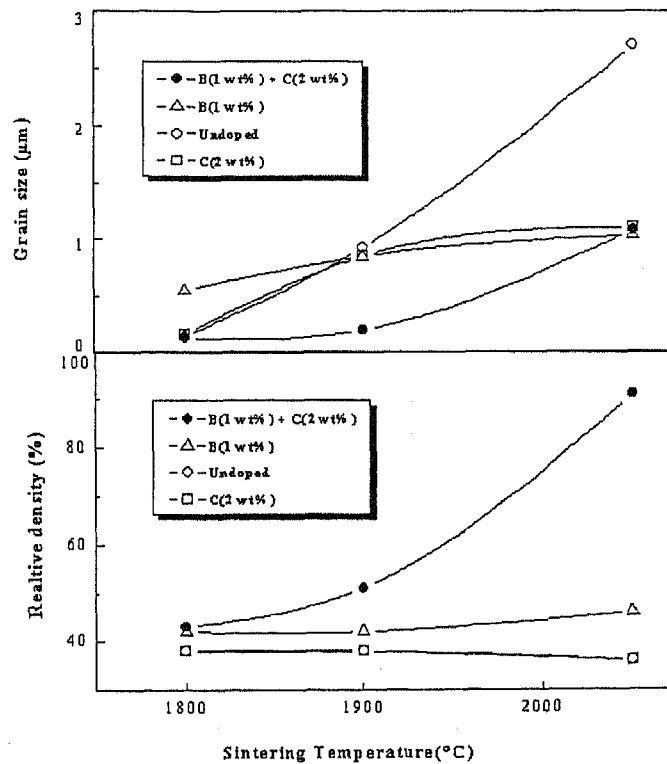


Figure 1.2: Effect of additives on grain growth and densification in sintering of SiC. (Heating rate $\sim 20^\circ\text{C}/\text{min}$; duration 1 min at 1800°C and 1900°C , 30mins at 2050°C)[13].

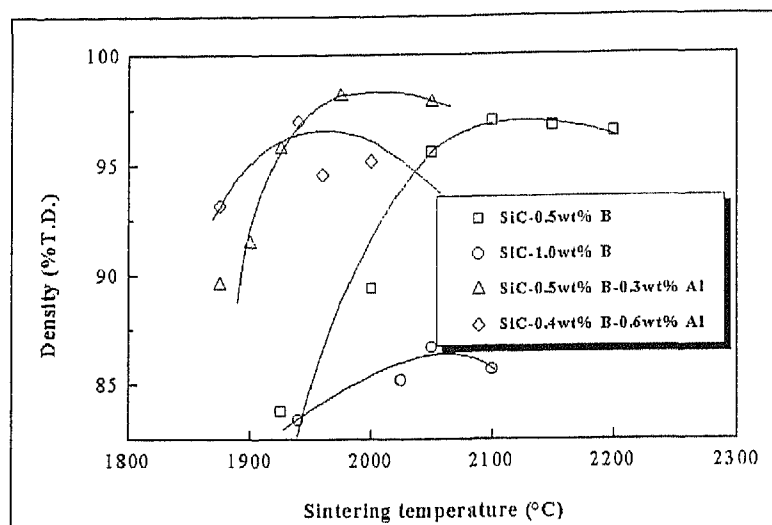


Figure 1.3: Effect of temperature on sintered density for B-doped, Al-doped and B+Al-doped silicon carbide[17].

Apart from the additives, the oxygen content of sinterable silicon powders also affects densification[21]. Lower oxygen content improves densification behaviour of SiC. It was observed that 9% sinter density difference was between standard sintered powder and heat treated powder with 0.64 wt% O₂. Morphology of the oxygen containing phases had influence on the densification. Hausner[14] discussed how the surface area of the powder had also a significant influence on the sintering behaviour. Powders having higher specific surface area had a higher densification rate with additions of sintering additives. Silicon carbide sintered body with a relative density of 95% or over was produced by pressureless sintering at 2050°C if an ultrafine raw material powder with particle size of less than 0.05 μm was used[22].

Control of sintering atmosphere[14, 23, 24] and heating rate[23] were also important to the sintering of silicon carbide powders. Inert gas atmosphere gave optimum results in B-doped powders. Higher pressure of inert gas atmosphere reduced the sinter density. Nitrogen had a retarding effect on the sintering of boron doped β-SiC[25]. Silicon vapour, oxygen and CO₂ gas in the system were deleterious to sintering as they resulted in loss of boron and consequently in inhibition of densification. Sintering was strongly inhibited by silicon vapour as a result of coarsening of the compacts. In terms of heating rate, it was observed[23] that rapid heating rate was also not favorable and with some additives slower

heating rate was the most effective way to increase sintered density of silicon carbide.

1.2.2 Hot pressing

Silicon carbide has poor self-sinterability, and additives are required in its sintering. As a result, the mechanical properties of conventional pressureless-sintered silicon carbide ceramics are insufficient for use in many kinds of applications.

Hot pressing of silicon carbide ceramics was studied because of its ability to produce dense sintered bodies. By this technique, some success in self bonding silicon carbide has been achieved[18]. Although pure silicon carbide powders can be hot pressed by conventional methods, to only $\sim 84\%$ of theoretical density, the addition of certain impurities enhances sintering, such that densities as high as 98% of theoretical value can be attained. Another possible way of densification is hot pressing under very high pressure(~ 50 kbar). Nadeau[26] investigated ultra-high-pressure hot pressing and reported that high densification(approximately 98% of theoretical density) is possible for both α -SiC and β -SiC under a pressure of 30 kbar at 1500°C . He concluded that the mass transport phenomena that may play a role in the hot pressing of silicon carbide powders are crushing and sliding of particles, plastic deformation, evaporation and condensation and bulk or surface(including grain boundaries) diffusion. The final stage densification occurs due to diffusion controlled processes like the last three named. Kalish and Clougherty[27] reported that the high pressure sintering was useful to prepare pure, fine grained and fully dense microstructures of SiC. Takatori *et al.*[28] also studied the high pressure sintering of β -SiC with no sintering additives. It was concluded that densification of SiC under high pressures depends strongly on sintering temperature, grain morphology and magnitude of the self diffusion constants. Prochazka[13] discovered that boron was an effective sintering aid, and by addition of 1% boron to a submicron silicon carbide powder and sintering under 70 MPa at 1950°C was able to obtain a SiC compact of 99% theoretical density. It was concluded that solid phase diffusion was the main mechanism for effective densification. Sakai and Aikawa[29] studied the phase transformation and thermal conductivity of hot-pressed β -SiC with Al_2O_3 and carbon additives. Upto 2% Al_2O_3 the simultaneous addition of carbon was required but specimens containing 3 wt% Al_2O_3 were densified to near the theoretical value regardless of the carbon content(*Figure 1.4*). In another investigation, Sakai and Hirosaki[30] pointed out that addition of BaO-C in SiC powders densifies the compact by hot pressing. Hot pressing of SiC powders was done by addition

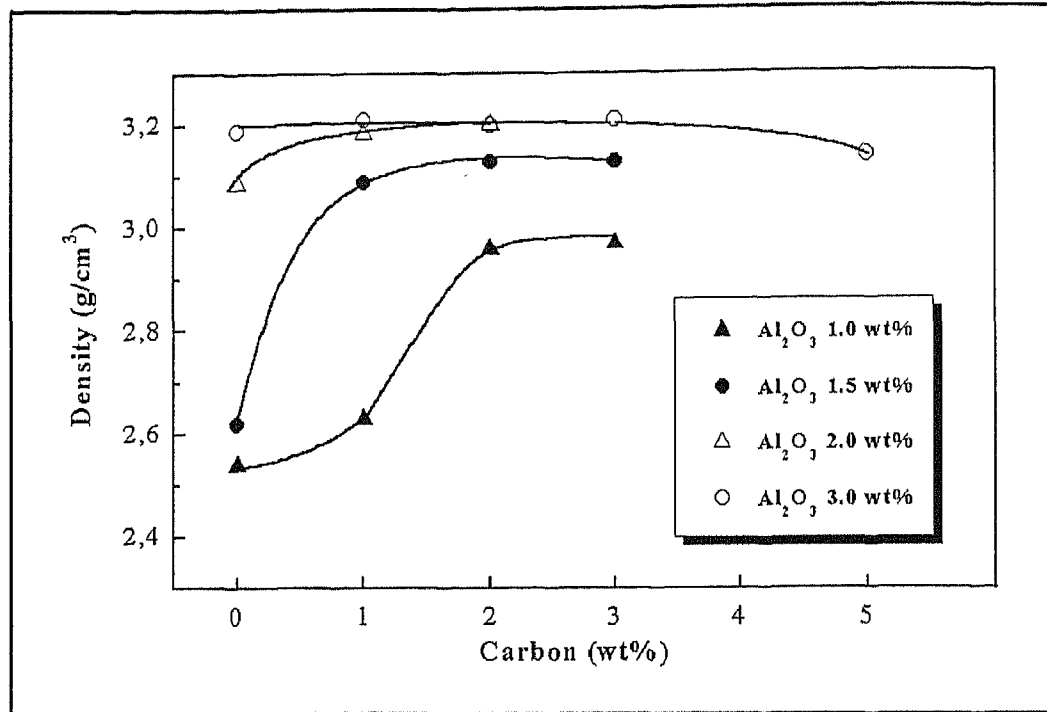


Figure 1.4: Effect of Al_2O_3 and carbon on sintered density of SiC (All specimens are hot-pressed at 2050°C for 30 mins) [29].

of AlN, although the sintering mechanism was not well understood by the authors[31]. Schoennahl *et al.*[32] in their extensive study found that dense SiC ceramic materials were produced by hot pressing of selected compositions in the systems Si-Al-C and Si-Ti-C. They observed that elemental Si, C or Al addition led to a considerable diminution of the hardness of the sintered samples. Addition of complex carbide Al_4SiC_4 or Ti_3SiC_2 to SiC aided in densification.

1.3 Liquid Phase Sintering

Liquid phase sintering has been extensively applied in order to obtain dense SiC ceramics. The innovative approach to sintering of SiC was initiated in early 1980s by Omori and Takei[33]. The major inspiration for the densification strategy used for SiC is adopting

the sintering procedures of Si_3N_4 with $\text{Al}_2\text{O}_3\text{-Y}_2\text{O}_3$ additive[34, 35, 36]. By doing so, superior self-reinforced SiC was fabricated successfully[37, 38]. Several sintering parameters were varied, and additives were added such that improved properties could be obtained. The advantage of using a liquid phase was that the silicon carbide, which was not easily sintered using conventional sintering aids, could be sintered to high densities(>95% TD) at temperatures well below 2000°C [39]. Another advantage of using liquid phase sintering was that SiC powder with higher oxygen content could be densified. The use of low sintering temperature and short sintering times also allowed to obtain fine grained materials with improved mechanical properties[39].

1.3.1 Effect of oxide additives

Pressureless sintering of silicon carbide powder with addition of oxide additives was first attempted by Omori and Takei[33]. Sintering was accomplished at 2100°C with oxide additives which were produced by the reaction of $\text{Al}(\text{OH})_3$ with HCl and of $\text{Y}(\text{OH})_3$ with HCOOH . In their study, they found that addition of Y_2O_3 additive did not promote densification. Al_2O_3 additions enhanced sintering, however equimolar additions of both the additives gave a denser material. In further studies, they[40] concluded that 3:5 ratio of binder additives were the optimum amount for sintering the β -SiC powder. It was suggested that the densification of SiC occurred by liquid phase of Al and Si which were produced by decomposition of $\text{Al}_2\text{Y}_4\text{O}_9$ above 2000°C and the gradual reaction with SiC. From Misra's[41] thermochemical analysis, it was concluded that SiC- Al_2O_3 system formed a liquid phase in the temperature zone of $1950\text{-}2150^\circ\text{C}$ (*Figure 1.5*). With free carbon, an eutectic melt would be likely to form even at a lesser temperature. These liquids helped the SiC to densify. Thus addition of both alumina along with some carbon as sintering aids would be beneficial.

Pressureless sintering of submicron SiC powder with the addition of aluminium oxide was also investigated by Suzuki[42]. He found that a sintered body with high density exceeding 97% of theoretical was obtained by the addition of at least 2 wt% Al_2O_3 . The densification proceeded via a liquid-phase sintering mechanism accompanied by a $\beta \rightarrow \alpha$ phase transformation and a reduction in the liquid phase. SiC with higher alumina content viz.15% did not densify after 10 hrs of holding. Lower alumina content viz.2% had less significant change in relative density. *Figure 1.6* shows the effect of alumina content and time on densification of silicon carbide. Sigl and Kleebe[43] investigated the densification

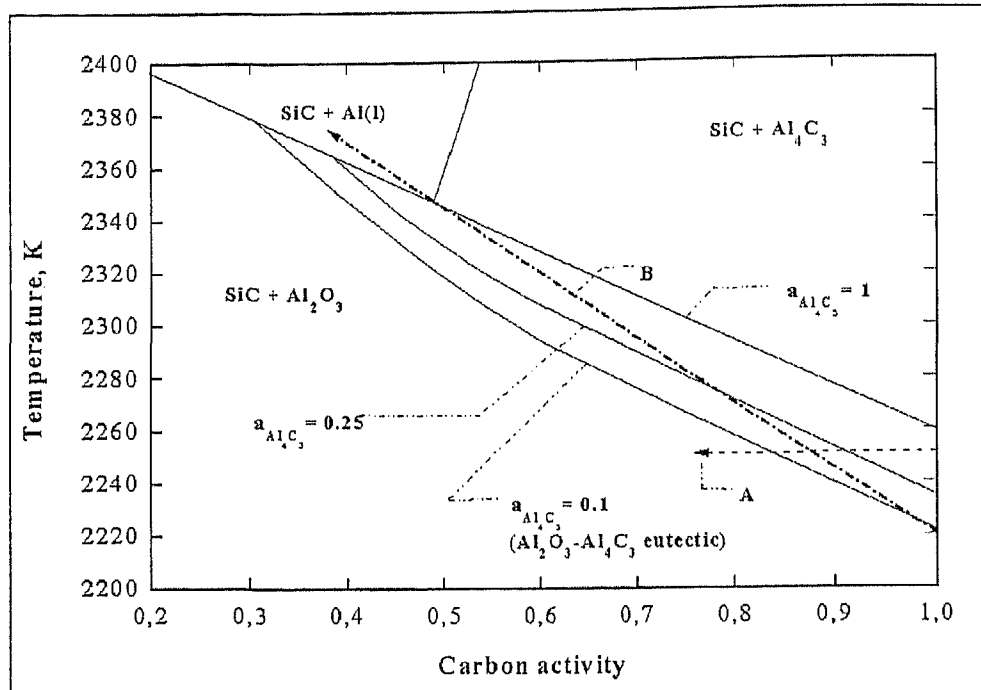


Figure 1.5: $\text{SiC}-\text{Al}_2\text{O}_3$ stability diagram for an ambient total pressure of 0.1 MPa showing the stability regions for the $\text{Al}_2\text{O}_3-\text{Al}_4\text{C}_3$ melt and the effect of the high vapour pressure of gaseous species on the stability of the melt: (A) Change in the melt composition due to the loss of the free carbon at a constant sintering temperature of 2250K; (B) Change in the melt composition as all of the free carbon is lost during the heating-up period for sintering at 2350K[41].

mechanism of silicon carbide using yttrium-aluminium garnet powder ($3\text{Y}_2\text{O}_3 \cdot 5\text{Al}_2\text{O}_3$). The core and rim structure in this system suggested that Ostwald ripening by solution and reprecipitation controls the sintering mechanism. Grande *et al.*[44] also investigated the $\text{Y}_2\text{O}_3-\text{Al}_2\text{O}_3$ additive systems and found that 7.5 wt% $\text{Y}_2\text{O}_3-\text{Al}_2\text{O}_3$ composition to SiC formed an eutectic and densification of SiC occurred by liquid phase sintering. It was reported that apart from alumina-yttria, relatively high density was, also, achieved by using several other rare-earth metal oxides, usually in combination with Al_2O_3 or boron compounds. Much lower sintering temperature viz. 1700-1800°C for SiC was observed by Mulla and Kristic[39], if a small amount of SiO_2 (only a few percent) was present in $\text{Al}_2\text{O}_3-\text{Y}_2\text{O}_3$ system (Figure 1.7). Thus a fraction of percent of oxygen was sufficient to reduce the temperature of liquid-phase formation.

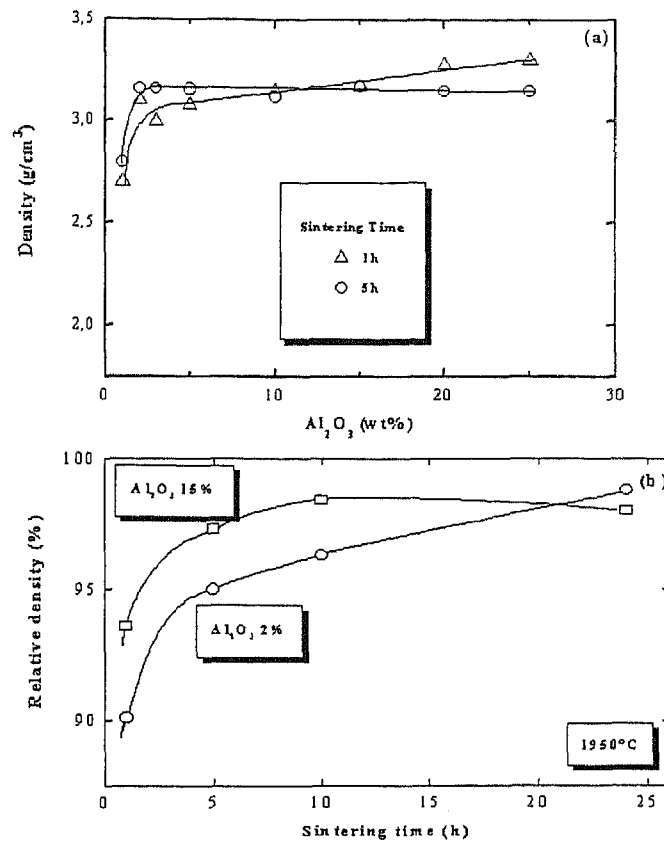


Figure 1.6: (a) Sintered density variation of SiC sintered at 2000°C for 1 and 5 hrs as a function of added amount of Al_2O_3 and (b) Sintered density variation of SiC as a function of sintering time. Sintered at 1950°C with 2% and 15% Al_2O_3 addition [42].

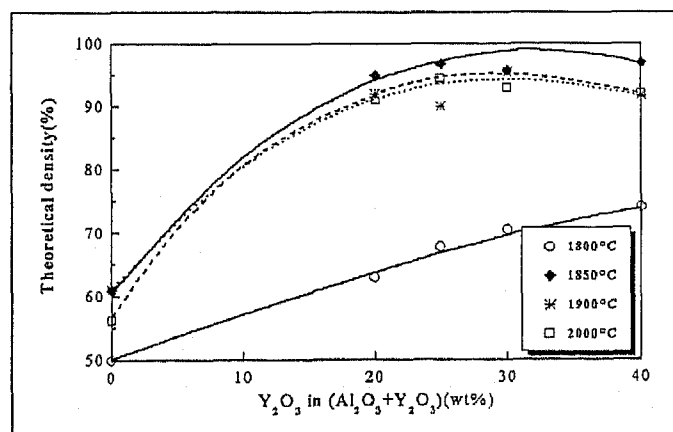


Figure 1.7: Change of sintered density of SiC with Y_2O_3 addition for samples containing 10 vol% $(\text{Al}_2\text{O}_3 + \text{Y}_2\text{O}_3)$ [39].

Lange[45] in his study observed that a liquid phase was responsible for the densification of SiC powder when Al_2O_3 was used as hot-pressing aid. However the composition of the liquid phase during densification was uncertain. The presence of SiO_2 and other impurities suggest the presence of an alumino-impurity-silicate phase. This fact was supported by the author as he reported that completely dense bodies were obtained at temperature(1800°C) which is less than the melting point of pure alumina. The mechanism was a rapid rearrangement during the initial period of pressure application and densification by a solution reprecipitation mechanism. Kim *et al.*[38] found that addition of Al_2O_3 - Y_2O_3 -CaO to β -SiC densified the compact to full density at 1750°C.

1.3.2 Effect of nitrides and other additives

The densification behaviour of β -SiC was investigated by Jun *et al.*[46] by adding AlN- Y_2O_3 as liquid phase sintering aids. It was reported that nitride phase or nitrogen atmosphere had a strong influence in terms of densification and grain growth behaviour of sintered body. *Figure 1.8* shows the effect of atmosphere and amount of sintering aids towards the densification of β -SiC sintered body. Lee and Wei[47] also observed the beneficial effect of AlN in liquid-phase-sintered SiC and found that the addition of AlN even improves the beneficial effects of yttria and/or alumina dopants. Nader[48] in his doctoral thesis also found the beneficial effect of N_2 atmosphere and concluded that 10 vol% additive with 60 mol% AlN and 40 mol% Y_2O_3 was the optimum although the eutectic point in the AlN- Y_2O_3 phase diagram lies at 40 mol% AlN and 60 mol% Y_2O_3 [49](*Figure 1.9*).

Other than nitride additives, B_4C , Al_4C_3 , etc are also reported as sintering aids for SiC. Lin *et al.*[50] studied the sintering behaviour of β -SiC powders with addition of Al, B and C and observed that a second phase ($\text{Al}_8\text{B}_4\text{C}_7$) was formed during hot pressing within the range of 1600°C to 1800°C with an applied pressure of 20 to 60 MPa. It was suggested that a liquid phase, which coexisted with this compound, enhanced densification. Suzuki[51] also reported on the densification of SiC by liquid phase sintering using aluminium and carbon. Stutz *et al.*[17] studied SiC sintering in presence of Al and B and reported that liquid formation that occurred in the system SiC- Al_4C_3 - B_4C at 1780 or 1860°C enhanced densification.

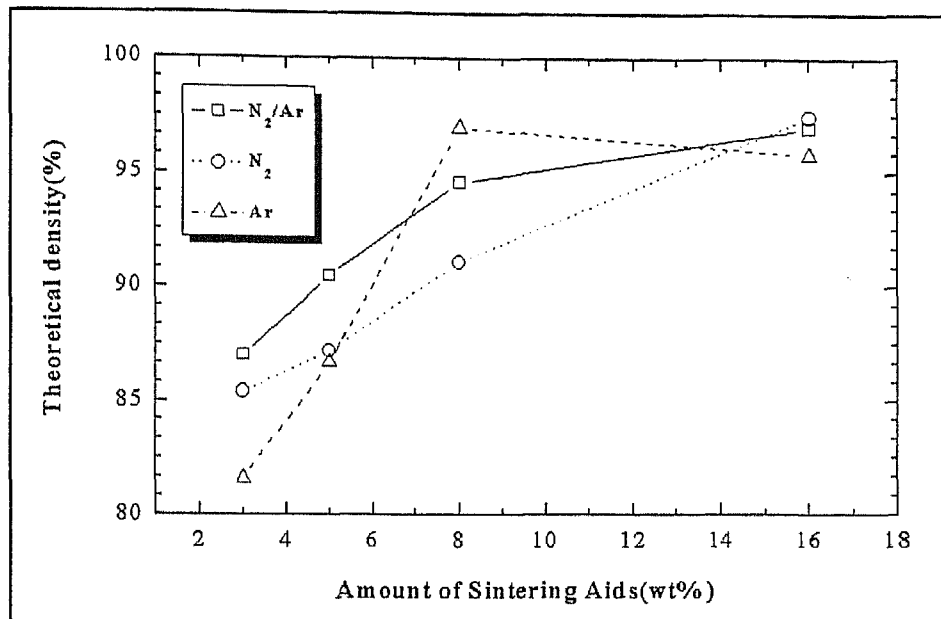


Figure 1.8: Plot of density versus amount of sintering aids for 95%SiC/5%AlN sintered at 2050°C for 1 hr in N₂, Ar and N₂/Ar[46].

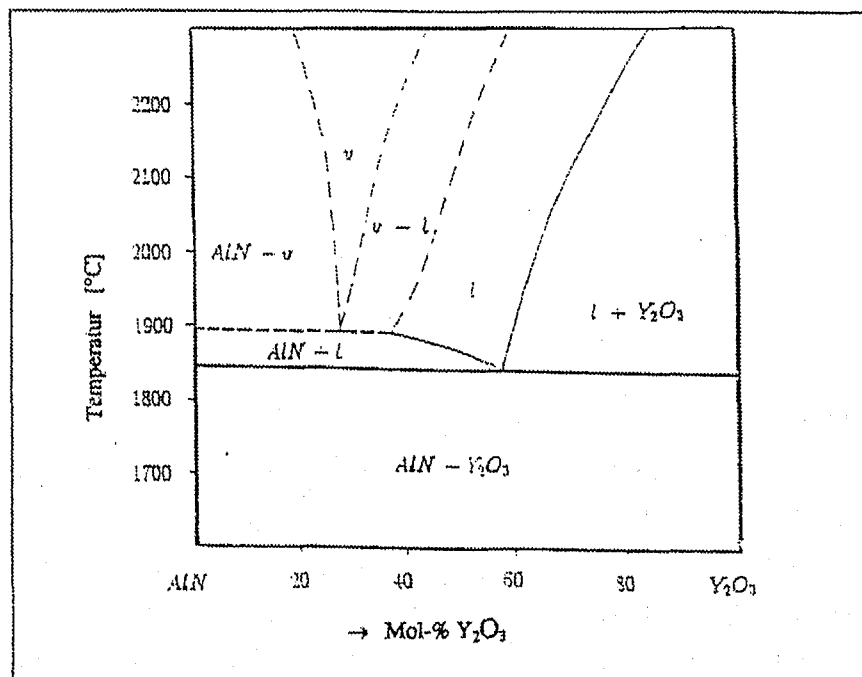


Figure 1.9: Quasibinary phase diagram of AlN-Y₂O₃[49].

1.4 Microstructural Aspects

1.4.1 Effect of B, Al and C

Pioneer work of Prochazka[13] on sintering and hot pressing of SiC with boron and carbon revealed that with boron addition, β -SiC frequently transformed into α -polytypes, mainly the 6H form. Grain growth occurred by a rate several orders of magnitude higher than the rate of grain growth of β -SiC. This phenomenon was undesirable as fine-grained microstructures were the desirable product. Hamminger *et al.*[52] investigated the microstructures of (B,C)- and (Al,C)-doped pressureless sintered SiC by wavelength dispersive X-ray analysis, Auger electron spectroscopy and microautoradiography. Clean grain boundaries were detected in (B,C)-doped materials, while (Al,C)-doped materials revealed the existence of thin Al-containing grain boundary films. In a similar type of study, Shinozaki *et al.*[53] and Greil *et al.*[54] found that addition of Al enhanced the β to α phase transformation and subsequent basal growth of α -SiC which prevented exaggerated grain growth. Homogeneous distribution of Al additive provided homogeneous fine α -platelets in SiC materials. Without Al additions, β -phase sheaths were observed in SiC grains which were very difficult to remove by heat treatment at higher temperature. Greil and Stutz[54] improved the microstructure of sintered β -SiC with 0.5 wt% B, 0.3 wt% Al and 1.5 wt% C by annealing between 1650-1850°C for 30mins before sintering at 2000°C. It prevented the formation of liquid phase which in turn hindered the polytype transformation and exaggerated grain growth.

1.4.2 Role of oxide additives

During pressureless sintering of SiC with alumina addition, Suzuki and Sasaki[55] observed fine plate-like interlocking grains. The grain growth proceeded predominantly within the direction of plates with increase in sintering time. *Figure 1.10* summarizes the three stages of microstructural development. The sintered body had no second phase along the grain boundaries, while aluminium oxide remained frequently at the triple points. Sasaki *et al.*[56], in a similar system, noted the presence of Si, C, Al, Ca and O on the surface of SiC grains with intergranular fracture mode (2 wt% Al₂O₃, 5 hrs sintering). Microstructural examination of β -SiC with addition of alumina-yttria revealed that most of the grains were uniform and equiaxed[39]. XRD pattern showed the presence of yttria-

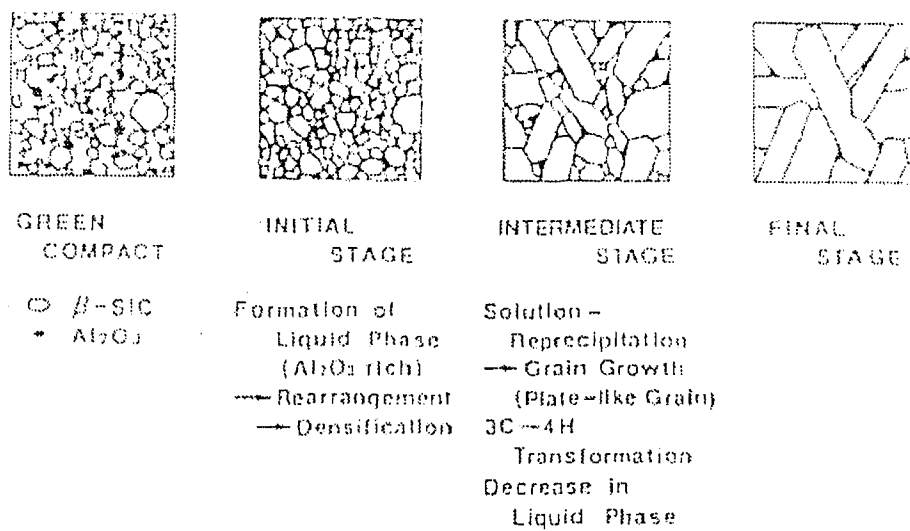


Figure 1.10: Schematic microstructure development of β -SiC with Al_2O_3 addition during pressureless sintering [55].

alumina-garnet eutectic liquid. β -to- α polytypes transformation was greatly reduced due to low temperature sintering. A polytype analysis of the relevant SiC peaks revealed that both the starting powder and the sintered body were dominated by the 6H structure[43]. It was also observed that an amorphous grain-boundary film was there between the SiC grains. Grande *et al.*[44] found that a homogeneous secondary phase formed during solid state sintering of SiC with Al_2O_3 - Y_2O_3 . Coarsening of this phase occurred with increasing sintering time. An inhomogeneous microstructure developed during sintering at 1820°C (LPS-SiC) and the secondary phase was identified as YAG crystal. Lee and Kim[57] studied the pressureless sintering of β -SiC and α -SiC powders with addition of Al_2O_3 - Y_2O_3 additives. The microstructure depended highly on the polytypes of the starting SiC powders. The microstructure of SiC obtained from α -SiC powder was composed of equiaxed grains, whereas SiC obtained from β -SiC powder was composed of a platelike grain structure resulting from the grain growth associated with $\beta \rightarrow \alpha$ phase transformation. Kim *et al.*[58] annealed the hot pressed β -SiC powders sintered with large seed grains of α -SiC or β -SiC at 1850°C and investigated the microstructural development. The introduction of large seeds($0.44\mu\text{m}$ as compared to $0.1\mu\text{m}$ β -SiC powders) accelerated the grain growth of elongated large grains during annealing, in which no appreciable $\beta \rightarrow \alpha$ phase transformation occurred. It was also observed that growth of matrix grains was slower in case of β -SiC seeds. A bimodal microstructure of small and large elongated grains was noted. In contrast, with α -SiC seeds, a uniform microstructure of elongated

grains was found. They concluded that further optimization of the microstructure could be possible with β -SiC seeds because of the remnant driving force for grain growth caused by the bimodal microstructure.

1.4.3 Effect of nitride and other additives

Rafaniello *et al.*[59] observed a phase separation leading to two phases of 2H wurtzite structure after annealing the hot pressed SiC-AlN samples below $\sim 2000^\circ\text{C}$. In a later work, Zangvil and Ruh[60] showed that at $2100\text{--}2300^\circ\text{C}$, the 4H solid solution was stable upto 14 mol% AlN and above 23 mol% AlN, 2H(δ) solid solution was stable.

The system AlN-Al₂O₃ was investigated by Kuo and Virkar[61] and they also observed a homogeneous solid solution to undergo phase separation when annealed at temperatures lower than $\sim 1900^\circ\text{C}$. The two phases formed here were also of 2H type of structure but with different compositions.

Both of the systems exhibited the formation of either a modulated structure or very uniform sized precipitates. The morphology of phase separation in these two systems was originally investigated by Kuo *et al.*[62, 63]. In the SiC-AlN system, a basket-weave type of morphology was observed. Whereas in the AlN-Al₂O₃ system, the morphology consisted of disk-shaped precipitates. The difference in morphology between the two systems was attributed to the orientation-dependent elastic energy function using the approach of Mayo and Tsakalakos[64]. Chen *et al.*[65] also observed the effect of coherency strain energy in the SiC-AlN pseudobinary system. Modulated, coherent, tweed-type structures were found at equimolar composition in the SiC-AlN system when annealed between $1600\text{--}1900^\circ\text{C}$. It was concluded that phase separation in this system under the conditions of composition and annealing temperature occurred by spinodal decomposition. In recent studies on the SiC-AlN-Y₂O₃ system, Nader[48] and Wiedmann[66] found that after sintering in N₂ atmosphere, the phases present in the system were mostly β -SiC(3C-polytype) with some existence of Y₁₀Al₂Si₃O₁₈N₄. They also noticed that after prolonged annealing of 16 hrs at 1950°C , all the β -SiC transformed into α -SiC of mostly 6H and 4H polytypes whereas the Y₁₀Al₂Si₃O₁₈N₄ decomposed into some oxide phases.

Sintering atmosphere effect on microstructure evolution in hot-pressed SiC was investigated by Jun *et al.*[46]. The microstructure consisted mainly of equiaxed grains regardless of sintering atmosphere and addition of AlN. However in annealed samples,

growth of large elongated grains was observed although the total amount of growth was not much due to grain growth inhibition by N_2 after 12 hrs annealing. N_2 atmosphere significantly retarded the $\beta \rightarrow \alpha$ transformation.

1.5 Mechanical Properties

1.5.1 Strength

The strength of SiC depends on a number of factors, including mechanical testing method, strain rate, temperature, impurity level, inclusion distribution, and in some cases on the orientation of the test specimen relative to the original material[67]. It was reported that surface flaws drastically lowered the strength, which increased with increasing density of the sintered body. A study on the influence of the mechanical testing method revealed that the values of strength measured in tension were lower than those obtained in bending because a large volume of material was tested. Although bending strength was independent of orientation of the test specimen, higher values were obtained in the pressing direction of hot pressed SiC[67]. Inclusions played a significant role in determining the strength of fully dense material as these inclusions were the crack initiating regions. The temperature dependence of the strength of hot pressed SiC containing B additions had been measured by Prochazka and Charies[68]. Edington *et al.*[67] also reported the variation of bend strength with temperature in hot pressed SiC(*Figure 1.11*).

Dutta[69, 70] in an extensive study noted that room-temperature strengths were somewhat higher than at 1370°C. Surface oxidation at 1370°C was found to be responsible for this. Addition of boron and carbon were found to be impartial to room temperature flexural strength of α -SiC while the strength at 1370°C was lower than the strength of commercial sintered α -SiC. Similarly, bending strength was lower at 1400°C than as room temperature in case of both 2 wt% and 15 wt% Al_2O_3 added SiC[55]. However, bending strength showed a tendency to increase with sintering time in case of 2 wt% and 15 wt% Al_2O_3 . Jun *et al.*[46] reported the effect of addition of AlN, TiN additives and atmosphere on the flexural strength. When the sintering was carried out in N_2/Ar atmosphere, subsequently improved flexural strength SiC was obtained due to higher sintered density and fine grain size. AlN addition also showed a similar influence on the flexural strength. Bending strength increased with the amount of sintering aids. Maximum

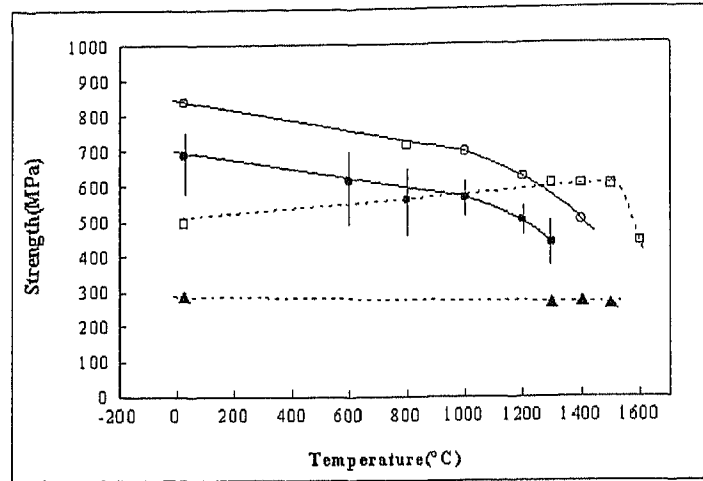


Figure 1.11: The variation of bend strength with temperature in hot pressed SiC. The open circles are three point bend data, while the closed circles are for four point measurements. The open squares are the best boron containing material while the closed triangles are the same material but containing coarse α -grains[67].

average strength of 953 MPa was obtained in the N_2/Ar -sintered sample with 16% sintering aids. This value was much higher as compared to conventional Ar-sintered SiC[46]. Keppeler *et al.*[71] also investigated the high temperature bending strength behaviour and concluded that the globular LPS-SiC material showed an increase of strength in the temperature between 1000°C to 1200°C due to healing of flaws and surface cracks by a glassy phase formed by oxidation. Higher strength will be achieved by maximizing fracture toughness and minimizing the size of defects through improved manufacturing processes[1].

1.5.2 Fracture toughness

The value of K_{IC} for SiC had been shown[72] to increase with decreased grain size and optimum fracture toughness was obtained for grain sizes less than $10\mu m$. Schwetz and Lipp[73] determined the value of K_{IC} at room temperature and at 1200°C using the SENB-method for the additive systems B+C and Al+C. The result showed that room temperature K_{IC} of both materials were identical. However with increase in temperature the value of fracture toughness also increased, and this was much more predominant in the

B+C system. Grathwohl *et al.*[74] also investigated a similar system and found that all materials exhibited a moderate resistance against static fatigue at 1300°C. The fracture mode was found to be clearly different for B+C and Al+C additive systems.

Suzuki and Sasaki[55] reported the K_{IC} values of sintered SiC with 2% and 15% Al_2O_3 and found that K_{IC} increased with sintering time. After 24 hrs of sintering, the sintered SiC with 15% Al_2O_3 revealed a K_{IC} of 5.7 MPa.m^{1/2} which was twice the fracture toughness of B-doped sintered α -SiC (2-3 MPa.m^{1/2})[75]. This value was also higher than K_{IC} of 3-4 MPa.m^{1/2} for an Al_2O_3 -fluxed hot pressed SiC[75]. The K_{IC} values strongly depended on the aspect ratio of the grains. Higher aspect ratio increased the K_{IC} value owing to the morphology with interlocking platelike grains. Improved fracture behaviour of novel SiC ceramics having rodlike grains was observed by Kodama and Miyoshi[76]. They concluded that the fracture toughness of these ceramics was better than that of ordinary SiC and its maximum value was 7.3 MPa.m^{1/2}. Grain pullout, grain bridging and crack deflection were considered to be the main operative mechanisms which led to improved fracture toughness. Based on the above principle, Lee *et al.*[57] and Cao *et al.*[77] toughened the SiC sintered material. Lee and Kim[57] showed that with α -SiC powder, the fracture toughness increased slightly whereas in case of β -SiC powder, it increased significantly which was attributed to crack bridging and crack deflection by the platelike grains. Keppler *et al.*[71] also observed a similar mechanism in 99% β -SiC, 1% α -SiC, although they consider pullout of platelets was not a toughening mechanism as platelet grains with an orientation normal to the crack propagation were broken without any debonding.

1.5.3 Creep and high temperature strength

Creep of SiC between 1900°C and 2200°C has been investigated[78, 79] in hot pressed materials and it was concluded that the creep of these forms of SiC was controlled by grain boundary diffusion, probably by carbon. The creep properties of SiC sintered bodies containing Al were somewhat different from those of bodies produced using B-C system sintering additives. It was observed that the high temperature creep rate was much higher than for those not containing Al[23] because diffusion of the materials was accelerated by the aluminium. Suzuki and Sasaki[55] confirmed that the SiC with addition of Al_2O_3 had higher creep rupture resistance upto 1200°C in air than B-doped sintered α -SiC.

Yamada and Mohri[1] reviewed that SiC possessed better high-temperature strength at temperatures above 1000°C than any other materials, including metals. There was a tendency for the strength of SiC to increase at high temperatures, and stress relaxation at the crack tip was reported as a possible responsible mechanism.

1.5.4 Fatigue resistance

Suzuki[42] reported the results of static and low-cycle fatigue tests for Al₂O₃ doped SiC. It was observed that in the static fatigue test, the load stress-time to rupture curve was virtually horizontal upto 1200°C, the number of fatigue cycle(N) was 100 or more and there was no evidence of slow crack growth.

Another work[80] on such material exhibited an N value of 27 at 1200°C accompanied by fatigue. A drop in N value(N = 27) and slow crack growth were also observed for Al₂O₃-added pressureless sintered SiC at 1400°C. The results of low cycle fatigue test were similar to those of the static fatigue test, indicating the superior fatigue resistance of SiC sintered bodies.

1.6 Oxidation Resistance

Suzuki[42], in his review, reported the oxidation-induced weight gain and change in strength before or after oxidation of HIPed SiC. It was found that at 1200°C and 1300°C weight gain increases linearly with oxidation time and the kinetics are parabolic upto 1000 hrs. It was also noticed that although room-temperature strength dropped by 11%, there was no change in 1300°C strength after oxidation for 1000 hrs.

It was further concluded that the lower the alumina content, the better the resistance to oxidation. A sintered body with density of at least 99% and containing less than 3 wt% Al₂O₃ exhibited superior oxidation resistance, with a weight gain of less than 1 mg/cm² after oxidation for 1000 hrs at 1300°C[42].

Chapter 2

Chapter 2

Experimental Procedure

2.1 Preparation of LPS-SiC Ceramics

2.1.1 Raw materials and greenbody fabrication

The starting materials used to fabricate green bodies were commercially available α -SiC, β -SiC, β' -SiC, AlN and Y₂O₃ powders. The characteristics of these powders are given in Table 2.1.

Table 2.1: Characteristics of initial powders

Powder	Manufacturer	Chemical analysis	Size distribution			Specific area m ² /g	Density g/cm ³
			d ₁₀ [μ m]	d ₅₀ [μ m]	d ₉₀ [μ m]		
α -SiC	A-10,H.C.Starck Goslar,Germany	C-30.0,O-0.9, Al-0.03,Ca-0.01, Fe-0.05	0.18	0.51	1.43	11.1	3.22
β -SiC	BF-12,H.C.Starck Goslar,Germany	C-30.0,O-1.2, Al-0.05,Ca-0.005, Fe-0.03	0.25	0.89	3.5	17.8	"
β' -SiC	E-hp,H.C.Starck Goslar,Germany	—	—	—	—	—	"
AlN	Grade C,H.C.Starck Goslar,Germany	N-30.0,C-0.1 O-2.5,Fe-0.005	0.34	0.92	3.07	5.0	3.26
Y ₂ O ₃	Grade C,H.C.Starck Goslar,Germany	Al-0.005,Ca-0.003 Fe-0.005	1.21	4.48	8.08	12.9	5.02

Compositional variation was done on the basis of initial $\alpha : \beta$ -SiC ratio, additive contents and the molar ratio of AlN to Y_2O_3 in the additive system. Different powder specifications are listed in Table 2.2.

Table 2.2: Specifications of the starting powders

Powder (symbol)	SiC (vol%)	Additive (vol%)	α -SiC: β -SiC (mol%)	AlN: Y_2O_3 (mol%)
90 β /10A/20AlN	90	10	10:90	20:80
90 β^* /10A/20AlN	90	10	10:90	20:80
90 β /10A/40AlN	90	10	10:90	40:60
90 β /10A/60AlN	90	10	10:90	60:40
90 β /10A/80AlN	90	10	10:90	80:20
90 β /8A/60AlN	92	8	10:90	60:40
90 β /7A/60AlN	93	7	10:90	60:40
96 β /10A/60AlN	90	10	4:96	60:40
90 β -10 β' /10A/60AlN	90	10	10 β' :90 β	60:40

β^* = Ibidem β -SiC Powder
 β' = Coarse Grained β -SiC

The powder mixtures were prepared by attrition milling in isopropanol with Si_3N_4 milling media for 4 hrs using a polyethylene container and stirrer. The slurry was separated from the milling media via a sieve chain and subsequently dried in a vacuum evaporator. Completely dried powders were obtained after 15 hrs of drying at 60°C in a drying oven. The processed powders were then sieved to obtain granules with a maximum size of 160 μ m and cold isostatically pressed at a pressure of 240MPa. The preparation method is schematically represented in Figure 2.1.

2.1.2 Sintering and HIPing

Sintering was performed in a gas pressure furnace(KCE Kessel GmbH) with a graphite heating element in a nitrogen atmosphere. Heating was performed at a rate of 20°C/min from room temperature to 1500°C and there-after at 10°C/min to the sintering temperature. Selection of the sintering temperature depends on the powder system. The main

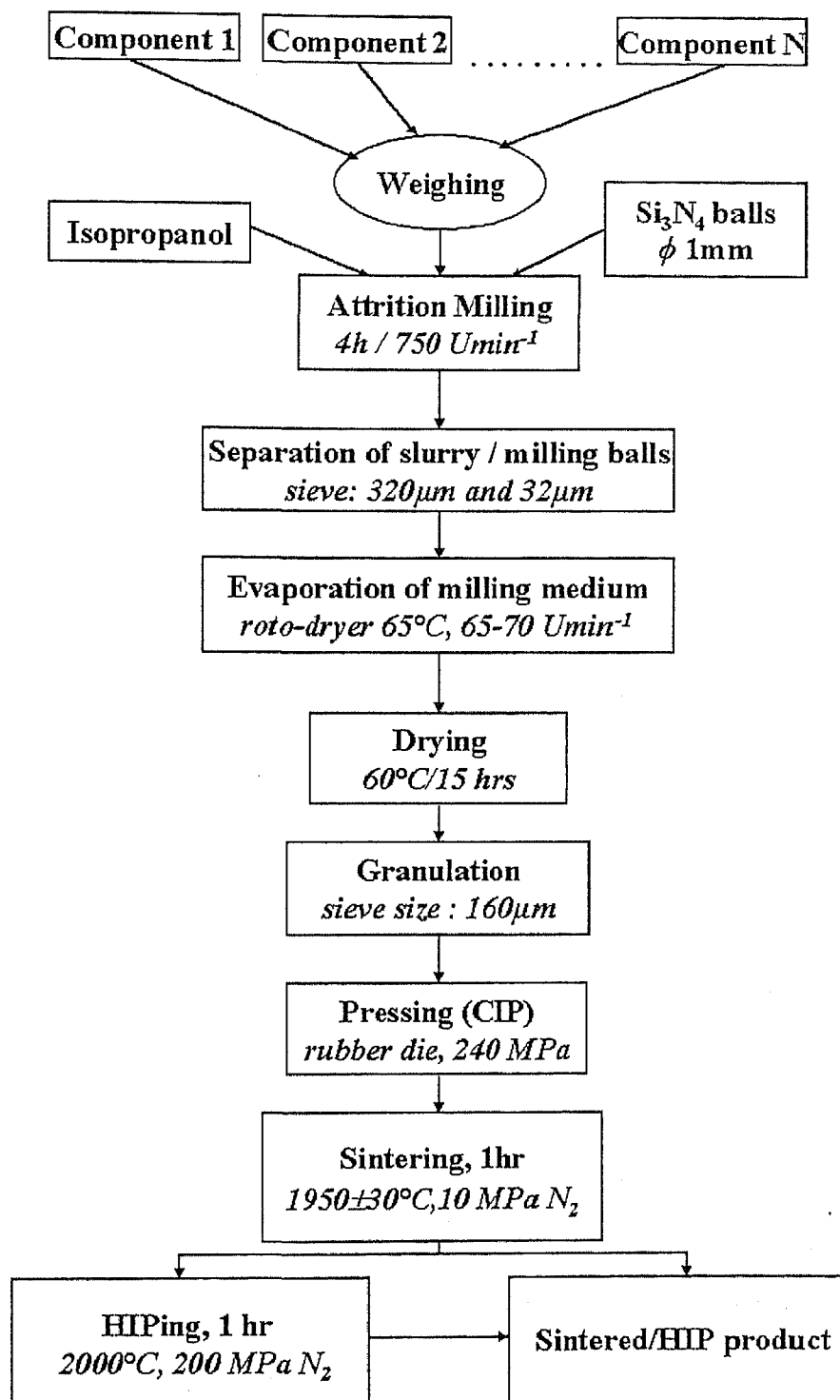


Figure 2.1: Schematic diagram of sample preparation method.

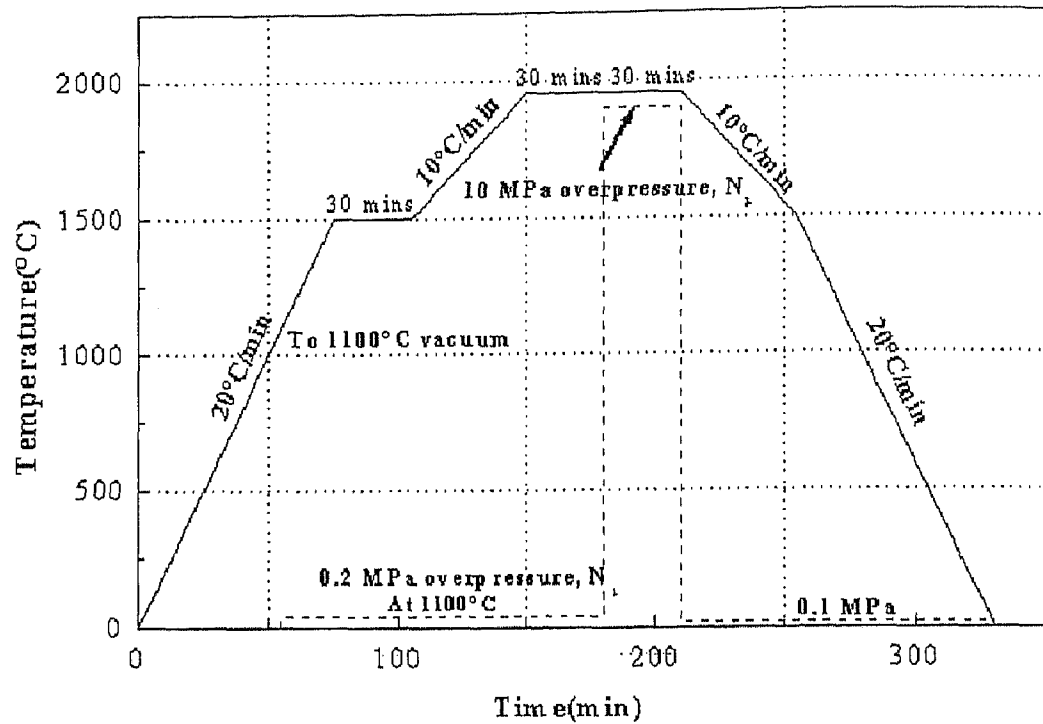


Figure 2.2: Schematic diagram of sintering cycle.

objective of the selected sintering temperature was to get fully dense samples. A first stage of sintering was carried out under a slight N_2 overpressure (0.2 MPa) for 30 mins, followed by a pressure sintering cycle of 30 mins at the same temperature under 10 MPa N_2 to achieve complete densification. A schematic diagram of the sintering cycle is shown in Figure 2.2. Hot Isostatic Pressing was done for the samples containing 20 vol% AlN as they were hard to sinter. HIPing was done at 2000°C for 1 hr at an N_2 overpressure of 200 MPa.

2.1.3 Annealing treatment

Annealing schedules were followed in a gas pressure furnace (Astro Industries, CA) in N_2 atmosphere. The specimens were kept in a BN-crucible and annealed at 1950°C for different times to obtain complete $\beta \rightarrow \alpha$ -SiC phase transformation. The heating and cooling rates were kept at 10°C/min.

2.2 Characterization of the Ceramics

2.2.1 Sinter density and mass loss

The sinter densities were measured using Archimedes' water displacement method:

$$\rho_s = \frac{m_s \cdot \rho_w}{m_s - m_w} \quad (2.1)$$

where ρ_s = sinter density (g/cm³)

ρ_w = density of water at room temperature(g/cm³)

m_s = mass of the sintered body(g)

m_w = mass of the sintered body in water(g)

The relative densities(ρ_{rel}) were calculated by dividing the sinter density(ρ_s) with the theoretical density(ρ_{th}). The theoretical densities were calculated from the rule of mixtures.

Mass losses(Δm) of the specimens were measured by using the following formula:

$$\Delta m = \frac{m_G - m_s}{m_G} \cdot 100 \quad (2.2)$$

where m_G = mass of the green body(g)

2.2.2 X-ray diffractometry

Sintered and annealed samples were cut and ground to fine powder to do qualitative phase analysis using the X-ray diffraction(Siemens D5000, Cu K $_{\alpha}$ radiation, $\lambda=1.5406\text{\AA}$) technique. The X-ray diffraction patterns were analyzed by using Siemens DIFFRAC-AT software to obtain the phases present in the system and to measure the extent of $\beta \rightarrow \alpha$ conversion. Percentage of α -SiC obtained after annealing was calculated from the ratio of the relative intensities of the (101) reflection of the α -SiC polytype 6H (F) and the SiC reflection with maximum intensity(F_{max}), followed by comparison of that ratio with the calibration curve(*Figure 2.3*) established by Nader[48].

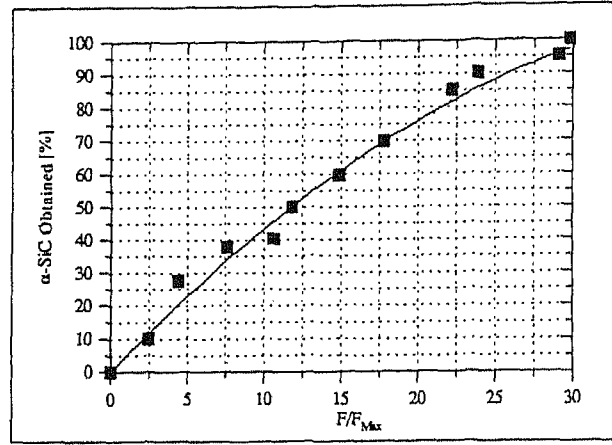


Figure 2.3: Percentage α -SiC obtained as a function of intensity ratio[48].

2.2.3 Metallography

For scanning electron microscopy observations, the specimens were Cu-resin mounted (Resin II, Wirtz) and polished in a semi-automatic polishing machine (Pedemax II, Struers). At first, mounted samples were ground with a diamond wheel ($60\mu\text{m}$) to flatten the surface. Polishing was done using the diamond suspensions DP-PLAN of size $15\mu\text{m}$ and DP-DAC of sizes 6, 3 and $1\mu\text{m}$. After polishing, specimens were dismounted and plasma etched using an RF Plasma Barrel Etcher PT7150 (Biorad Laboratoric GmbH, Munich, Germany) for 3-3.5 min in a mixture of CF_4 and O_2 in 1:1 ratio.

2.2.4 Microstructural analysis

Microstructures of the initial powders, sintered and annealed specimens were examined with scanning electron microscopes of type DSM 982 GEMINI, Zeiss and type S200, Cambridge Instruments. Grain size and aspect ratio were measured by use of an image analysis software (IMAGE C, Imtronic GmbH).

2.3 Mechanical properties evaluation

Mechanical characterization was done on the basis of room temperature indentation fracture toughness of sintered and annealed samples, 4-point bending strength of sintered

specimens at room temperature and at high temperature(1000°C, 1200°C, 1400°C and 1500°C).

2.3.1 Room temperature fracture toughness

Fracture toughness was determined by using the Indentation Method. The samples were polished down to 1 μ m and mounted in a specimen holder. For each specimen, 12 indentations were made by a Vickers Indentor with a load of 5kg at a constant loading speed of 70 μ m/s and loading time of 15 sec. Measuring the crack length and diagonals of the indentation, a software allows to calculate the fracture toughness value using the following formula:

$$K_{IC} = 0.16\sqrt{\frac{E}{H}}.F.L^{3/2} \quad (2.3)$$

where E = Elasticity modulus, taken as 400GPa for SiC ceramics

H = Vickers hardness(GPa)

L = crack length(μ m)

F = load(N)

The hardness(H) was calculated by the formula:

$$H = \frac{1.8544F}{d_H^2} \quad (2.4)$$

where d_H = diagonals of Vickers indentation(μ m)

2.3.2 Bending strength

Four-point bending strength measurements of as sintered specimens were performed at room temperature and at high temperatures between 1000°C to 1500°C in air. For strength measurements, bar shaped samples were cut and ground to a size of 3 \times 4 \times 50mm³. The tensile surface of the test specimens was polished to 3 μ m diamond finish and the tensile edges were blunted to avoid stress concentrations and large edge flaws caused by sectioning.

Room temperature testing was accomplished with a testing machine(Schenck, Hydropuls PSA 2017, Darmstadt, Germany) with a cross head speed of 5 mm/s. For each

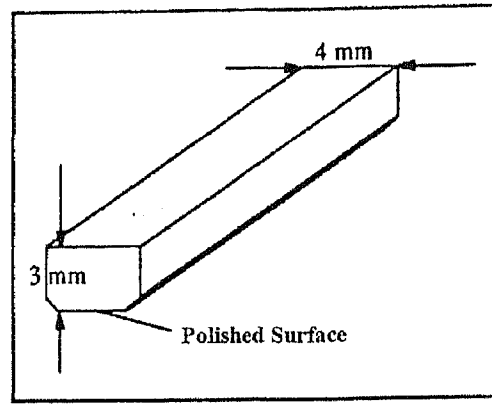


Figure 2.4: Schematic drawing of 4-point bending strength specimen.

composition, at least 6 specimens of the dimension 3mm×4mm×50mm(see Figure 2.4) were tested. Special care was taken during specimen preparation in order to avoid any occurrence of surface flaws.

High temperature tests were performed at 1000°C, 1200°C, 1400°C and 1500°C with a Zwick 1476 testing machine. The specimens were heated up at a rate of 10°C/min upto 50°C below the testing temperature and then at a rate of 5°C/min to the testing temperature. This heating profile was followed in order to avoid thermal shock. A dwell time of 10 mins was allowed to ensure a homogeneous temperature when tested. The specimens were loaded with a constant cross head displacement rate of 0.1 mm/s.

The bending strength was calculated according to formula:

$$\sigma_{4P} = \frac{3}{2} \cdot \frac{F(l_o - l_i)}{bh^2} \quad (2.5)$$

where σ_{4P} = 4-point bending strength(MPa)

F = Force(N)

l_o = length between the two outer supports(40mm)

l_i = length between the two inner supports(20mm)

b = breadth of the specimen(mm)

h = height of the specimen(mm)

Chapter 3

Chapter 3

Results and Discussion

3.1 Characteristic properties

3.1.1 Sinter density and mass loss

Average sinter densities and mass losses of all the materials are reported in *Table 3.1*. The

Table 3.1: Sinter density and mass loss data

Sample	Densification operation	Temperature (°C)	N ₂ -pressure (MPa)	Avg mass loss δm (%)	ρ_{theo} (g/cm ³)	ρ_{sample} (g/cm ³)	ρ_{rel} (%)
90 β /10A/20AlN	Sintering(run-1)	2020	10	0.95	3.36	3.11	92.7
90 β^* /10A/20AlN	"	2010	"	1.50	3.36	3.23	96.1
90 β /10A/20AlN	Sintering(run-2)	2020	"	1.30	3.36	3.13	93.1
90 β^* /10A/20AlN	"	2030	"	1.60	3.36	3.20	95.2
90 β /10A/20AlN	HIPing	2000	200	-1.47	3.36	3.30	98.2
90 β^* /10A/20AlN	"	"	"	-0.36	3.36	3.34	99.4
90 β /10A/40AlN	Sintering	1975 \pm 5	10	2.25	3.34	3.33	99.7
90 β /10A/60AlN	"	1945	"	1.90	3.32	3.34	100.6
90 β /10A/80AlN	"	2000	"	2.28	3.28	3.30	100.5
90 β /8A/60AlN	"	2020	"	2.60	3.29	3.31	100.5
90 β /7A/60AlN	"	2020	"	3.05	3.28	3.29	100.3
96 β /10A/60AlN	"	1980	"	2.50	3.32	3.33	100.3
90 β -10 β' /10A/60AlN	"	1980	"	2.40	3.32	3.33	100.3

results show that, in case of 90 β /10A/20AlN and 90 β^* /10A/20AlN, both materials were not fully dense after sintering as well as after HIPing. SEM micrographs (*Figure 3.1*) of HIPed samples revealed residual porosity distributed within these two materials. It is

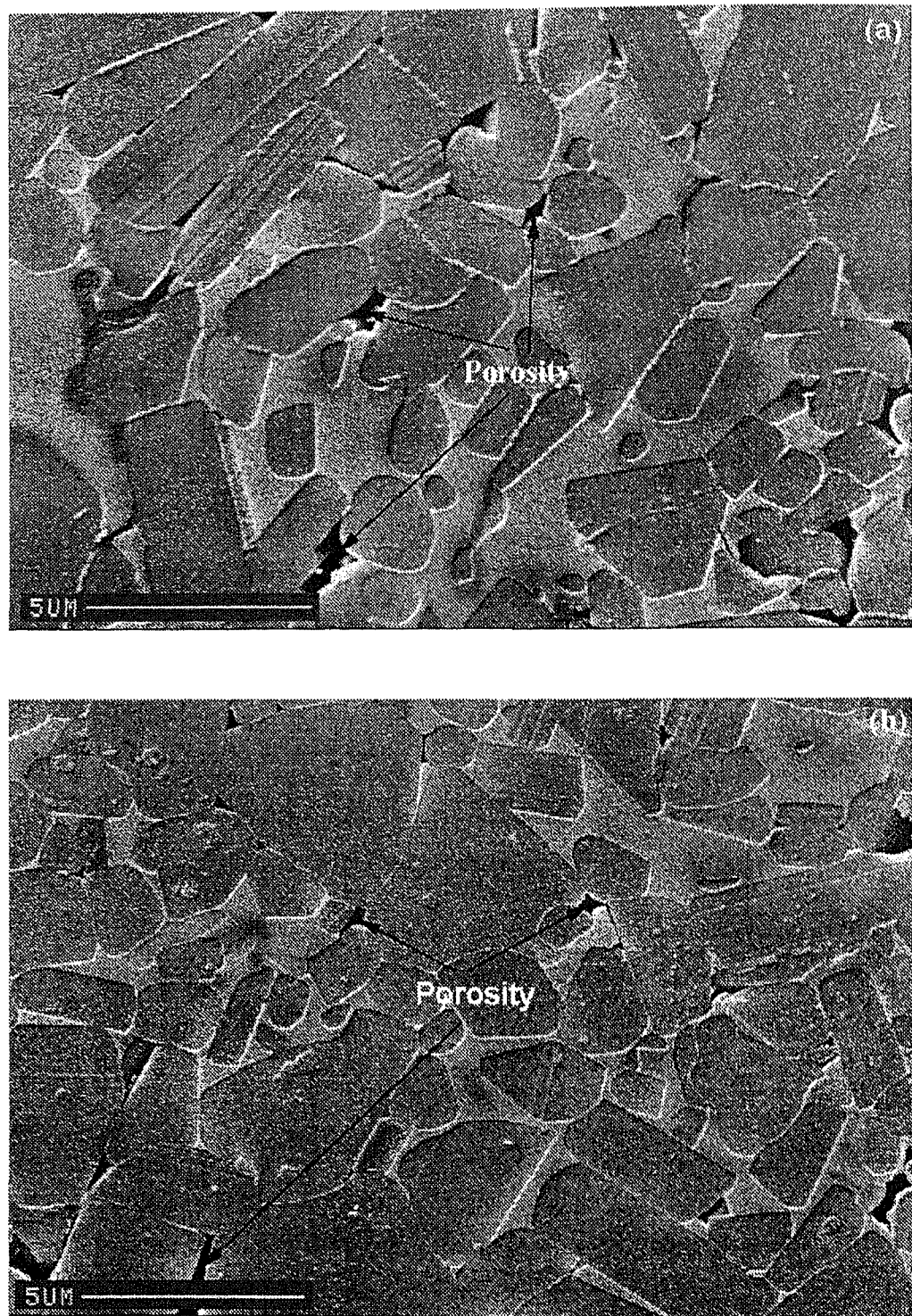
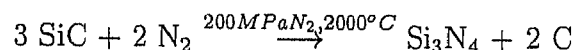


Figure 3.1: SEM micrographs of Hot Isostatic Pressed material; (a) $90\beta/10A/20AlN$ and (b) $90\beta^*/10A/20AlN(\times 5000)$.

presumed that inherent glassy phase composition was the prime controlling parameter for non sinterability of these materials. HIPing was also not fruitful to overcome this problem. Probably, during HIPing at a very high N_2 pressure of 200MPa, some SiC transforms into Si_3N_4 chiefly by the following reaction:



This leads to excessive porosity. In XRD patterns of these two materials the existence of some free carbon and silicon nitride confirms the above reaction (see later section for XRD patterns).

3.1.2 X-ray diffractometry

X-ray analyses of all the samples were done at each step of annealing to observe the gradual phase change and also $\beta \rightarrow \alpha$ -conversion as a function of annealing time. *Figure 3.2* represents the XRD-pattern of HIPed material. Phase analysis reveals the existence of C and Si_3N_4 which were formed during HIP operation. *Figure 3.3, 3.4 and 3.5* represent typical X-ray diffraction patterns of 90 β /10A/60AlN, 90 β /7A/60AlN and 90 β -10 β' /10A/60AlN materials. In general, it was observed that after annealing treatments, most of the silicon polytypes transformed into the 6H-polytype. Beside this, the grain boundary phases which are mostly oxinitride phases transform primarily to oxide phases due to loss of nitrogen at $\sim 1950^\circ\text{C}$. The most important phases found in this system are reported in *Table 3.2*.

Gradual transformation from β -SiC to α -SiC was calculated as a function of annealing time and presented in the *Figure 3.6*. It was observed that material with 60AlN and 10 α -SiC seed, complete transformation from β -SiC to α -SiC occurs within 6 to 10 hrs of annealing at 1950°C . However, starting with no α -SiC seed results in only 54% conversion after 20 hrs of annealing.

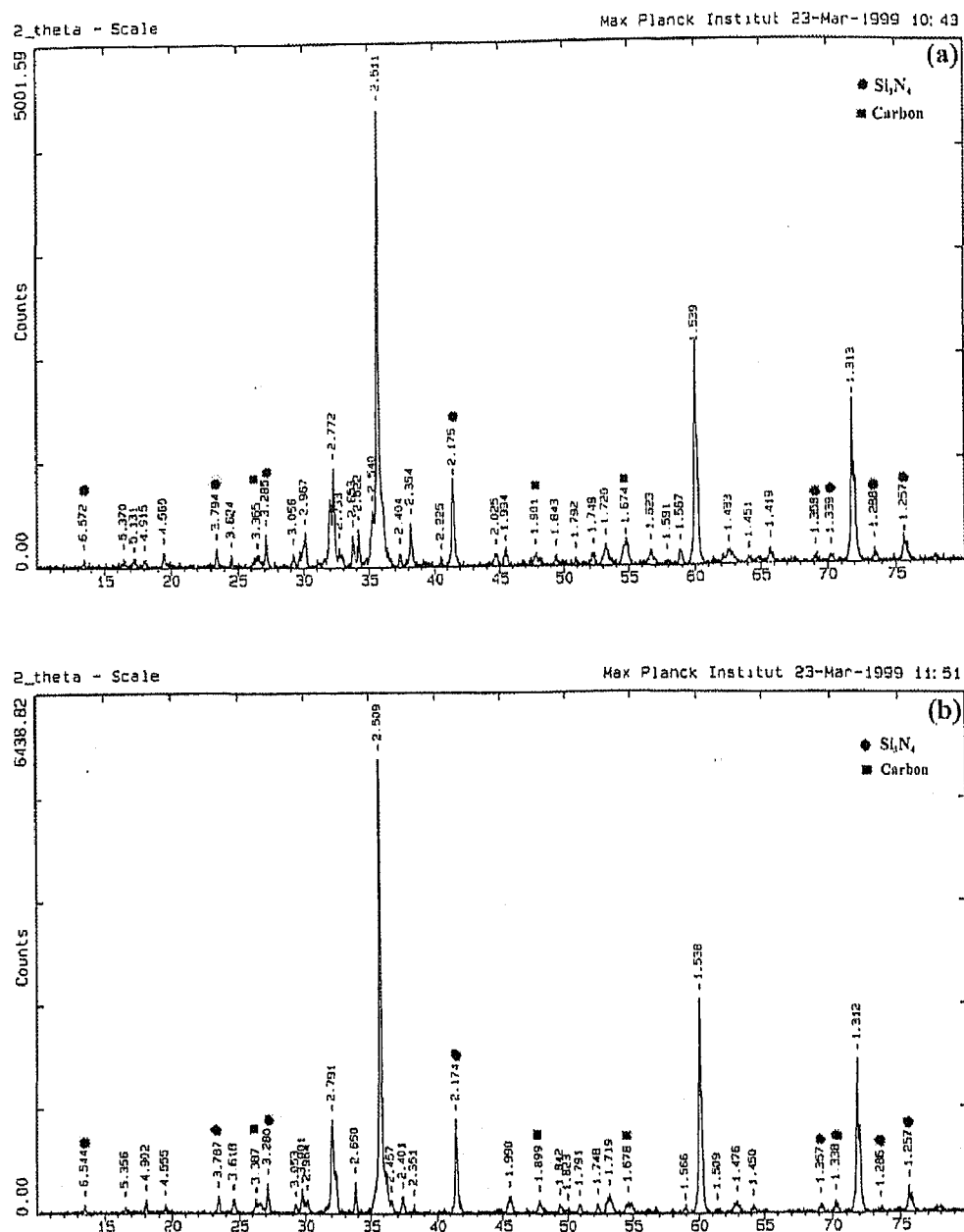


Figure 3.2: X-ray diffraction pattern of hot isostatically pressed material; (a) 90β/10A/20AlN and (b) 90β*/10A/20AlN.

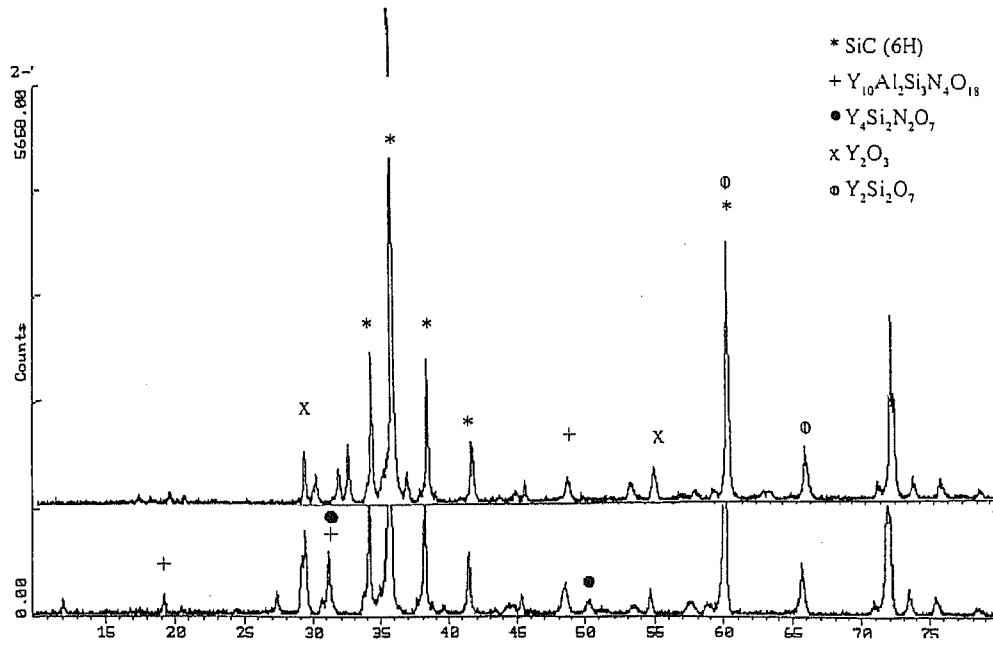


Figure 3.3: X-ray diffraction pattern of 90β/10A/60AlN sample.

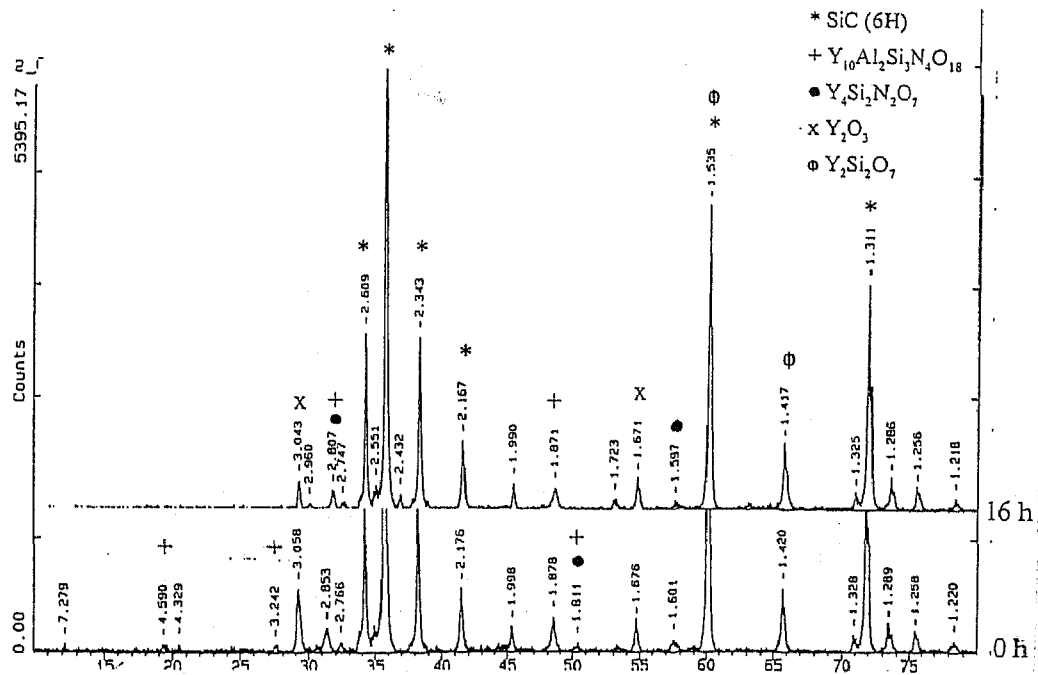


Figure 3.4: X-ray diffraction pattern of 90β/7A/60AlN sample.

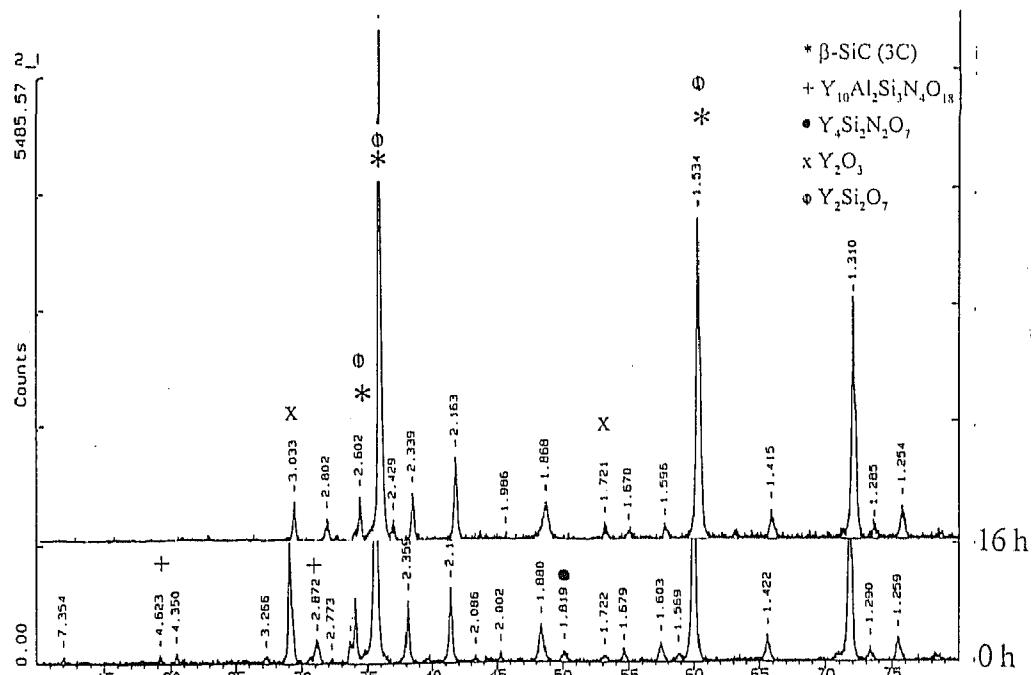


Figure 3.5: X-ray diffraction pattern of 90β-10β'/10A/60AlN sample.

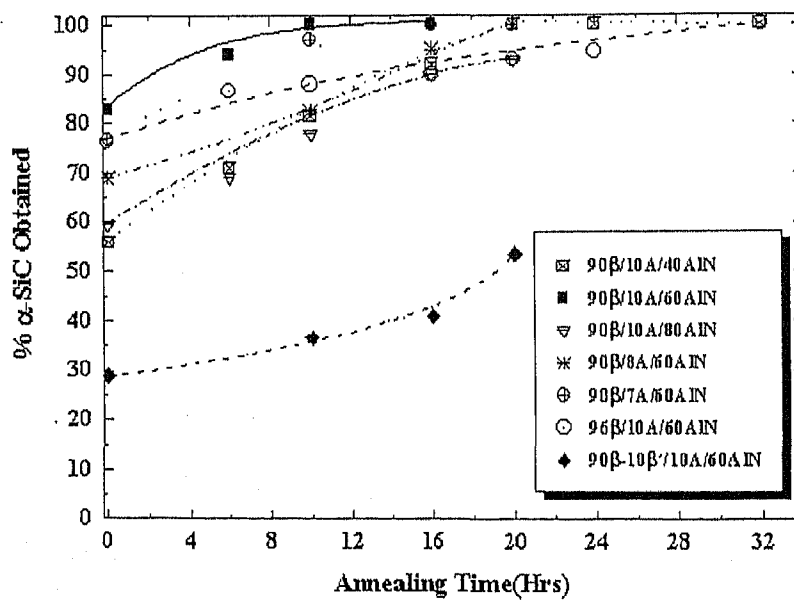


Figure 3.6: $\beta \rightarrow \alpha$ -SiC phase transformation as a function of annealing time.

Table 3.2: Phase analysis data as a function of annealing time

Material	Crystalline phases	Sintered	Annealed(16 h)
90 β /10A/60AlN	α -SiC(6H)	✓	✓
	β -SiC(3C)	✓	—
	$Y_{10}Al_2Si_3O_{18}N_4$	✓	—
	$Y_4Si_2N_2O_7$	✓	—
	$Y_2Si_2O_7$	✓	✓
	$Al_2Y_4O_9$	✓	✓
	Y_2O_3	✓	✓
90 β /7A/60AlN	α -SiC(6H)	✓	✓
	β -SiC(3C)	✓	—
	$Y_{10}Al_2Si_3O_{18}N_4$	✓	✓
	$Y_4Si_2N_2O_7$	✓	✓
	$Y_2Si_2O_7$	✓	✓
	$Al_2Y_4O_9$	—	—
	Y_2O_3	✓	✓
90 β -10 β' /10A/60AlN	α -SiC(6H)	—	✓
	β -SiC(3C)	✓	✓
	$Y_{10}Al_2Si_3O_{18}N_4$	✓	—
	$Y_4Si_2N_2O_7$	✓	—
	$Y_2Si_2O_7$	✓	✓
	$Al_2Y_4O_9$	✓	✓
	Y_2O_3	✓	✓

3.2 Mechanical properties

3.2.1 Fracture toughness

Effect of AlN-content in additive

The results (Table 3.3) show that in materials with 20AlN, the fracture toughness values are rather high with a error of about $\pm 25\%$. This large variation is probably due to the porosity distribution which may also contribute to the higher indentation fracture tough-

Table 3.3: Fracture toughness and hardness variation data for the materials containing different mol% AlN in the additive system

Sample	$K_{IC}(\text{MPa}\cdot\sqrt{m})$	Vickers hardness(VHN)
90 β /10A/20AlN	5.0 \pm 24%	1663 \pm 10%
90 β^* /10A/20AlN	3.7 \pm 8%	1577 \pm 5%
90 β /10A/40AlN	3.4 \pm 8%	1958 \pm 2%
90 β /10A/60AlN	4.9 \pm 6%	1806 \pm 2%
90 β /10A/80AlN	3.9 \pm 8%	2101 \pm 3%

ness values. This conforms also to a lower Vickers hardness. From the plot(*Figure 3.7*) of the remaining fracture toughness values as a function of AlN-content in the additive system, it is evident that there is a maximum in fracture toughness at 60mol% AlN. The SEM micrographs of these samples(*Figure 3.8*) reveal that in case of 40AlN, the grain size is much finer as compared to 60 or 80AlN samples. The reason for the increase of the fracture toughness of the platelet grain containing materials(60 and 80AlN) as compared to fine globular material(40AlN) is obvious from the crack path(*Figure 3.9*)[37, 48, 71, 81]. Crack bridging(1), crack deflection(2) and mechanical interlocking(3) are the prime toughening mechanisms[71]. Compared to the grain morphology of the material 60AlN, the material 80AlN has a lower aspect ratio. So the crack deflection mechanism is not so predominant in this case resulting a lower fracture toughness value.

Effect of additive content

Keeping 60mol% AlN constant in the additive system, the effect of additive content on the fracture toughness of the sintered materials was investigated. An increased fracture toughness was noticed for higher additive content materials(*Table 3.4*). The microstructural observation(see *Figure 3.8(b)* and *Figure 3.10*) of these materials reveals that for 10vol% additive, the grains are much more elongated, i.e., the aspect ratio of grains is higher which yields a higher K_{IC} value owing to the intergranular crack deflection toughening mechanism.

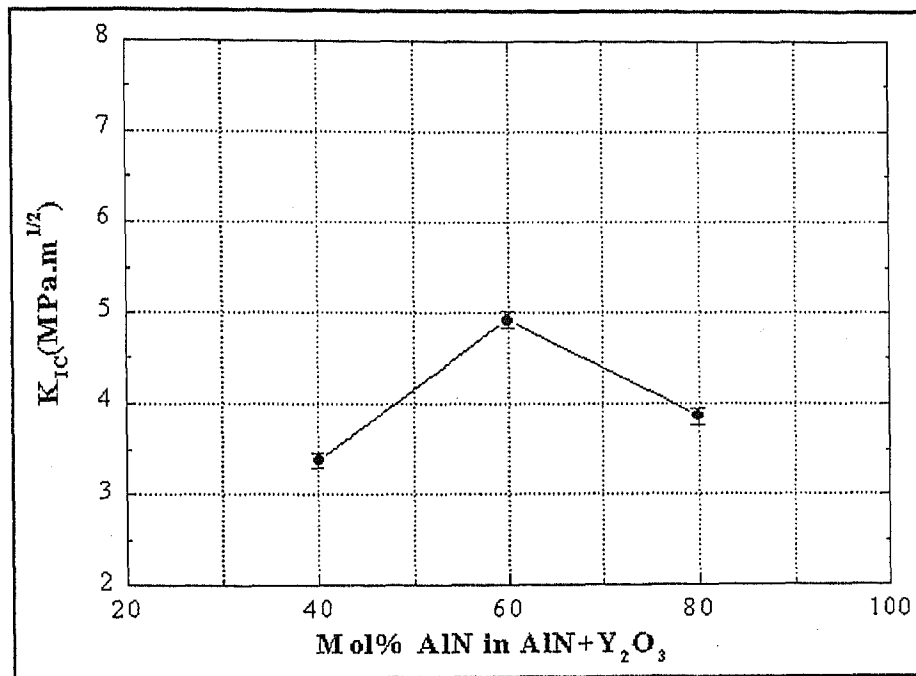


Figure 3.7: Fracture toughness variation as a function of AlN-content in the additive system AlN-Y₂O₃.

Effect of initial α -SiC content

From the tabulated values (Table 3.5), it is evident that fracture toughness increases with increasing α -SiC content. Substitution of α -SiC by large β -SiC powder also lowers the fracture toughness. The probable explanation lies in the difference of the crack trajectory in these material which is attributable to the difference in grain morphology, in particular, aspect ratio of grains. Elongated grains are observed by scanning electron microscopy in the case of 10% α -SiC (Figure 3.8 (b)). For the other two materials the grains are much finer and almost square-shaped (Figure 3.11) which will cause the crack path to remain relatively straight indicating low fracture toughness.

Effect of annealing time on fracture toughness

Figure 3.12 shows the variation of fracture toughness with annealing time in the case of samples with different AlN contents. For all the materials, K_{IC} values increase with annealing time. It has been observed that for the 60AlN material, the fracture toughness

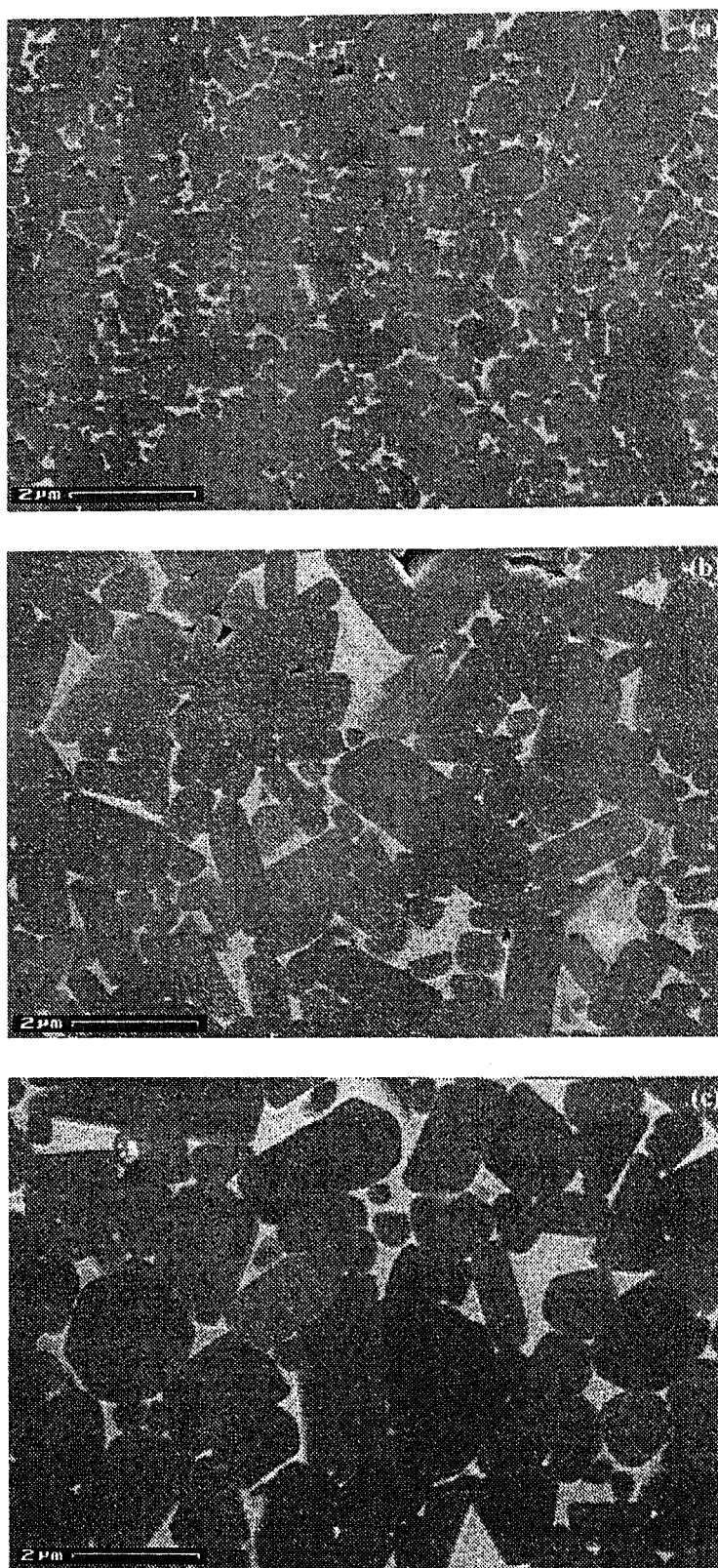


Figure 3.8: Scanning electron micrographs of as sintered specimens; (a) $90\beta/10A/40AlN$, (b) $90\beta/10A/60AlN$ and (c) $90\beta/10A/80AlN(\times 10000)$.

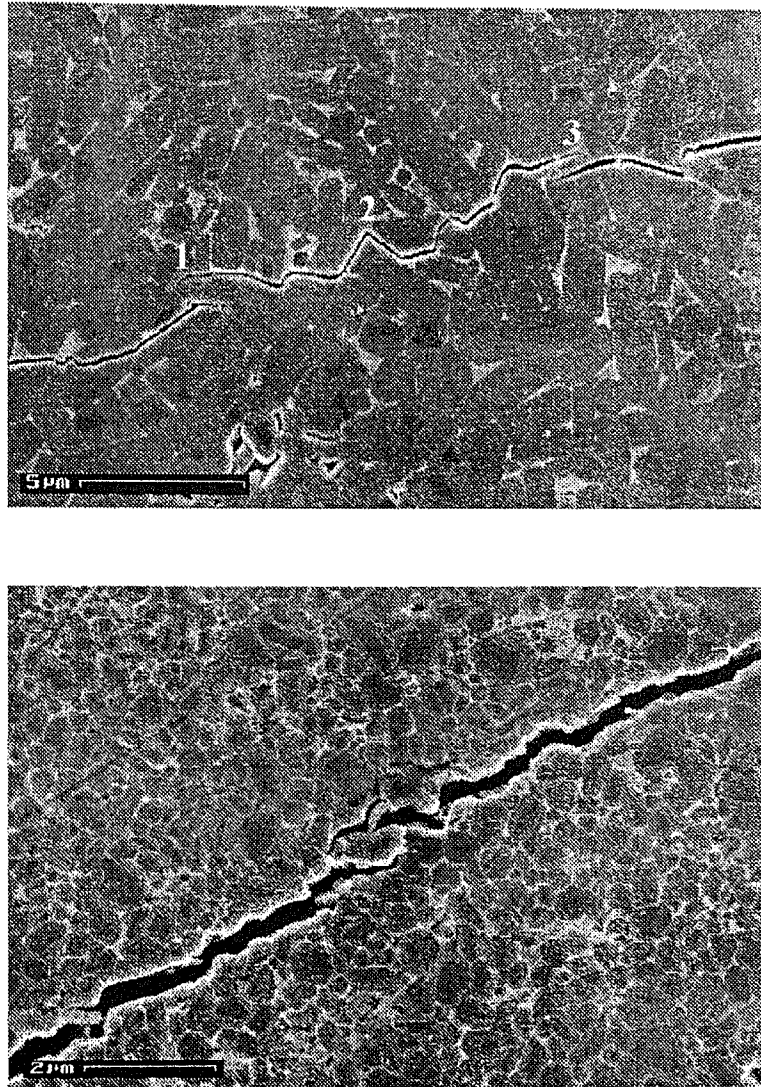


Figure 3.9: Differences in crack propagation in the globular and platelet materials (a) for platelet($\times 5000$) and (b) for globular($\times 10000$).

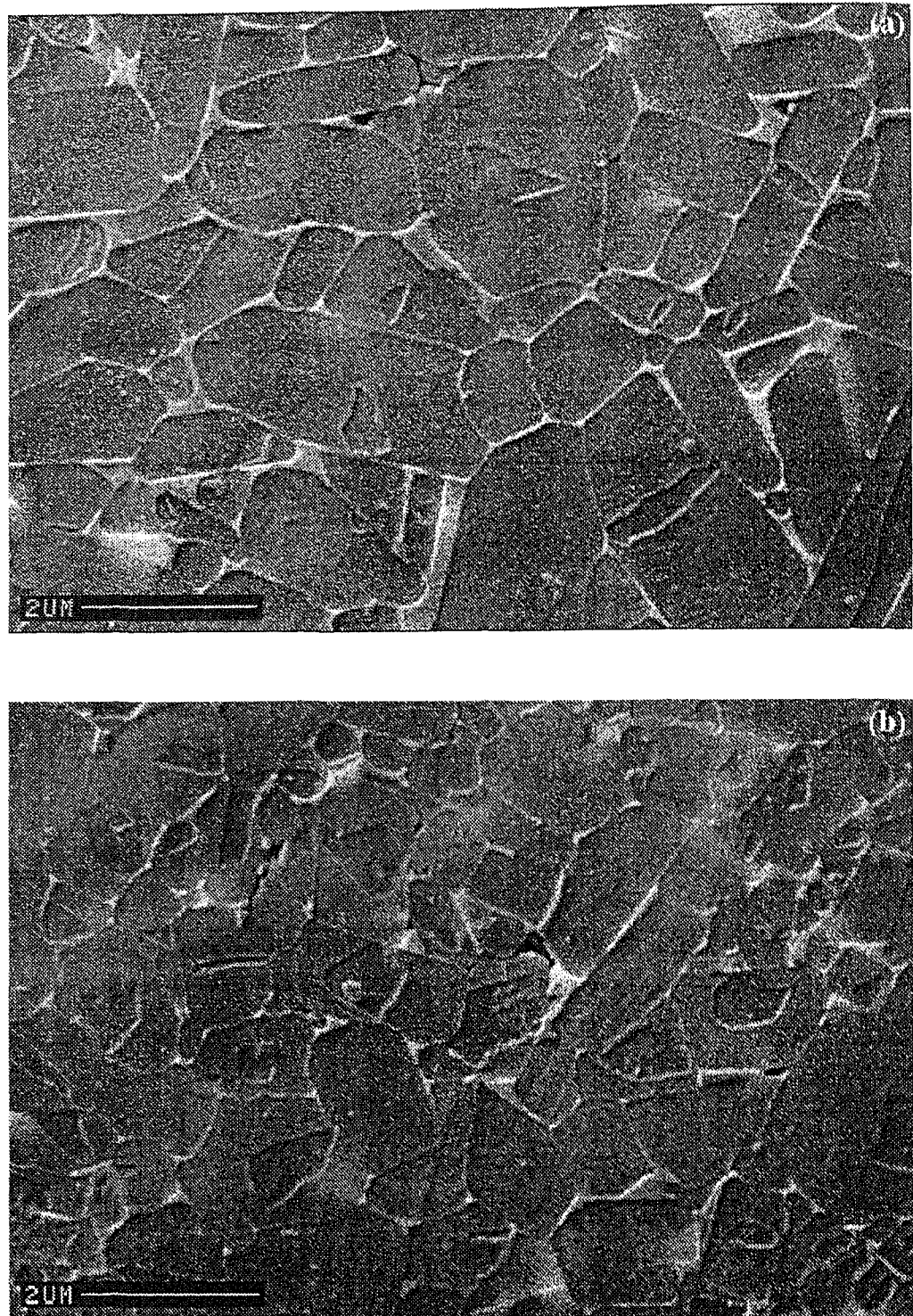


Figure 3.10: Scanning electron micrographs of as sintered specimens containing different vol% of additive; (a) $90\beta/7A/60AlN$ and (b) $90\beta/8A/60AlN(\times 10000)$.

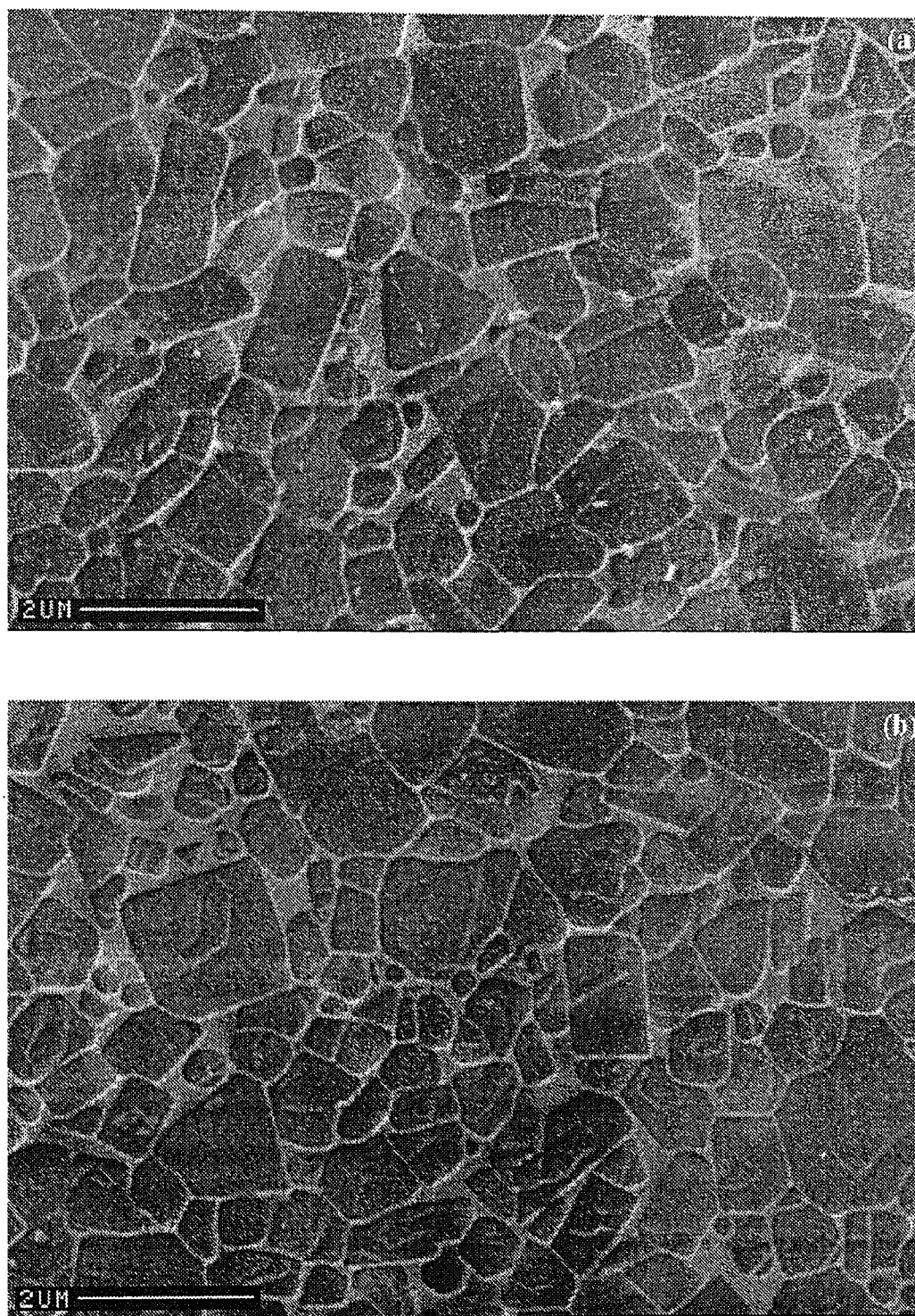


Figure 3.11: Scanning electron micrographs of as sintered specimens containing different amounts of α -SiC seeds; (a) 90β - $10\beta'$ /10A/60AlN and (b) 96β /10A/60AlN($\times 10000$).

Table 3.4: Fracture toughness and hardness variation data for the materials containing different vol% of additive

Sample	$K_{IC}(\text{MPa}.\sqrt{m})$	Vickers hardness(VHN)
90 β /7A/60AlN	$4.0 \pm 10\%$	$2148 \pm 4\%$
90 β /8A/60AlN	$4.1 \pm 5\%$	$2128 \pm 3\%$
90 β /10A/60AlN	$4.9 \pm 6\%$	$1806 \pm 2\%$

Table 3.5: Fracture toughness and hardness variation data for the materials containing different vol% of additive

Sample	$K_{IC}(\text{MPa}.\sqrt{m})$	Vickers hardness(VHN)
90 β -10 β' /10A/60AlN	$3.8 \pm 10\%$	$2137 \pm 5\%$
96 β /10A/60AlN	$3.9 \pm 5\%$	$2010 \pm 2\%$
90 β /10A/60AlN	$4.9 \pm 6\%$	$1806 \pm 2\%$

reaches a maximum value of $5.9 \text{ MPa}.\sqrt{m} \pm 13\%$ after 10hrs of annealing. From the XRD analysis, complete $\beta\text{-SiC} \rightarrow \alpha\text{-SiC}$ conversion is observed after 10hrs of annealing. The importance of this $\beta \rightarrow \alpha$ conversion is that, unless and until it is completed, the chance of grain growth is minimum as the $\alpha\text{-SiC}$ grows in a preferential direction. Prolonged annealing, however, has the effect of grain coarsening; at the same time the aspect ratio decreases from 2.3 to 2 (Figure 3.13). For 40AlN, the fracture toughness reaches a constant value of almost $5.0 \text{ MPa}.\sqrt{m} \pm 8\%$ after 20hrs of annealing. In this case also, full $\beta \rightarrow \alpha$ conversion occurs after 20hrs of annealing. But for 80AlN, there is no such saturation observed even after 20hrs of annealing. In this material, the transformation remains incomplete owing to the highly viscous glassy phase (due to the high AlN content), which makes the diffusion process sluggish.

For different additive contents, fracture toughness was also monitored as a function of annealing time (Figure 3.14). Similar trends are noticed conforming to the earlier

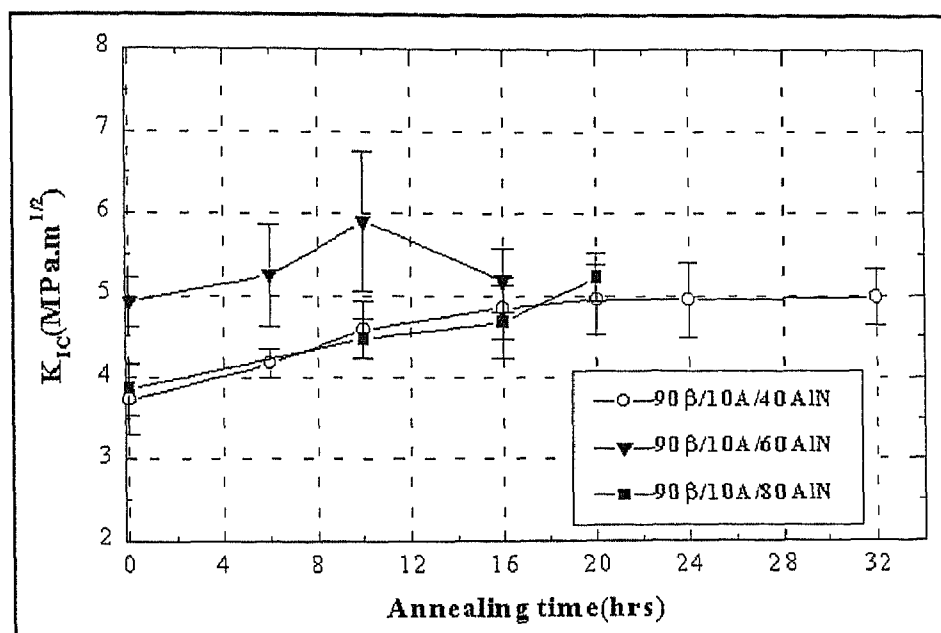


Figure 3.12: Fracture toughness variation as a function of annealing time and with different AlN-contents in the additive system.

discussion. For the 7vol% additive material, the complete $\beta \rightarrow \alpha$ transformation consumes a little more time owing to the less amount of liquid phase which acts as a carrier phase in diffusion.

The fracture toughness values of sintered SiC with different initial α -SiC contents are plotted in Figure 3.15 as a function of annealing time. In all cases, K_{IC} increases with increasing annealing time similar to the earlier cases. The material with 4% α -SiC shows a promising result of $6.5 \text{ MPa} \cdot \sqrt{\text{m}} \pm 7\%$ after 32 hrs of annealing. SEM micrographs (Figure 3.16) and XRD analysis show that large elongated grains with an aspect ratio of 2.5 and complete $\beta \rightarrow \alpha$ conversion after 32 hrs of annealing are the prime controlling parameters for achieving this high fracture toughness at room temperature.

The material in which the α -SiC seeds were substituted by coarse β -SiC powder shows a gradual increase of fracture toughness till 20 hrs of annealing. However, XRD reveals that the $\beta \rightarrow \alpha$ transformation is only 54% completed after 20 hrs of annealing. It is expected that further annealing can improve the fracture toughness of this material.

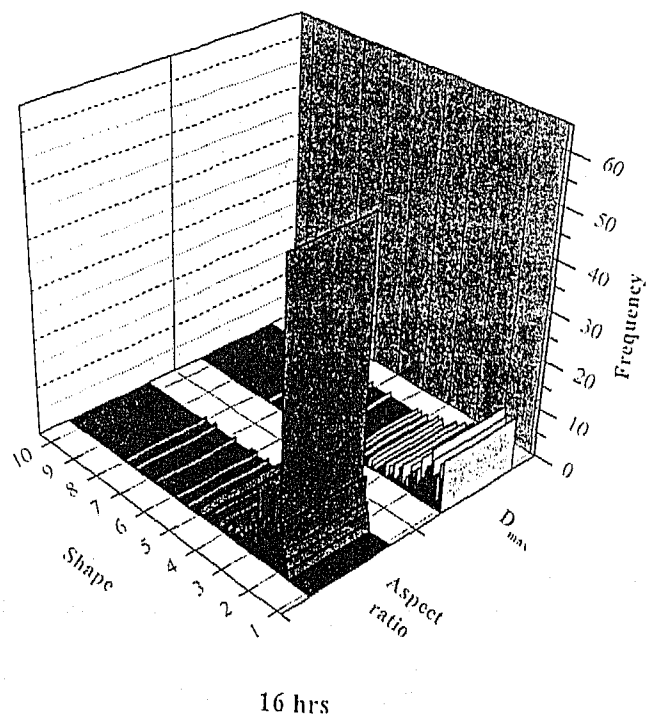
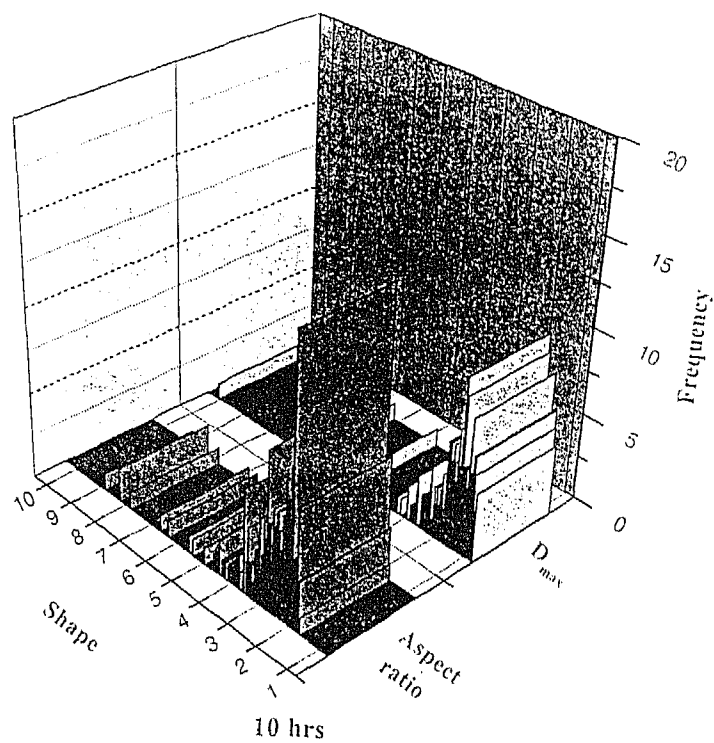


Figure 3.13: Effect of prolong annealing on grain size and aspect ratio.

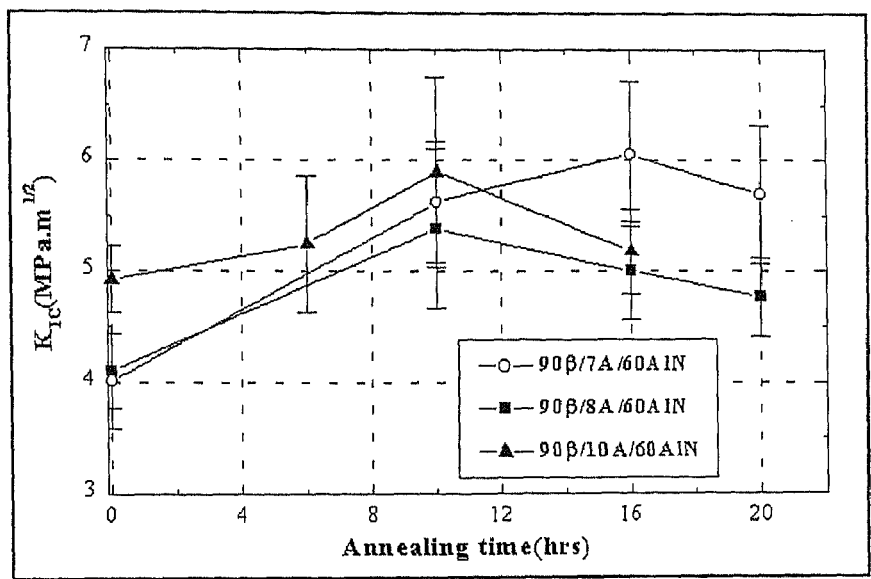


Figure 3.14: Fracture toughness variation with annealing time and additive content.

3.2.2 Bending strength

Effect of AlN-content in additive

Figure 3.17 shows the results of the bending strength measurements at room temperature. A slightly decreasing trend was observed as a function of increasing AlN content in the additive. Scanning electron micrographs(Figure 3.8) show that material 40AlN has much finer globular grains as compared to the others. This leads to a somewhat higher bending strength value.

High temperature results are plotted in Figure 3.18 . For the material 40AlN, high temperature strength increases upto 1200°C followed by a drastic decrease at 1400°C whereas 60AlN material shows a almost constant bending strength upto 1200°C. At 1400°C the bending strength increases to 551 MPa followed by a sharp decrease to 419 MPa at 1500°C. The increase in bending strength of the former material is comparable to the behaviour of globular α-SiC material observed by Keppeler *et al.*[71] in the temperature range between 1000°C and 1200°C. The authors explained this behaviour by the healing of flaws and surface cracks with glassy phase formed by oxidation of intergranular phase. In another investigation by Rixecker *et al.*[82], it was observed that during high temperature testing, a surface layer was formed in which the oxynitride grain boundary

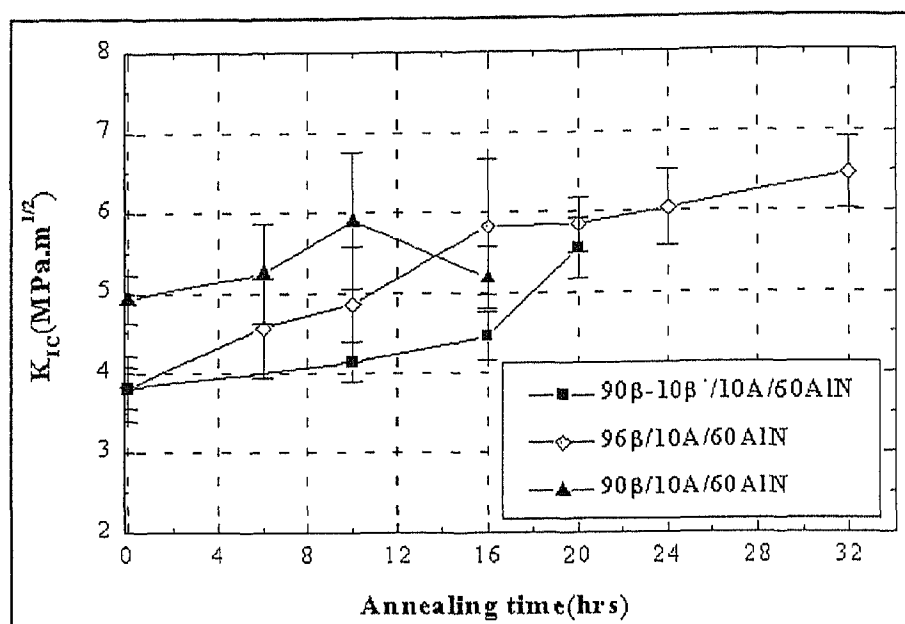


Figure 3.15: Fracture toughness variation as a function of annealing time and with different α -SiC content in additive system.

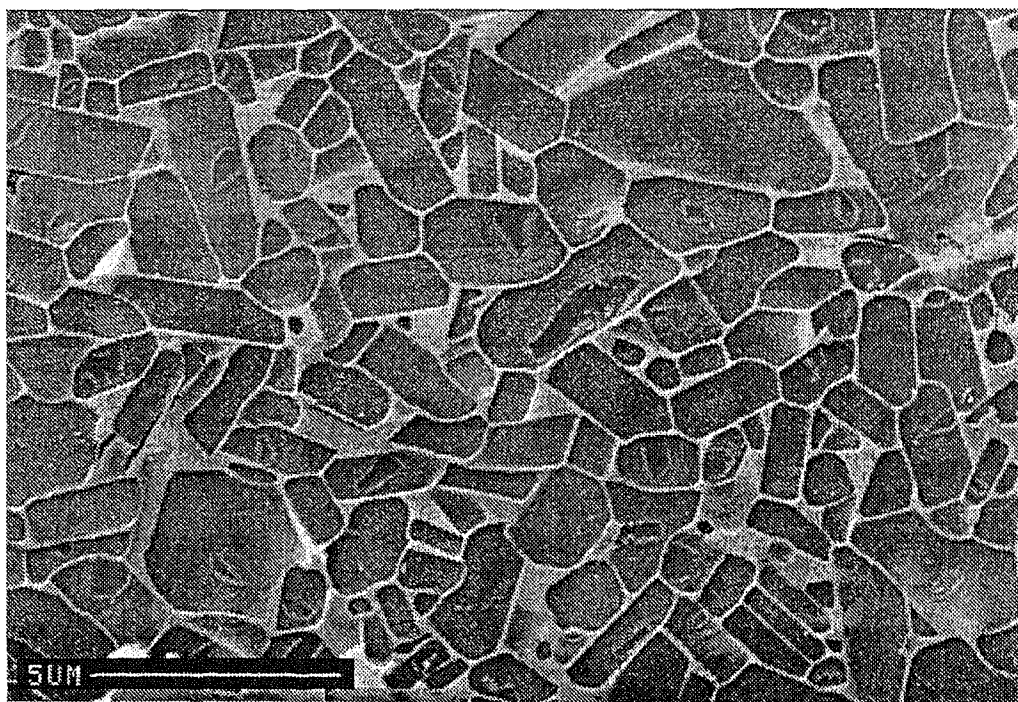


Figure 3.16: SEM micrograph of 96β/10A/60AlN after 32 hrs of annealing ($\times 5000$).

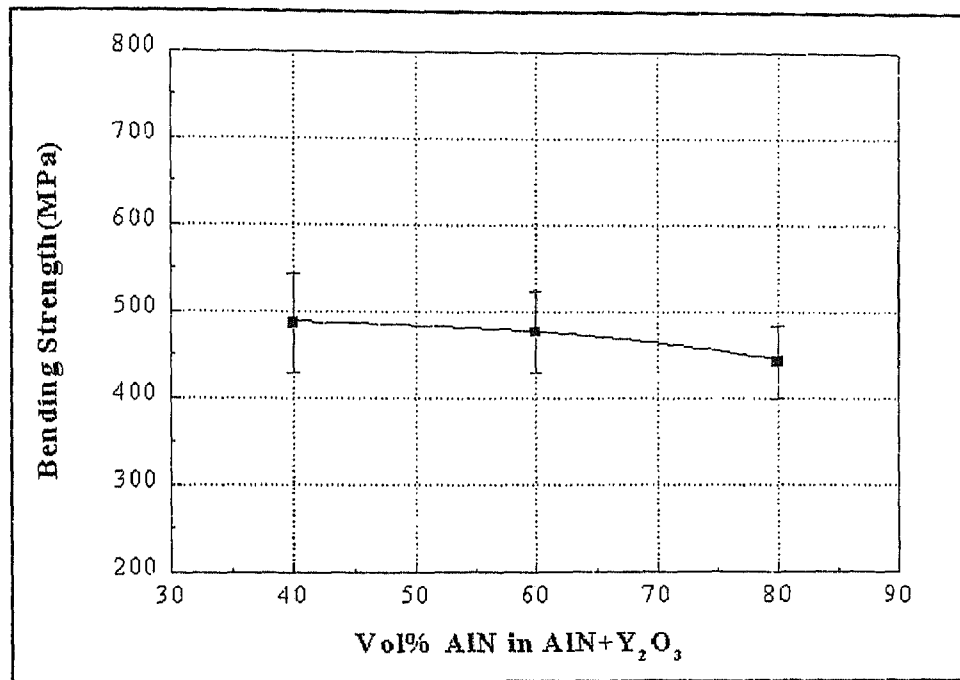


Figure 3.17: Bending strength variation with AlN-content in additive system.

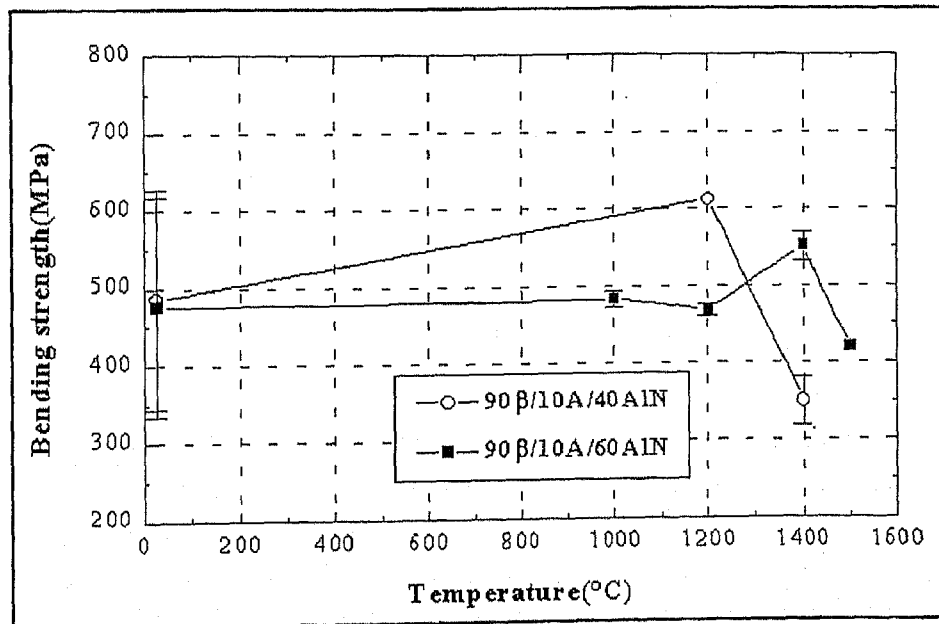


Figure 3.18: High temperature bending strength variation with AlN-content in additive system.

phases present in as sintered samples were converted to oxides and a compressive stress was induced due to the associated volume expansion. This compressive stress generated by formation of low density oxide phases prevents any prior surface cracks or flaws to grow. Most probably, both these mechanisms were operating in the present case. At 1400°C and 1500°C, the bending strength value decreases due to softening of the grain boundary phases. Probably a delayed oxidation takes place in 60AlN due to morphological change in grains and grain boundary phases in this particular system. Further investigation is going on in order to understand this behaviour.

Effect of additive content

Room temperature bending strength variation with increasing amount of additive is projected in *Figure 3.19*. It was observed that bending strength decreases with increasing additive content due to the increase in the amount of the weak secondary phase. Czechowski *et al.*[83] in their investigation, correlated the bending strength of SiC with the $\text{Al}_2\text{O}_3/\text{Y}_2\text{O}_3$ additive content and found that contiguity of the glassy phase has a great influence on the mechanical behaviour of the material.

From the plot(*Figure 3.20*) of the high temperature bending strength variation, it can be observed that with less additive content, the strength remains almost constant till 1200°C followed by a sharp decrease. As discussed in the preceding section, the oxidation of nitride phase plays a significant role in this system. However with 7 and 8% of additive, these effects are not so predominant as less amount of oxynitride phase is present. With 10vol% additive, the strength behaviour was already explained in the earlier section.

Effect of initial α -SiC content

The bending strength variation by varying the initial α -SiC content was followed. From the plot(*Figure 3.21*), no significant difference in bending strength was observed upon decreasing the α -SiC content from 10% to 4%. However, substitution of all the α -SiC by coarse β -SiC powder improves the room temperature bending strength because a bimodal microstructure is formed *Figure 3.11*. The high temperature behaviour suggests that there is a tradeoff between grain boundary softening and the compressive stress generation due to oxidation of the oxynitride phases which yields a fairly constant bending strength level between 1200°C and 1400°C(*Figure 3.22*).

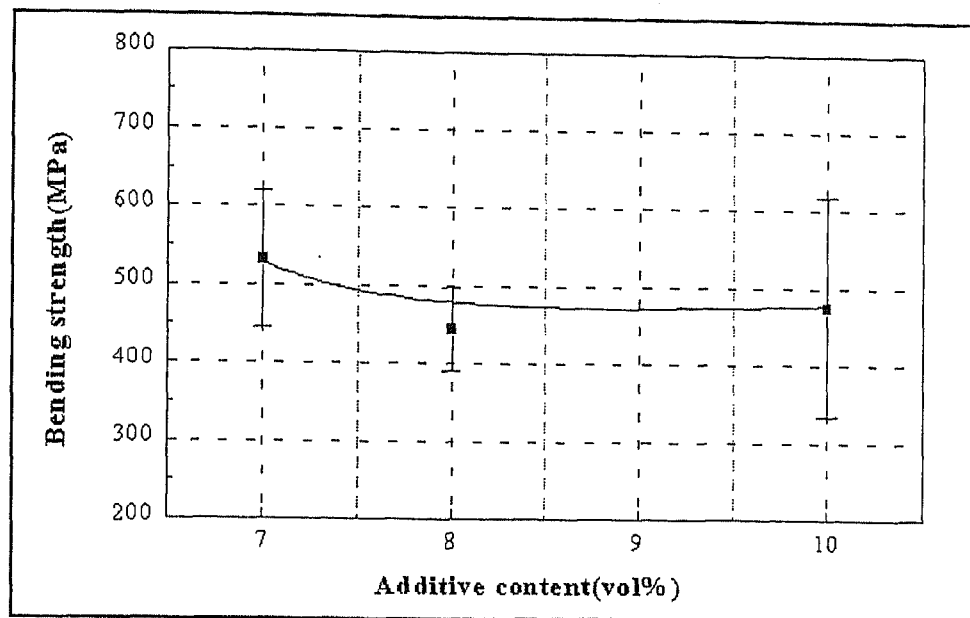


Figure 3.19: Bending strength variation with additive content.

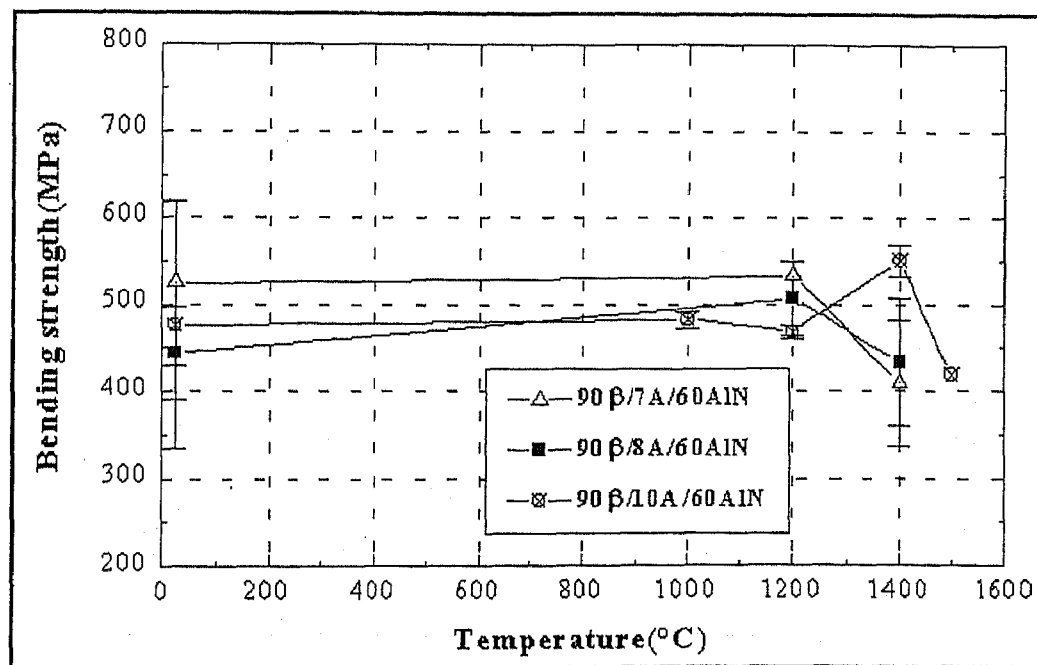


Figure 3.20: High temperature bending strength variation with additive content.

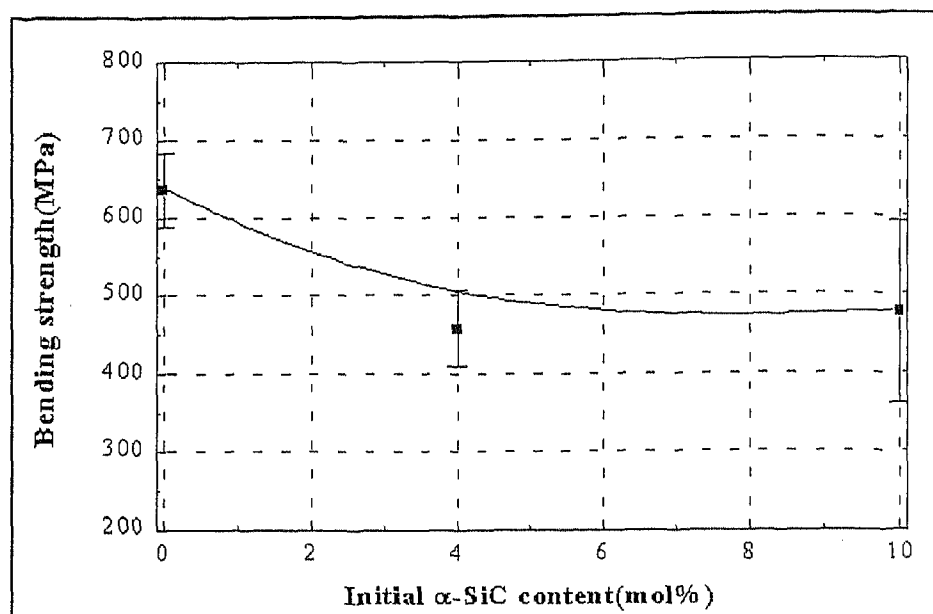


Figure 3.21: [Bending strength variation with initial α -SiC content.

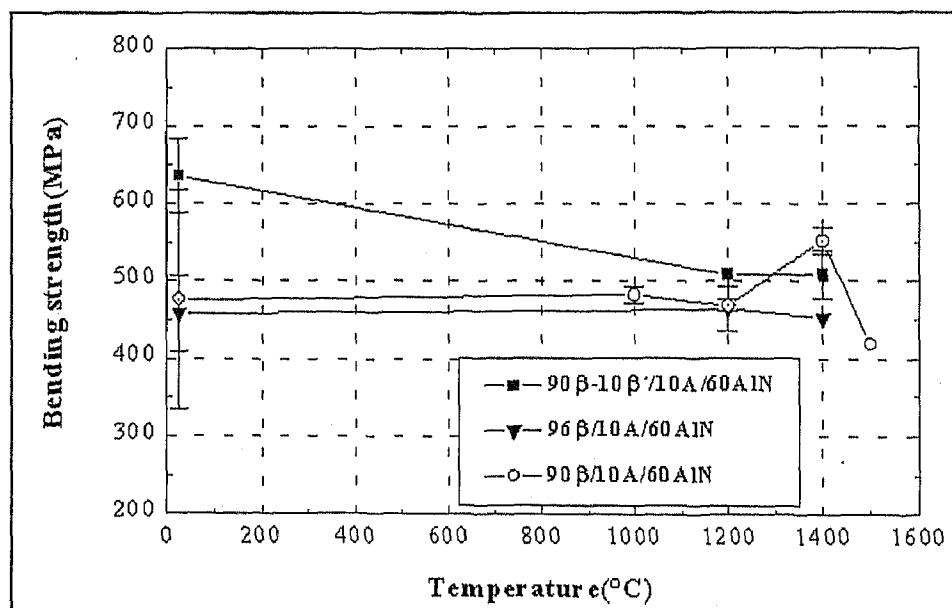


Figure 3.22: High temperature bending strength variation with initial α -SiC content.

Chapter 4

Chapter 4

Conclusions and future scope of work

β -SiC with α -SiC or coarse β -SiC seeds was successfully sintered for all compositional variations except for 20mol% AlN-containing additive system. Even HIPing under a high pressure of N₂(200 MPa) at 2000°C was not fruitful to densify these materials.

X-ray diffraction patterns reveal that most of the as-sintered materials contain primarily β -SiC(3C) phase along with some α -SiC(6H). After sintering the secondary phases that are predominantly present in these systems are Y₁₀Al₂Si₃O₁₈N₄, Y₄Si₂N₂O₇ and some Y₂Si₂O₇ and Al₂Y₄O₉. After annealing presence of the oxynitride phases vanish as they get transformed to oxide phases. However, in HIPed samples, the XRD patterns confirmed the presence of Si₃N₄ and free carbon which formed due to high N₂ overpressure. From the XRD-patterns the phase transformation from $\beta \rightarrow \alpha$ was monitored and it was found that for materials with 60AlN, phase transformation takes place rather very quickly. This was attributed to the second phase composition. Materials having less α -SiC seeds require more time to get fully converted.

Scanning electron microscopy reveals the grain growth and change in morphology of the grains with annealing time. In most of the samples it was found that grain growth is directly related to phase transformation, and substantial grain growth was observed in materials with 60mol% AlN after 6-10 hrs of annealing. This is attributed to the completion of the phase transformation from $\beta \rightarrow \alpha$ -SiC.

Room temperature fracture toughness results demonstrate that fracture toughness depends directly on the grain morphology i.e. shape, size and aspect ratio. Increased fracture toughness was observed in case of 60AlN due to formation of. platelet grains

formation. Crack bridging, crack deflection and mechanical interlocking are the prime toughening mechanisms in this system. Conforming to these mechanisms, fracture toughness increases with increasing annealing time due to formation of platelet grains. However, prolonged annealing had an adverse effect due to reduction of the average aspect ratio. Fracture toughness of $6.5 \text{ MPa}\cdot\sqrt{m}$ was found for $96\beta/10A/60\text{AlN}$ samples after annealing for 32 hrs. however in some samples, the phase transformation from $\beta \rightarrow \alpha\text{-SiC}$ was not completed. Perhaps one can find even better fracture toughness by prolonged annealing of these materials.

Bending strength results suggest that at room temperature, the strength only depends on the grain morphology and the second phase content of the system. With a bimodal microstructure, the strength value of 635 MPa was found for $90\beta\text{-}10\beta'/10A/60\text{AlN}$ material. However, at a high temperature the strength of the materials is primarily influenced by the softening of the glassy phase. The nitrogen content is also of great importance because oxydation of the initial or Y-nitride phases induces a high compressive stress at the surface, thus providing a strengthening mechanism. It was found that for $90\beta/10A/60\text{AlN}$ material, the bending strength increases at 1400°C due to this process. However, the reason for the particularly good high temperature behaviour of the material with 60mol% AlN was not well understood, and experiments with different temperatures and annealing times to be performed to clarify this point.

Considering all the properties, it was shown that in the material $90\beta/10A/60\text{AlN}$, excellent high temperature strength along with high fracture toughness can be achieved. Further investigations on this system will help to develop superior good potent material for high temperature applications.

References

Bibliography

- [1] K. Yamada and M. Mohri, in 'Silicon Carbide Ceramics', **Vol.1**, ed. S. Sōmiya and Y. Inomata, Elsevier, Barking, U.K., 1991, p.13.
- [2] P. Popper, in 'Special Ceramics', ed. P. Popper, The British Ceramic Research Association, Stoke-on-Trent, U.K., 1960, p.209.
- [3] P. Matje and K. A. Schwetz, in 'Ceram. Trans., Ceramic Powder Science II', **A, Vol.1**, ed. G. L. Messing, E. R. Fuller, Jr. and H. Hausner, The Am. Ceram. Soc., Westerville, Ohio, 1988, p.460.
- [4] Y. Okaba, J. Hojo and A. Kato, J. Chem. Soc. Japan, 1980, p.188.
- [5] Y. Okaba, J. Hojo and A. Kato, J. Less-Common Metals, **Vol.68**, No.1, 1979, p.29.
- [6] G. C. Wei, C. R. Kennedy and L. A. Harris, Am. Ceram. Soc. Bull., **Vol.63**, No.8, 1984, p.1054.
- [7] T. Hase and H. Suzuki, J. Ceram. Soc. Japan, **Vol.86**, No.12, 1978, p.606.
- [8] Y. Ando *et al.*, J. Cryst. Growth, **Vol.52**, 1981, p.178.
- [9] W. R. Cannon, S. C. Danforth, J. H. Flint, J. S. Haggerty and R. A. Marra, J. Am. Ceram. Soc., **Vol.65**, No.7, 1982, p.324.
- [10] W. R. Cannon, S. C. Danforth, J. S. Haggerty and R. A. Marra, J. Am. Ceram. Soc., **Vol.65**, No.7, 1982, p.330.
- [11] M. Luce, O. Croix, C. Robert and M. Cauchetier, in 'Ceram. Trans., Ceramic Powder Science III', **Vol.12**, ed. G. L. Messing, S. Hirano and H. Hausner, The Am. Ceram. Soc. Inc., Westerville, Ohio, 1990, p.267.
- [12] C. Greskovich and J. H. Rosolowski, J. Am. Ceram. Soc., **Vol.59**, No.7, 1976, p.336.

- [13] S. Prochazka, in 'Mass Transport Phenomena in Ceramics', ed. A. R. Cooper and A. H. Heuer, **Vol.9**, Plenum Press, New York, 1975, p.421.
- [14] H. Hausner, in 'Energy and Ceramics', *Matls. Sc. Monographs*, 6, ed. P. Vincenzini, Elsevier Scientific Pub. Company, Amsterdam, 1980, p.582.
- [15] H. Suzuki and T. Hase, in 'Proc. of Int. Sympo. on factors in Densification and Sintering of Oxide and Non-Oxide Ceramics', ed. S. Sōmiya and S. Saito, Gakujutsu Bunken, Fukyu-kai, Tokyo, 1979, p.345.
- [16] Y. Murata and R. H. Smoak, in 'Proc. of Int. Sympo. on factors in Densification and Sintering of Oxide and Non-Oxide Ceramics', ed. S. Sōmiya and S. Saito, Gakujutsu Bunken, Fukyu-kai, Tokyo, 1979, p.383.
- [17] D. H. Stutz, S. Prochazka and J. Lorenz, *J. Am. Ceram. Soc.*, **Vol.68**, No.9, 1985, p.479.
- [18] R. A. Alliegro, L. B. Coffin and J. R. Tinklepaugh, *J. Am. Ceram. Soc.*, **Vol.39**, No.11, 1956, p.386.
- [19] W. Bröcker, H. Landfermann and H. Hausner, *Powder Met. Int.*, **Vol.11**, No.2, 1979, p.83.
- [20] S. Shinozaki, J. Haugas, W. T. Donlon, R. M. Williams and B. N. Juterbock, in 'Advanced Ceramics II', ed. S. Sōmiya, Elsevier Applied Science, London, 1988, p.7.
- [21] A. Kerber, H. Hofmann and P. Wirth, in 'Ceram. Trans., Ceramic powder science III', **Vol.12**, ed. G. L. Messing, S. Hirano and H. Hausner, The Am. Ceram. Soc., Westerville, Ohio, 1990, p.895.
- [22] J. Hojo, in 'Silicon Carbide Ceramics', **Vol.1**, ed. S. Sōmiya and Y. Inomata, Elsevier, Barking, U.K., 1991, p.149.
- [23] H. Tanaka, in 'Silicon Carbide Ceramics', **Vol.1**, ed. S. Sōmiya and Y. Inomata, Elsevier, Barking, U.K., 1991, p.213.
- [24] S. Prochazka, C. A. Johnson and R. A. Giddings, in 'Proc. of Int. Sympo. on factors in Densification and Sintering of Oxide and Non-Oxide Ceramics', ed. S. Sōmiya and S. Saito, Gakujutsu Bunken, Fukyu-kai, Tokyo, 1979, p.366.
- [25] M. N. Rahaman, *Ceramic Processing and Sintering*, Marcel Dekkar, Inc., New York, 1995, p.707.

- [26] J. S. Nadeau, *Am. Ceram. Soc. Bull.*, **Vol.52**, No.2, 1973, p.170.
- [27] D. Kalish and E. V. Clougherty, *Am. Ceram. Soc. Bull.*, **Vol.48**, No.5, 1969, p.570.
- [28] K. Takatori, N. Ogawa, M. Shimada and M. Koizumi, in 'Energy and Ceramics', *Matls. Sc. Monographs*, 6, ed. P. Vincenzini, Elsevier Scientific Pub. Company, Amsterdam, 1980, p.525.
- [29] T. Sakai and T. Aikawa, *J. Am. Ceram. Soc.*, **Vol.71**, No.1, 1988, p.C-7.
- [30] T. Sakai and N. Hirosaki, *J. Am. Ceram. Soc.*, **Vol.68**, No.8, 1985, p.C-191.
- [31] R. Ruh, A. Zangvil and J. Barlowe, *Am. Ceram. Soc. Bull.*, **Vol.64**, No.10, 1985, p.1368.
- [32] J. Schoennahl, B. Willer and M. Daire, in 'Sintering—New Developments', ed. M. M. Ristić, Elsevier Scientific Pub. Company, Amsterdam, 1979, p.338.
- [33] M. Omori and H. Takei, *J. Am. Ceram. Soc.*, **Vol.65**, No.6, 1982, p.C-92.
- [34] N. P. Padture and B. R. Lawn, *J. Am. Ceram. Soc.*, **Vol.77**, No.10, 1992, p.2518.
- [35] M. A. Mulla and V. D. Kristic, *J. Mat. Sci.*, **Vol.29**, No.3, 1994, p.934.
- [36] M. A. Mulla and V. D. Kristic, *Acta Metall.*, **Vol.42**, No.1, 1994, p.303.
- [37] N. P. Padture, *J. Am. Ceram. Soc.*, **Vol.77**, No.2, 1994, p.519.
- [38] Y. W. Kim, M. Mitomo and H. Hirotsumi, *J. Am. Ceram. Soc.*, **Vol.78**, No.11, 1995, p.3145.
- [39] M. A. Mulla and V. D. Kristic, *Am. Ceram. Soc. Bull.*, **Vol.70**, No.3, 1991, p.439.
- [40] M. Omori and H. Takei, *J. Mat. Sci.*, **Vol.23**, No.10, 1988, p.3744.
- [41] A. K. Misra, *J. Am. Ceram. Soc.*, **Vol.74**, No.2, 1991, p.345.
- [42] K. Suzuki, in 'Silicon Carbide Ceramics', **Vol.2**, ed. S. Sōmiya and Y. Inomata, Elsevier, Barking, U.K., 1991, p.163.
- [43] L. S. Sigl and H. J. Kleebe, *J. Am. Ceram. Soc.*, **Vol.76**, No.3, 1993, p.773.
- [44] T. Grande, H. Sommerset, E. Hagen, K. Wiik and M. A. Einarsrud, *J. Am. Ceram. Soc.*, **Vol.80**, No.4, 1997, p.1047.

- [45] F. F. Lange, *J. Mat. Sci.*, **Vol.10**, No.2, 1975, p.314.
- [46] H. W. Jun, H. W. Lee, G. H. Kim, H. S. Song and B. H. Kim, *Ceramic Engg. and Sc. Proceedings*, **Vol.18**, No.4, 1997, p.487.
- [47] R. R. Lee and W. C. Wei, *Ceramic Engg. and Sc. Proceedings*, **Vol.11**, 1990, p.1094.
- [48] M. Nader, Doctoral Thesis, University of Stuttgart, 1995.
- [49] A. Jeutter, Diplom Thesis, University of Stuttgart, 1993.
- [50] B. W. Lin, M. Imai, T. Yano and T. Iseki, *J. Am. Ceram. Soc.*, **Vol.69**, No.4, 1986, p.C-67.
- [51] K. Suzuki, *Bull. Ceram. Soc. Japan*, **Vol.21**, 1986, p.590.
- [52] R. Hamminger, G. Grathwohl and F. Thümmeler, in 'Science of Ceramics', **Vol.12**, ed. P. Vincenzini, Ceramurgica s.r.l., Faenza, Italy, 1984, p.299.
- [53] S. S. Shinozaki, W. T. Donlon, R. M. Williams, B. N. Juterbock and T. J. Whalen, in 'Advanced Ceramics', ed. S. Sōmiya and R. C. Bradt, Terra Scientific Pub. Company, Tokyo, 1987, p.35.
- [54] P. Greil and D. Stutz, in 'Advanced Ceramics', ed. S. Sōmiya and R. C. Bradt, Terra Scientific Pub. Company, Tokyo, 1987, p.49.
- [55] K. Suzuki and M. Sasaki in *Fundamental Structural Ceramics*, ed. S. Sōmiya and R. C. Bradt, Terra Scientific Pub. Company, Tokyo, 1987, p.75.
- [56] M. Sasaki, K. Suzuki, H. Nishimura and M. Noshiro in *Proc. of the World Congr. on High Tech. Ceramics, 6th CIMTEC*, ed. P. Vincenzini, Elsevier Sc. Pub., B. V., Amsterdam, 1987, p.1101.
- [57] S. K. Lee and C. H. Kim, *J. Am. Ceram. Soc.*, **Vol.77**, No.6, 1994, p.1655.
- [58] Y. W. Kim, M. Mitomo and H. Hirotsuru, *J. Am. Ceram. Soc.*, **Vol.80**, No.1, 1997, p.99.
- [59] W. Rafaniello, M. R. Plichta and A. V. Virkar, *J. Am. Ceram. Soc.*, **Vol.66**, No.4, 1983, p.272.
- [60] A. Zangvil and R. Ruh, *J. Am. Ceram. Soc.*, **Vol.71**, No.10, 1988, p.884.

- [61] S. Y. Kuo and A. V. Virkar, *J. Am. Ceram. Soc.*, **Vol.72**, No.4, 1989, p.540.
- [62] S. Y. Kuo, A. V. Virkar and W. Rafaniello, *J. Am. Ceram. Soc.*, **Vol.70**, No.6, 1987, p.C-125.
- [63] S. Y. Kuo and A. V. Virkar, *J. Am. Ceram. Soc.*, **Vol.73**, No.9, 1990, p.2640.
- [64] W. E. Mayo and T. Tsakalakos, *Metall. Trans. A*, **Vol.11A**, 1980, p.1637.
- [65] J. Chen, Q. Tian and A. V. Virkar, *J. Am. Ceram. Soc.*, **Vol.75**, No.4, 1992, p.809.
- [66] I. Wiedmann, Doctoral Thesis, University of Stuttgart, 1998.
- [67] J. W. Edington, D. J. Rowcliffe and J. L. Hawshall, *Powder Met. Int.*, **Vol.7**, No.2, 1975, p.82.
- [68] S. Prochazka and R. J. Charies, *Am. Ceram. Soc. Bull.*, **Vol.52**, No.8, 1973, p.885.
- [69] S. Dutta, *J. Mat. Sci.*, **Vol.19**, No.4, 1984, p.1307.
- [70] S. Dutta, *J. Am. Ceram. Soc.*, **Vol.68**, No.10, 1985, p.C-269.
- [71] M. Keppeler, H. G. Reichert, J. M. Broadley, G. Thurn, I. Wiedmann and F. Aldinger, *J. Eur. Ceram. Soc.*, **Vol.18**, 1998, p.521.
- [72] J. W. Edington, D. J. Rowcliffe and J. L. Hawshall, *Powder Met. Int.*, **Vol.7**, No.3, 1975, p.136.
- [73] K. A. Schwetz and A. Lipp, in 'Science of Ceramics', **Vol.10**, ed. H. Hausner, Deutsche Keramische Gesellschaft, Köln, 1980, p.149.
- [74] G. Grathwohl, R. Hamminger, H. Iwanek and F. Thümmeler, in 'Science of Ceramics', **Vol.12**, ed. P. Vincenzini, Ceramurgica s.r.l., Faenza, Italy, 1984, p.583.
- [75] K. T. Faber and A. G. Evans, *J. Am. Ceram. Soc.*, **Vol.66**, No.6, 1983, p.C-94.
- [76] H. Kodama and T. Miyoshi, *J. Am. Ceram. Soc.*, **Vol.75**, No.6, 1992, p.1558.
- [77] J. J. Cao, W. J. MoberlyChan, L. C. DeJonghe, C. J. Gilbert and R. O. Ritchie, *J. Am. Ceram. Soc.*, **Vol.79**, No.2, 1996, p.461.
- [78] P. L. Farnsworth and R. L. Coble, *J. Am. Ceram. Soc.*, **Vol.49**, No.5, 1966, p.264.
- [79] T. L. Francis and R. L. Coble, *J. Am. Ceram. Soc.*, **Vol.51**, No.2, 1968, p.115.

- [80] R. K. Govila, J. Mat. Sci., Vol.18, No.7, 1983, p.1967.
- [81] I. Wiedmann, M. Nader, M. J. Hoffmann and F. Aldinger, in 'Proc. Werkstoffwoche'96, Symp.7, eds. F. Aldinger and H. Mughrabi, DGM Informationsgesellschaft, Frankfurt, 1996, p.512.
- [82] G. Rixecker, I. Wiedmann, K. Biswas and F. Aldinger, in 'Proc. Werkstoffwoche'98, Symp.9b, DGM Informationsgesellschaft, Frankfurt, 1999(in press).
- [83] Z. S. Rak and J. Czechowski, Proc. Eur. Conf. Adv. Mater. Processes Appl., 5th, Vol.2, No.2, 1997, p.363.

